Topic 14

Solution of Nonlinear Dynamic Response—Part II

Contents:

- **Mode superposition analysis in nonlinear dynamics**
- **Substructuring in nonlinear dynamics, a schematic example of a building on a flexible foundation**
- **Study of analyses to demonstrate characteristics of procedures for nonlinear dynamic solutions**
- **Example analysis: Wave propagation in a rod**
- **Example analysis: Dynamic response of a three degree of freedom system using the central difference method**
- **Example analysis: Ten-story tapered tower subjected to blast loading**
- **Example analysis: Simple pendulum undergoing large displacements**
- **Example analysis: Pipe whip solution**
- **Example analysis: Control rod drive housing with lower support**
- **Example analysis: Spherical cap under uniform pressure loading**
- **Example analysis: Solution of fluid-structure interaction problem**

Textbook: Sections 9.3.1, 9.3.2, 9.3.3, 9.5.3, 8.2.4

Examples: 9.6, 9.7, 9.8, 9.11

References:

The use of the nonlinear dynamic analysis techniques is described with example solutions in

Bathe, K. J., "Finite Element Formulation, Modeling and Solution of Nonlinear Dynamic Problems," Chapter in *Numerical Methods for Partial Differential Equations,* (Parter, S. V., ed.), Academic Press, 1979.

Bathe, K. J., and S. Gracewski, "On Nonlinear Dynamic Analysis Using Substructuring and Mode Superposition," *Computers & Structures, 13,* 699–707, 1981.

Ishizaki, T., and K. J. Bathe, "On Finite Element Large Displacement and Elastic-Plastic Dynamic Analysis of Shell Structures," *Computers & Structures, 12,* 309–318, 1980.

THE SOLUTION OF THE DYNAMIC EQUILIBRIUM EQUATIONS CAN BE ACHIEVED USING

- DIRECT INTEGRATION METHODS
  - EXPLICIT INTEGR.
  - IMPLICIT INTEGR.
- MODE SUPERPOSITION
- SUBSTRUCTURING

WE DISCUSS THESE TECHNIQUES BRIEFLY IN THIS LECTURE

EXAMPLES

EX.1 WAVE PROPAGATION IN A ROD

EX.2 RESPONSE OF A 3 D.O.F. SYSTEM

EX.3 ANALYSIS OF TEN STORY TAPERED TOWER

EX.4 ANALYSIS OF PENDULUM

EX.5 PIPE WHIP RESPONSE SOLUTION

SLIDES REGARDING

- ANALYSIS OF CRD HOUSING
- SOLUTION OF RESPONSE OF SPHERICAL CAP
- ANALYSIS OF FLUID-STRUCTURE INTERACTION PROBLEM (PIPE TEST)

THE DETAILS OF THESE PROBLEM SOLUTIONS ARE GIVEN IN THE PAPERS, SEE STUDY GUIDE

Markerboard 14-1

Transparency 14-1

Mode superposition:

- The modes of vibration change due to the nonlinearities, however we can employ the modes at a particular time as basis vectors (generalized displacements) to express the response.
- This method is effective when, in nonlinear analysis,
  - the response lies in only a few vibration modes (displacement patterns)
  - the system has only local nonlinearities

Transparency 14-2

The governing equations in implicit time integration are (assuming no damping matrix)

$$\underline{M}\ {}^{t+\Delta t}\ddot{\underline{U}}^{(k)} + {}^{\tau}\underline{K}\ \Delta\underline{U}^{(k)} = {}^{t+\Delta t}\underline{R} - {}^{t+\Delta t}\underline{F}^{(k-1)}$$

Let now $\tau = 0$, hence the method of solution corresponds to the initial stress method.

Using

$${}^{t+\Delta t}\underline{U} = \sum_{i=r}^{s} \underline{\phi}_i\ {}^{t+\Delta t}x_i$$

$${}^{0}\underline{K}\ \underline{\phi}_i = \omega_i^2\ \underline{M}\ \underline{\phi}_i$$

The modal transformation gives

$$ {}^{t+\Delta t}\ddot{\underline{X}}^{(k)} + \underline{\Omega}^2\,\Delta\underline{X}^{(k)} = \underline{\Phi}^T \underbrace{\left({}^{t+\Delta t}\underline{R} - {}^{t+\Delta t}\underline{F}^{(k-1)}\right)} $$

equations cannot be solved individually over the time span
Coupling!

where

$$ \underline{\Omega}^2 = \begin{bmatrix} \omega_r^2 & & \\ & \ddots & \\ & & \omega_s^2 \end{bmatrix} $$

$$ \underline{\Phi} = [\underline{\phi}_r \cdots \underline{\phi}_s] $$

$$ {}^{t+\Delta t}\underline{X}^T = [{}^{t+\Delta t}x_r \cdots {}^{t+\Delta t}x_s] $$

Transparency 14-3

Typical problem:

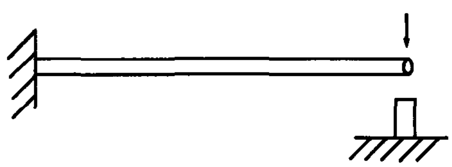

Pipe whip: Elastic-plastic pipe
Elastic-plastic stop

- Nonlinearities in pipe and stop. But the displacements are reasonably well contained in a few modes of the linear (initial) system.

Transparency 14-4

Transparency 14-5

Substructuring

- Procedure is used with implicit time integration. All linear degrees of freedom can be condensed out prior to the incremental solution.
- Used for local nonlinearities:
  Contact problems
  Nonlinear support problems

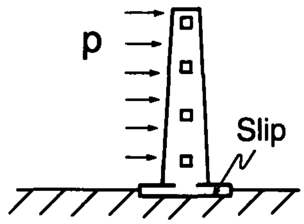

Transparency 14-6

Example:

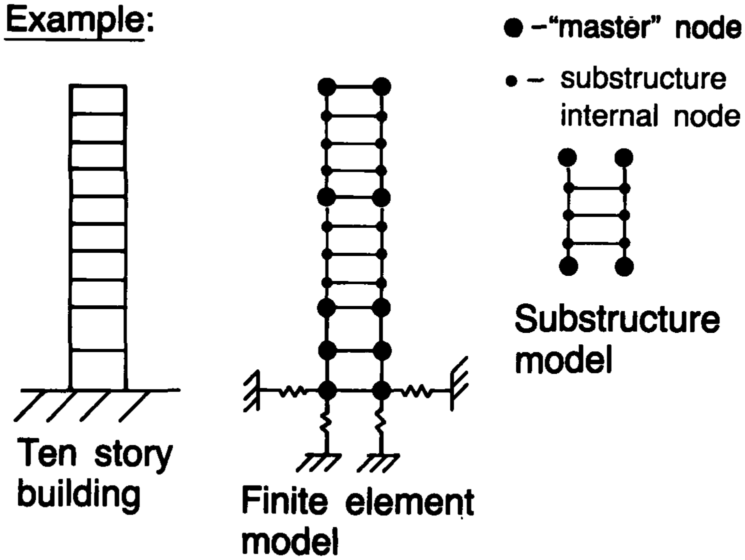

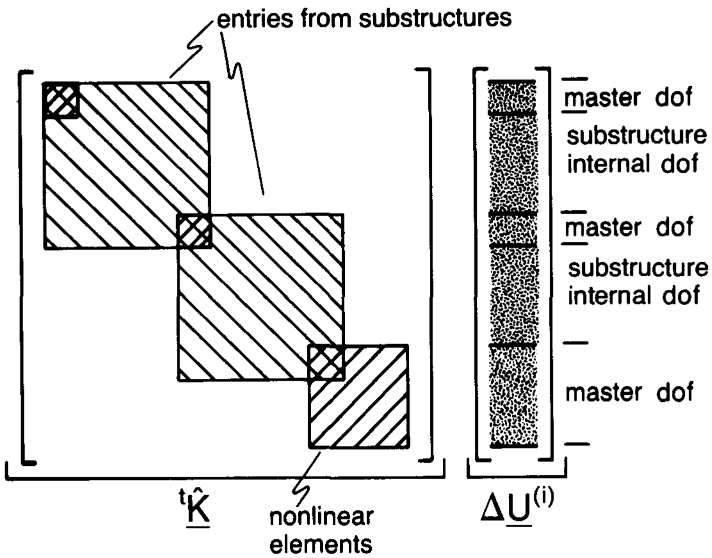

Transparency 14-7

Here

$$
{}^t\hat{\underline{K}} = \left(\underline{K} + \frac{4}{\Delta t^2}\,\underline{M}\right) + {}^t\underline{K}_{\text{nonlinear}}
$$

total mass matrix

all nonlinear stiffness effects

all linear element contributions

$$
= \hat{\underline{K}} + {}^t\underline{K}_{\text{nonlinear}}
$$

Transparency 14-8

Transparency 14-9

After condensing out all substructure internal degrees of freedom, we obtain a smaller system of equations:

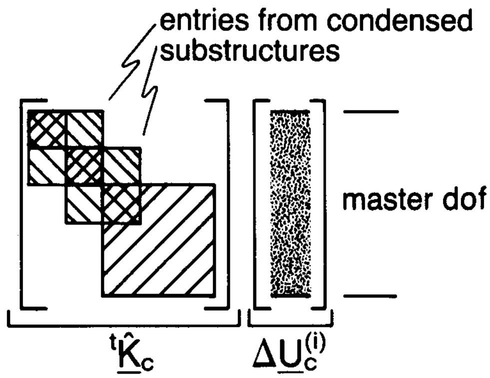

Transparency 14-10

Major steps in solution:

- Prior to step-by-step solution, establish $\hat{\underline{K}}$ for all mass and constant stiffness contributions. Statically condense out internal substructure degrees of freedom to obtain $\hat{\underline{K}}_c$.

  We note that

$$\underbrace{^{t}\hat{\underline{K}}_{c}}_{\text{condensed}} = \hat{\underline{K}}_{c} + \underbrace{^{t}\underline{K}_{\text{nonlinear}}}_{\text{all nonlinear effects}}$$

$$\text{from } \hat{\underline{K}} = \underline{K} + \frac{4}{\Delta t^2}\underline{M}$$

all linear element contributions ($\underline{K}$)

total mass matrix ($\underline{M}$)

- For each time step solution (and each equilibrium iteration):
  - Update condensed matrix, $\hat{\underline{K}}_c$, for nonlinearities.
  - Establish complete load vector for all degrees of freedom and condense out substructure internal degrees of freedom.
  - Solve for master dof displacements, velocities, accelerations and calculate all substructure dof disp., vel., acc.

    The substructure internal nodal disp., vel., acc. are needed to calculate the complete load vector (corresponding to all dof).

Transparency 14-11

Solution procedure for each time step(and iteration):

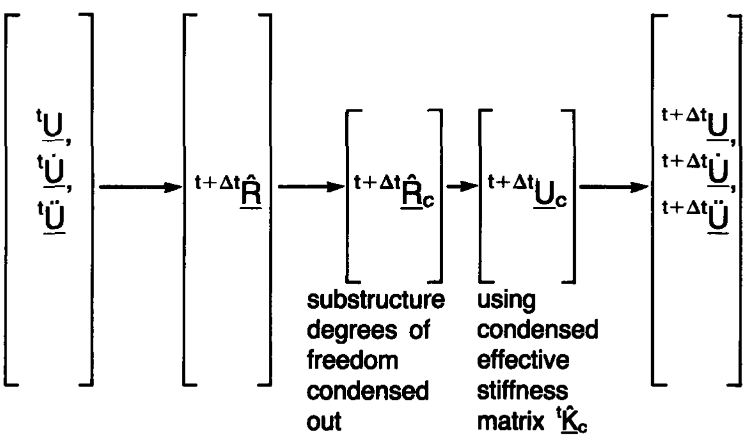

Transparency 14-12

Transparency 14-13

Example: Wave propagation in a rod

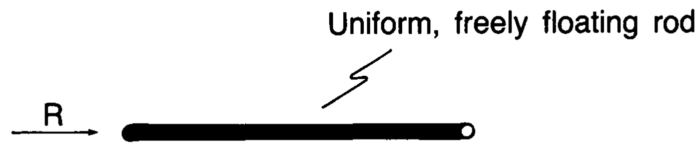

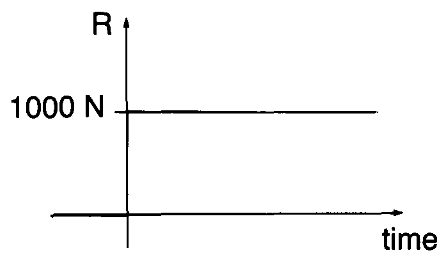

$L = 1.0$ m
$A = 0.01$ m^2
$\rho = 1000$ kg/m^3
$E = 2.0 \times 10^9$ Pa

Transparency 14-14

Consider the compressive force at a point at the center of the rod:

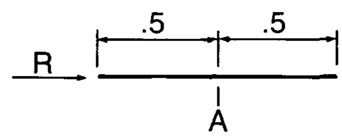

The exact solution for the force at point A is shown below.

t^* = time for stress wave to travel through the rod

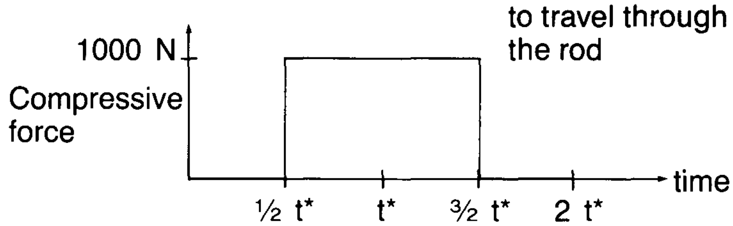

Transparency 14-15

We now use a finite element mesh of ten 2-node truss elements to obtain the compressive force at point A.

All elements uniformly spaced

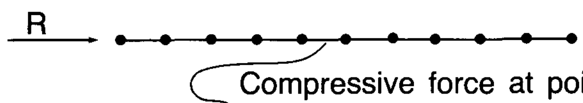

Compressive force at point A is measured using this element.

Transparency 14-16

Central difference method:

- The critical time step for this problem is

$$\Delta t_{cr} = L_e/c = t^* \left(\frac{1}{\text{number of elements}}\right)$$

  $\Delta t > \Delta t_{cr}$ will produce an unstable solution

- We need to use the inital conditions as follows:

$$\underline{M}\,{}^0\ddot{\underline{U}} + \cancelto{0}{\underline{K}\,{}^0\underline{U}} = {}^0\underline{R}$$

$$\downarrow$$

$${}^0\ddot{U}_i = \frac{{}^0R_i}{m_{ii}}$$

Transparency 14-17

- Using a time step equal to Δt_{cr}, we obtain the correct result:
  - For this special case the exact solution is obtained

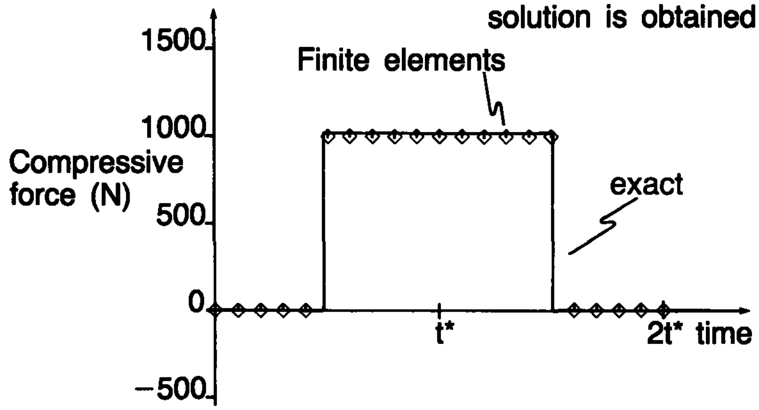

Transparency 14-18

- Using a time step equal to $\frac{1}{2}\Delta t_{cr}$, the solution is stable, but highly inaccurate.

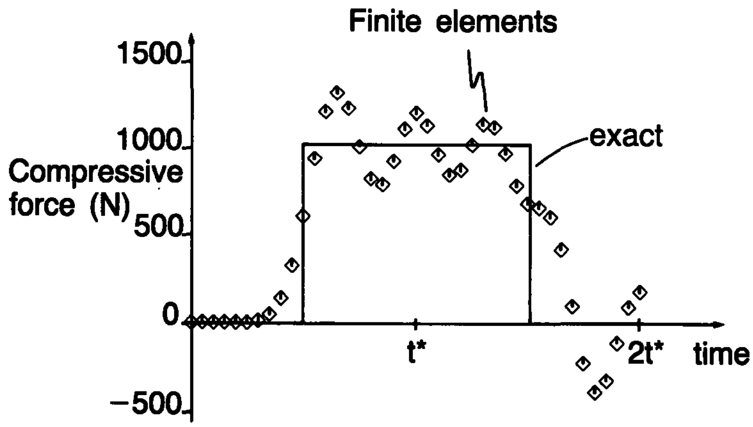

Now consider the use of the trapezoidal rule:

- A stable solution is obtained with any choice of Δt.
- Either a consistent or lumped mass matrix may be used. We employ a lumped mass matrix in this analysis.

Transparency 14-19

Trapezoidal rule, $\Delta t = \Delta t_{cr}|_{CDM}$, initial conditions computed using $\underline{M}\,{}^0\ddot{\underline{U}} = {}^0\underline{R}$.

— The solution is inaccurate.

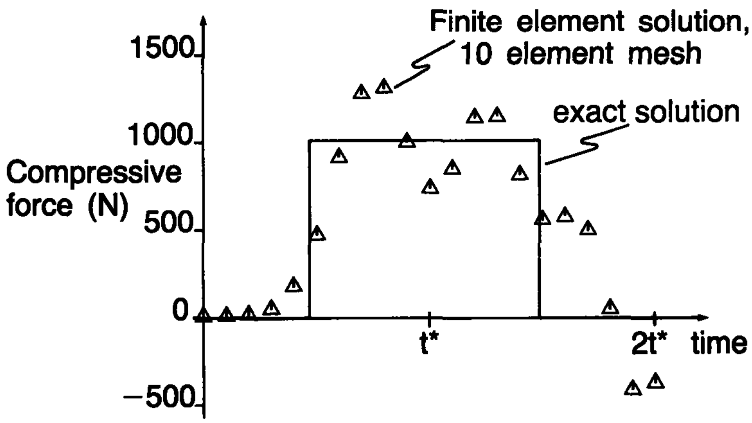

Transparency 14-20

Transparency 14-21

Trapezoidal rule, $\Delta t = \Delta t_{cr}|_{CDM}$, zero initial conditions.

— Almost same solution is obtained.

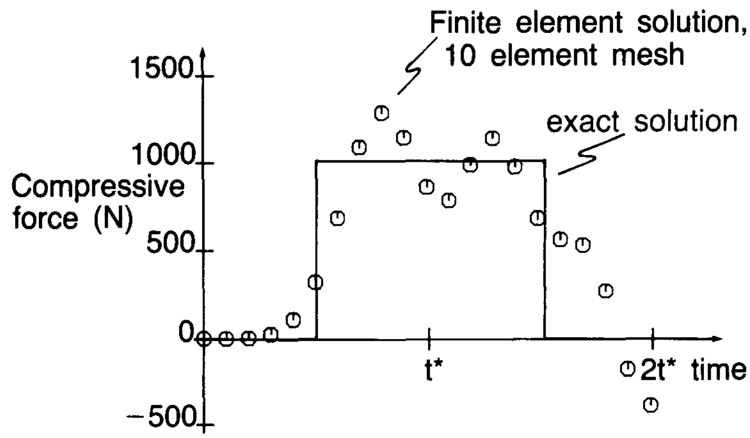

Transparency 14-22

Trapezoidal rule, $\Delta t = 2\Delta t_{cr}|_{CDM}$

— The solution is stable, although inaccurate.

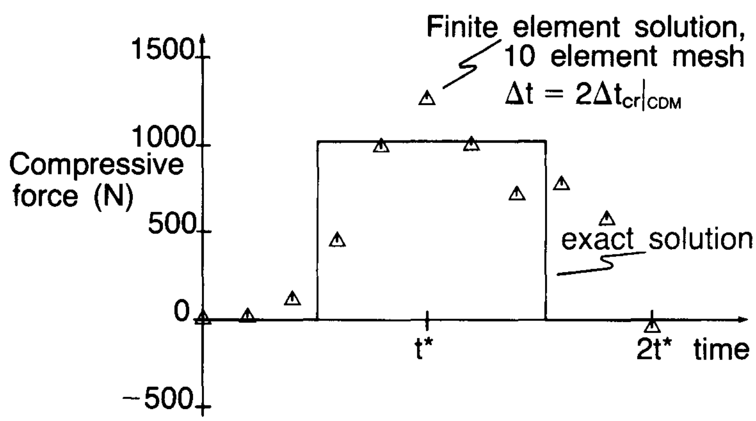

Trapezoidal rule, $\Delta t = \frac{1}{2}\, \Delta t_{cr}|_{CDM}$

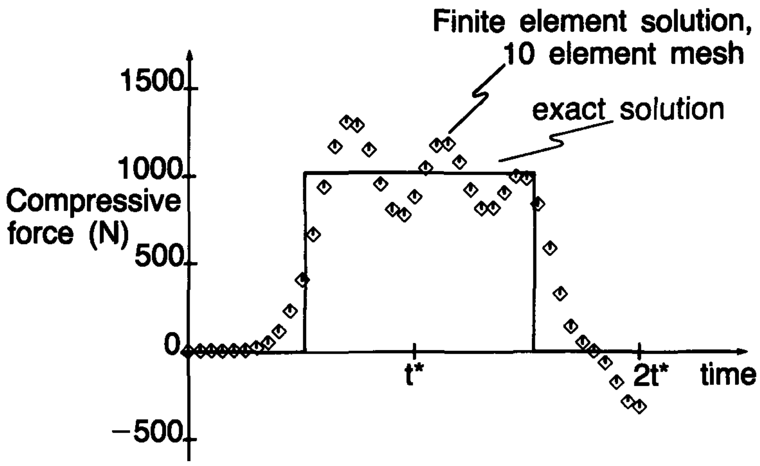

Transparency 14-23

The same phenomena are observed when a mesh of one hundred 2-node truss elements is employed.

— Here $\Delta t_{cr} = t^*/100$

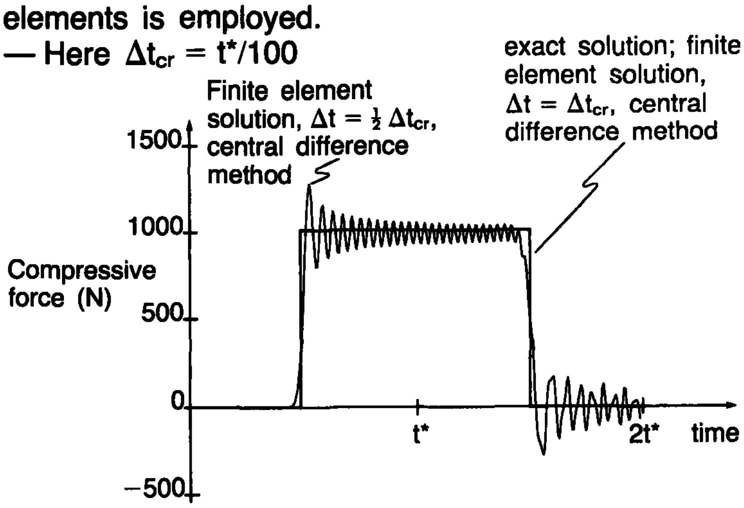

Transparency 14-24

Transparency 14-25

Trapezoidal rule, $\Delta t = \Delta t_{cr}|_{CDM}$

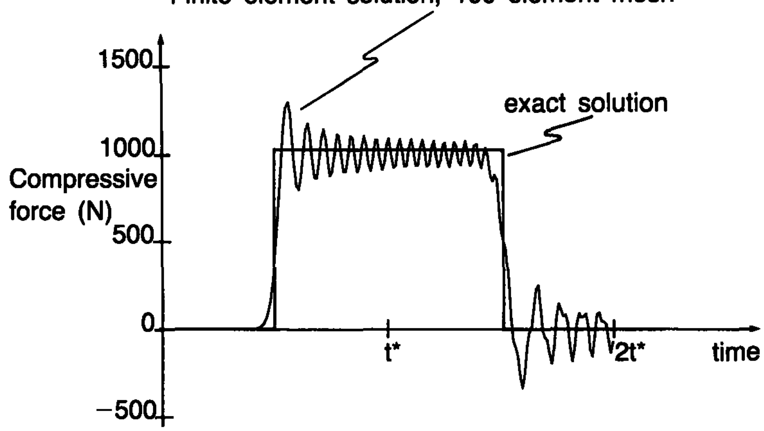

Transparency 14-26

Now consider a two-dimensional model of the rod:

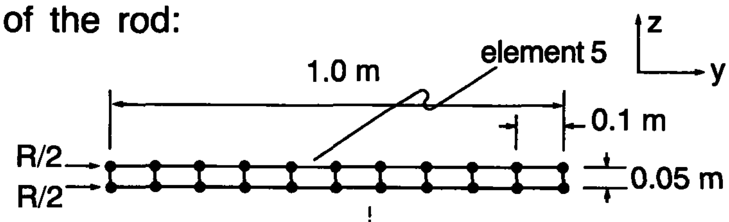

thickness = 0.2 m
$E = 2 \times 10^9$ Pa
$\nu = 0$
$\rho = 1000$ kg/m^3

Central difference method is employed

For this mesh, $\Delta t_{cr} \neq t^*/(10 \text{ elements})$ because the element width is less than the element length.

Transparency 14-27

If $\Delta t = t^*/(10 \text{ elements})$ is used, the solution diverges

— In element 5,

$$|\tau_{zz}| > \left(\frac{1000\,N}{0.01\,m^2}\right)$$

at $t = 1.9\,t^*$

Transparency 14-28

Example: Dynamic response of three degree-of-freedom system using central difference method

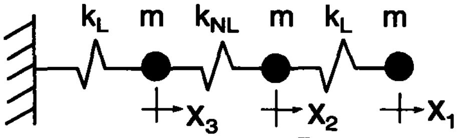

$k_L = 1$ lbf/ft
$m = 1$ slug

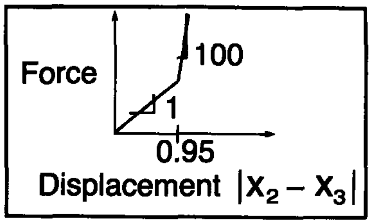

${}^0x_1 = {}^0x_2 = {}^0x_3 = 0$

${}^0\dot{x}_1 = 0.555$ ft/sec
${}^0\dot{x}_2 = 1.000$ ft/sec
${}^0\dot{x}_3 = 1.247$ ft/sec

$(\Delta t_{crit})_{linear} = 1.11$ sec
$(\Delta t_{crit})_{nonlinear} = 0.14$ sec

Transparency 14-29

Results: Response of right mass

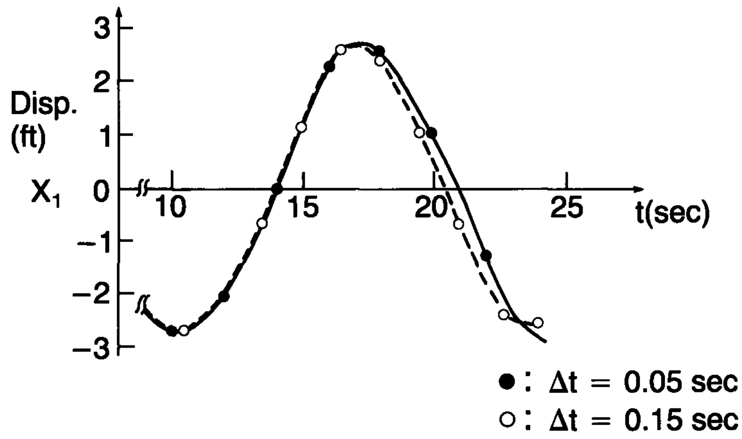

Transparency 14-30

Response of center mass:

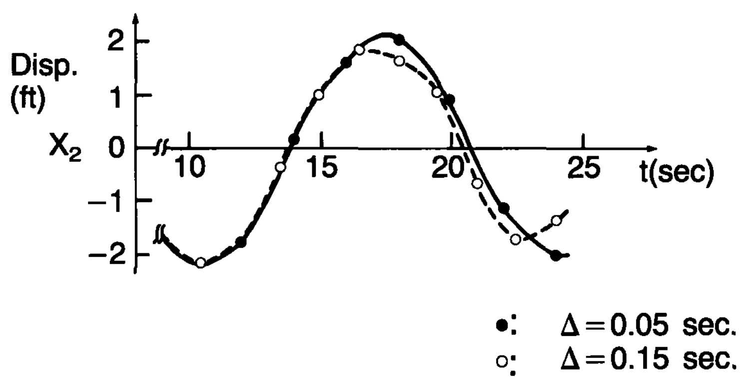

Response of left mass:

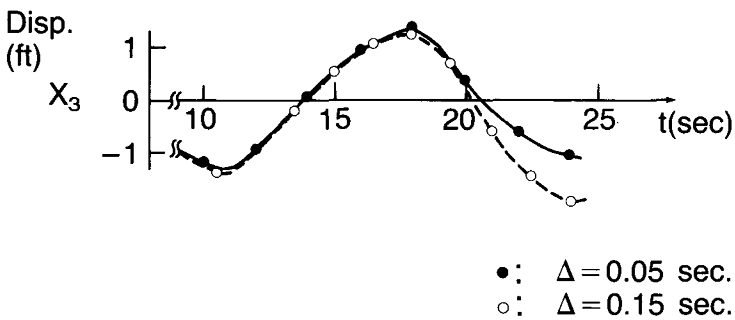

Transparency 14-31

Force (lbf) in center truss:

TIME	Δt=0.05	Δt=0.15
9.0	−0.666	−0.700
12.0	−0.804	−0.877
15.0	0.504	0.503
18.0	0.648	−0.100
21.0	−0.132	−0.059
24.0	−0.922	0.550

Transparency 14-32

Transparency 14-33

Example: 10 story tapered tower

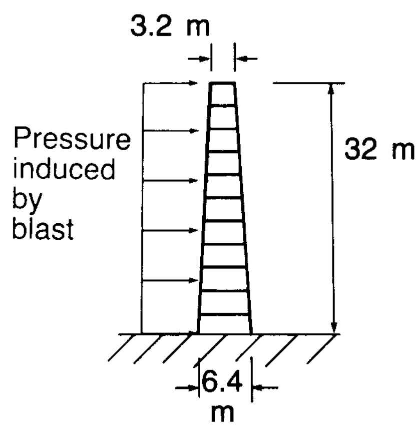

Girder properties:
$E = 2.07 \times 10^{11}$ Pa
$\nu = 0.3$
$A = 0.01\ m^2$
$A_s = 0.009\ m^2$
$I = 8.33 \times 10^{-5}\ m^4$
$\rho = 7800\ kg/m^3$

Transparency 14-34

Applied load (blast):

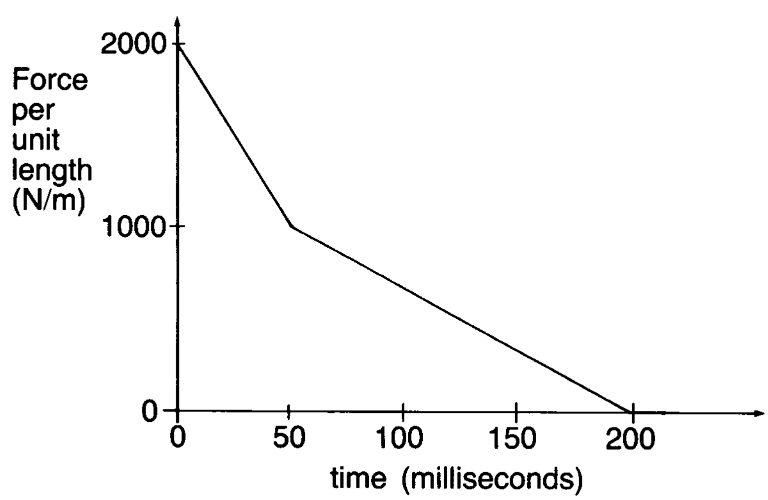

Purpose of analysis:

- Determine displacements, velocities at top of tower.
- Determine moments at base of tower.

We use the trapezoidal rule and a lumped mass matrix in the following analysis.

Transparency 14-35

We must make two decisions:

- Choose mesh (specifically the number of elements employed).
- Choose time step Δt.

These two choices are closely related:

The mesh and time step to be used depend on the loading applied.

Transparency 14-36

Transparency 14-37

Some observations:

- The choice of mesh determines the highest natural frequency (and corresponding mode shape) that is accurately represented in the finite element analysis.
- The choice of time step determines the highest frequency of the finite element mesh in which the response is accurately integrated during the time integration.

Transparency 14-38

- Hence, it is most effective to choose the mesh and time step such that the highest frequency accurately "integrated" is equal to the highest frequency accurately represented by the mesh.
- The applied loading can be represented as a Fourier series which displays the important frequencies to be accurately represented by the mesh.

Consider the Fourier representation of the load function:

$$f(t) = \frac{a_0}{2} + \sum_{n=1}^{\infty}(a_n \cos(2\pi f_n t) + b_n \sin(2\pi f_n t))$$

Including terms up to

case 1: $f_n = 17$ Hz

case 2: $f_n = 30$ Hz

The loading function is represented as shown next.

Transparency 14-39

Fourier approximation including terms up to 17 Hz:

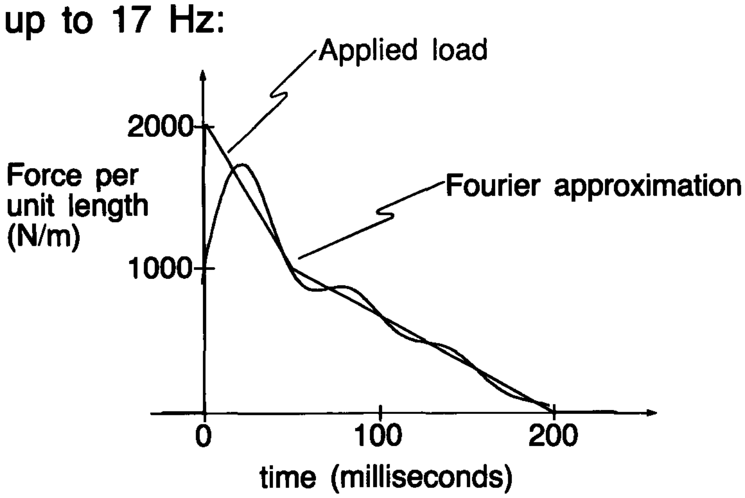

Transparency 14-40

Transparency 14-41

Fourier approximation including terms up to 30 Hz:

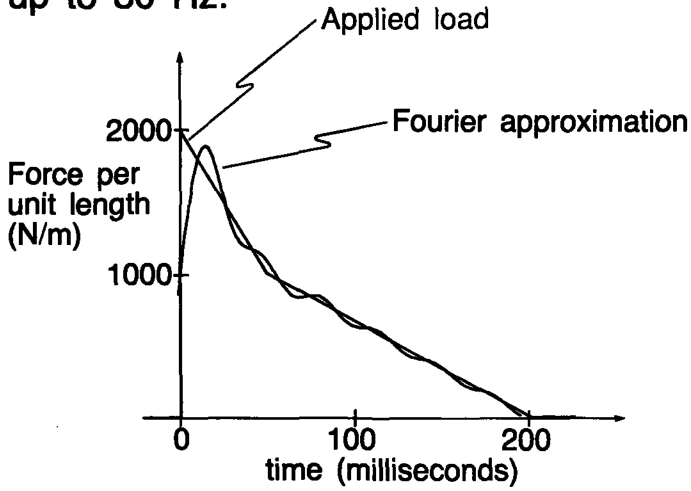

Transparency 14-42

- We choose a 30 element mesh, a 60 element mesh and a 120 element mesh. All elements are 2-node Hermitian beam elements.

30 elements	60 elements	120 elements

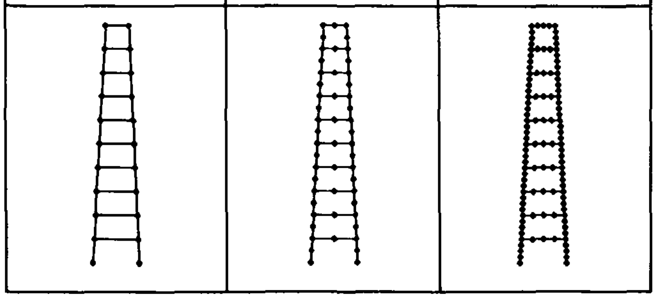

Determine "accurate" natural frequencies represented by 30 element mesh:

From eigenvalue solutions of the 30 and 60 element meshes, we find

mode number	natural frequencies (Hz)	
	30 element mesh	60 element mesh
1	1.914	1.914
2	4.815	4.828
3	8.416	8.480
4	12.38	12.58
5	16.79	17.27
6	21.45	22.47
7	26.18	28.08
8	30.56	29.80

accurate

inaccurate

Transparency 14-43

Calculate time step:

$$T_{co} = \frac{1}{17\,\text{Hz}} = .059 \text{ sec}$$

$$\Delta t \doteq \frac{1}{20} T_{co} = .003 \text{ sec}$$

- A smaller time step would accurately "integrate" frequencies, which are not accurately represented by the mesh.
- A larger time time step would not accurately "integrate" all frequencies which are accurately represented by the mesh.

Transparency 14-44

Transparency 14-45

Determine "accurate" natural frequencies represented by 60 element mesh:

From eigenvalue solutions of the 60 and 120 element meshes, we find

mode number	natural frequencies (Hz)	
	60 element mesh	120 element mesh
5	17.27	17.28
6	22.47	22.49
7	28.08	28.14
8	29.80	29.75
9	32.73	33.85
10	33.73	35.06
11	36.30	38.96

accurate (modes 5–8) ↔ inaccurate (modes 9–11)

Transparency 14-46

Calculate time step:

$$T_{co} = \frac{1}{30}\,\text{Hz} = .033 \text{ sec}$$

$$\Delta t \doteq \frac{1}{20} T_{co} = .0017 \text{ sec}$$

- The meshes chosen correspond to the Fourier approximations discussed earlier:

30 element mesh ⟷ Fourier approximation including terms up to 17 Hz.

60 element mesh ⟷ Fourier approximation including terms up to 30 Hz.

Pictorially, at time 200 milliseconds, we have (note that the displacements are amplified for visibility):

30 elements	60 elements
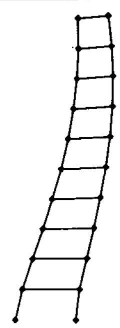	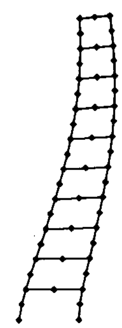

Transparency 14-47

Pictorially, at time 400 milliseconds, we have (note that the displacements are amplified for visibility):

30 elements	60 elements
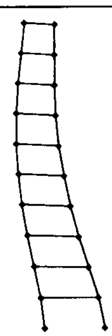	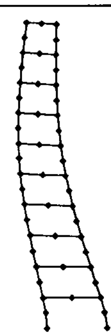

Transparency 14-48

Transparency 14-49

Consider the moment reaction at the base of the tower:

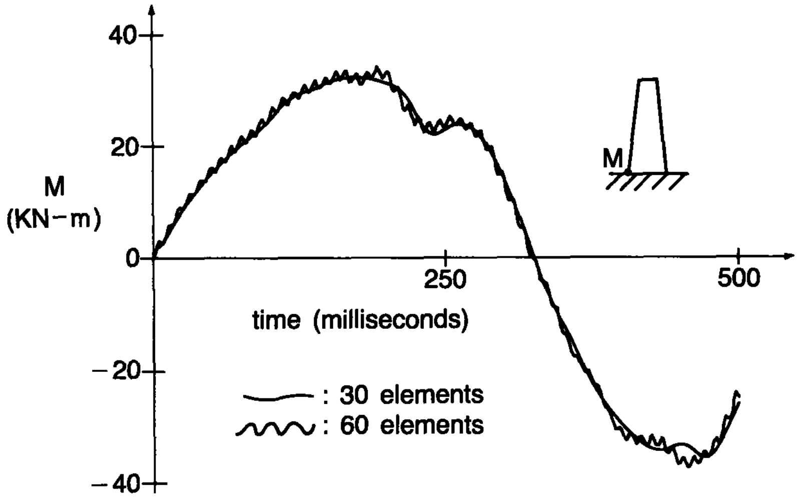

Transparency 14-50

Consider the horizontal displacement at the top of the tower:

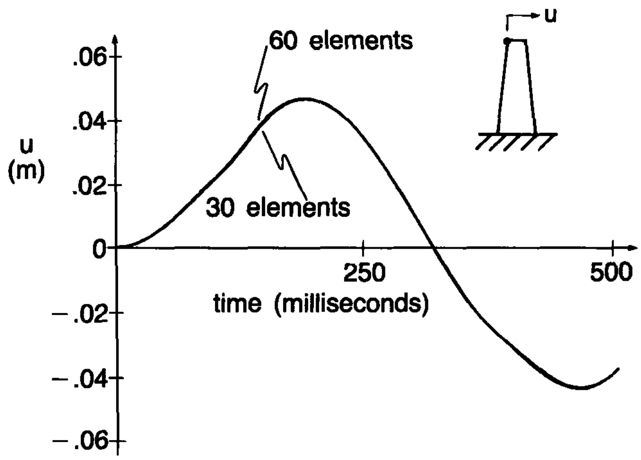

Consider the horizontal velocity at the top of the tower:

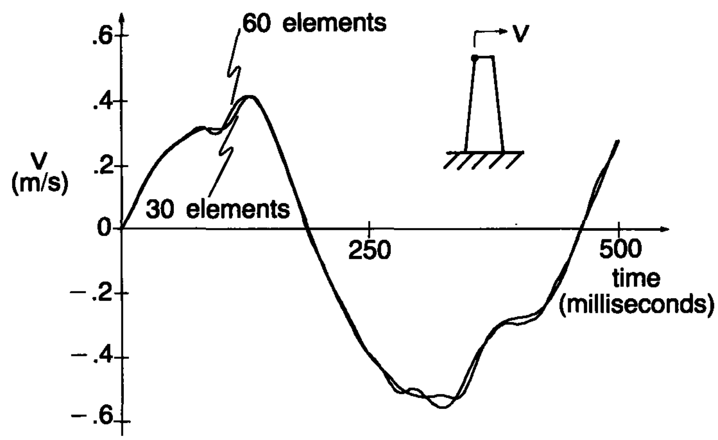

Transparency 14-51

Comments:

- The high-frequency oscillation observed in the moment reaction from the 60 element mesh is probably inaccurate. We note that the frequency of the oscillation is about 110 Hz (this can be seen directly from the graph).
- The obtained solutions for the horizontal displacement at the top of the tower are virtually identical.

Transparency 14-52

Transparency 14-53

Example: Simple pendulum undergoing large displacements

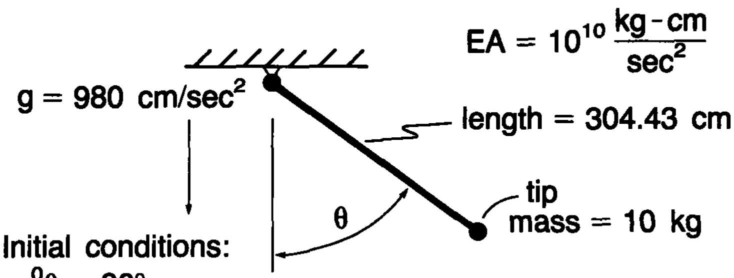

Initial conditions:
${}^{0}\theta = 90°$
${}^{0}\dot{\theta} = 0$

One truss element with tip concentrated mass is employed.

Transparency 14-54

Calculation of dynamic response:

- The trapezoidal rule is used to integrate the time response.
- Full Newton iterations are used to reestablish equilibrium during every time step.
- Convergence tolerance:
  $ETOL = 10^{-7}$
  (a tight tolerance)

Choose $\Delta t = 0.1$ sec. The following response is obtained:

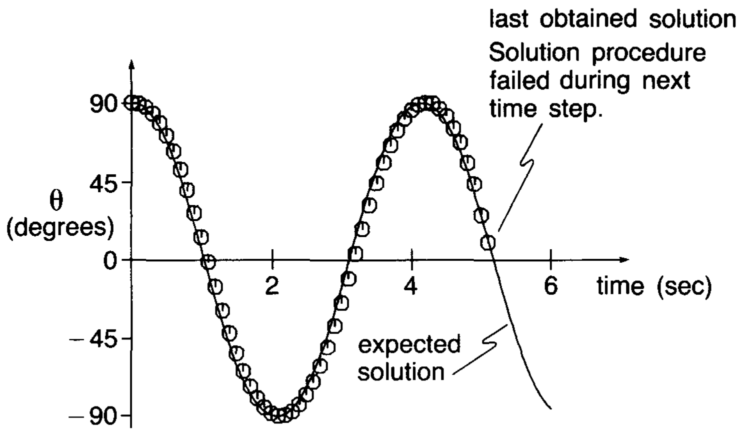

Transparency 14-55

The strain in the truss is plotted:

- An instability is observed.

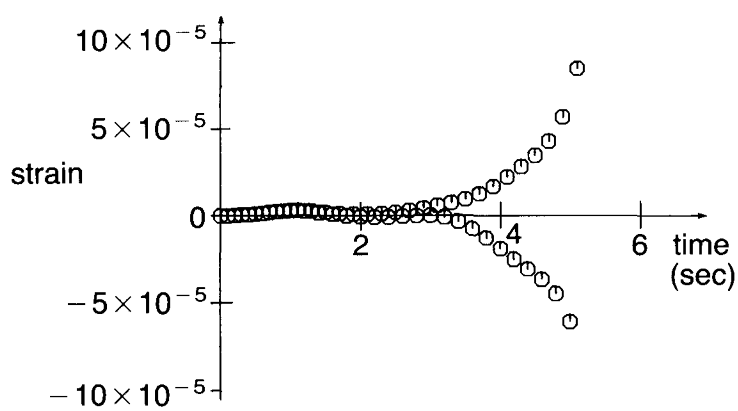

Transparency 14-56

Transparency 14-57

- The instability is unchanged when we tighten our convergence tolerances.
- The instability is also observed when the BFGS algorithm is employed.
- Recall that the trapezoidal rule is unconditionally stable only in linear analysis.

Transparency 14-58

Choose $\Delta t = 0.025$ sec, using the original tolerance and the full Newton algorithm (without line searches).

- The analysis runs to completion.

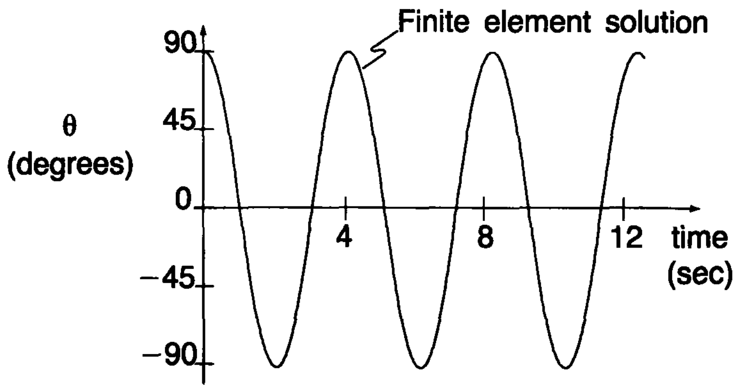

The strain in the truss is stable:

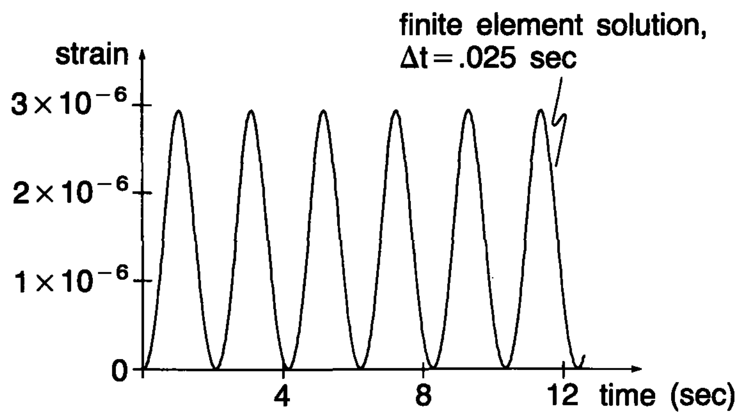

Transparency 14-59

It is important that equilibrium be accurately satisfied at the end of each time step:

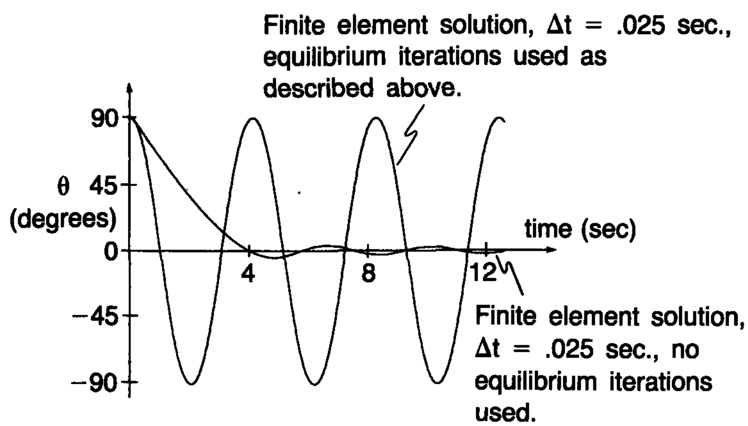

Transparency 14-60

Transparency 14-61

Although the solution obtained without equilibrium iterations is highly inaccurate, the solution is stable:

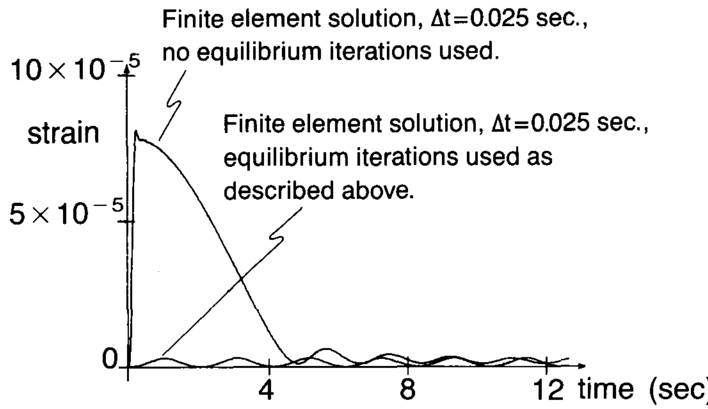

Transparency 14-62

Example: Pipe whip analysis:

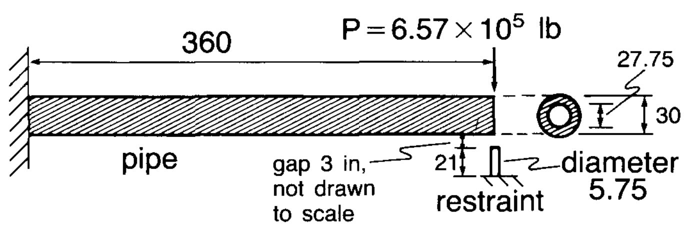

all dimensions in inches

- Determine the transient response when a step load P is suddenly applied.

Finite element model:

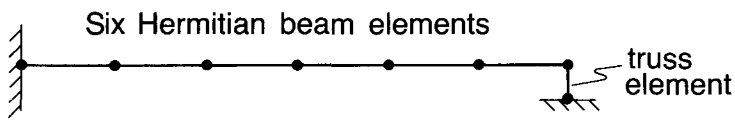

- The truss element incorporates a 3 inch gap.

Transparency 14-63

Material properties:

Pipe: $E = 2.698 \times 10^7$ psi
$\nu = 0.3$
$\sigma_y = 2.914 \times 10^4$ psi
$E_T = 0$
$\rho = 8.62 \times 10^{-3} \dfrac{\text{slug}}{\text{in}^3} = 7.18 \times 10^{-4} \dfrac{\text{lbf-sec}^2}{\text{in}^4}$

Restraint: $E = 2.99 \times 10^7$ psi
$\sigma_y = 3.80 \times 10^4$ psi
$E_T = 0$

Transparency 14-64

Transparency 14-65

The analysis is performed using

— Mode superposition (2 modes)

— Direct time integration

We use, for each analysis,

— Trapezoidal rule

— Consistent mass matrix

A convergence tolerance of ETOL $= 10^{-7}$ is employed.

Transparency 14-66

Eigenvalue solution:

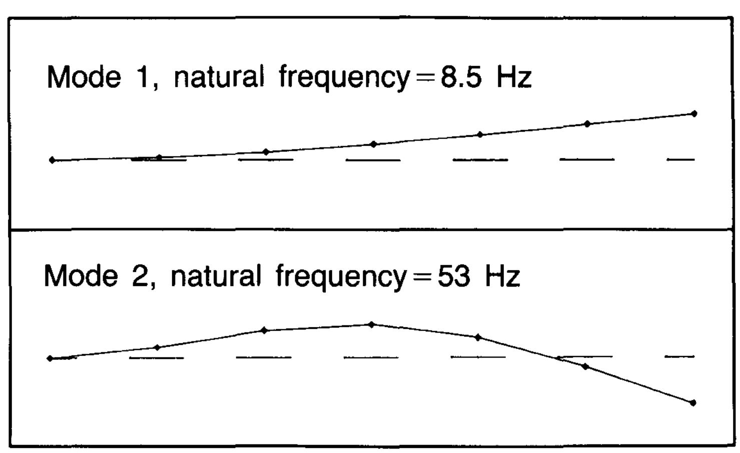

Transparency 14-67

Choice of time step:

We want to accurately integrate the first two modes:

$$\Delta t \doteq \frac{1}{20}\, T_{co} = \frac{1}{20}\left(\frac{1}{\text{(frequency of mode 2)}}\right)$$

$= .001$ sec

Note: This estimate is based solely on a linear analysis (i.e, before the pipe hits the restraint and while the pipe is still elastic).

Transparency 14-68

Determine the tip displacement:

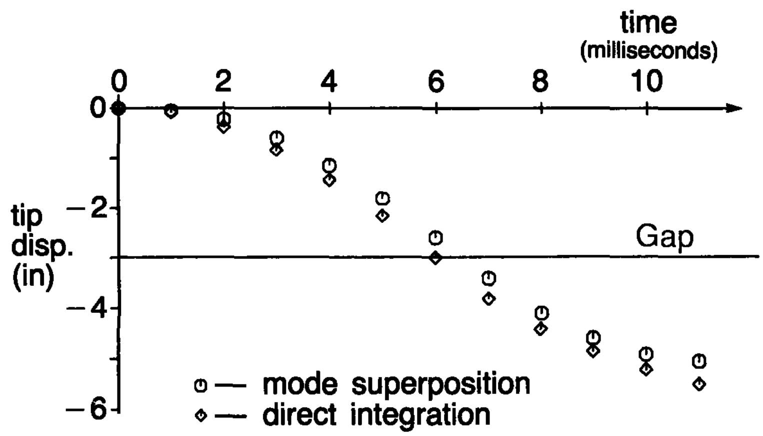

Transparency 14-69

Determine the moment at the built-in end of the beam:

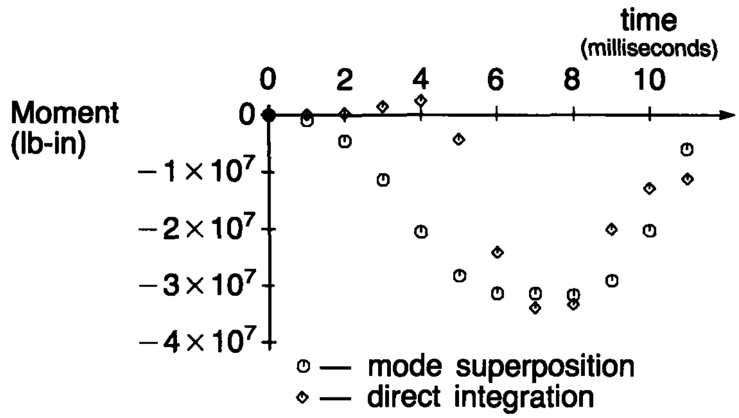

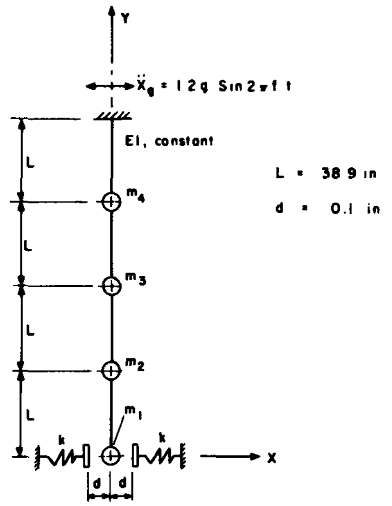

Analysis of CRD housing with lower support

Slide 14-1

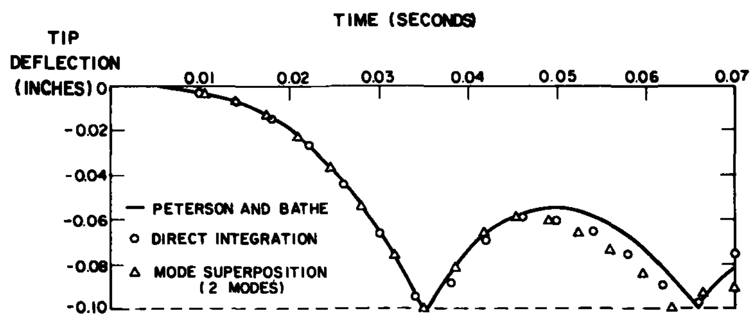

CRD housing tip deflection

Slide 14-2

Slide 14-3

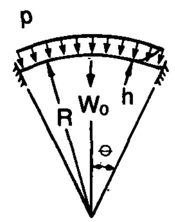

R = 22.27 in.
h = 0.41 in.
θ = 26.67°

E = 1.05×10^7 lb/in^2
$\nu = 0.3$
$\sigma_y = 2.4 \times 10^4$ lb/in^2
$E_T = 2.1 \times 10^5$ lb/in^2
$\rho = 9.8 \times 10^{-2}$ lb/in^3

Ten 8-node axisymmetric els.
Newmark inte ($\delta = 0.55$, $\alpha = 0.276$)
2×2 Gauss integration
consistent mass
$\Delta t = 10 \mu$sec, T.L.

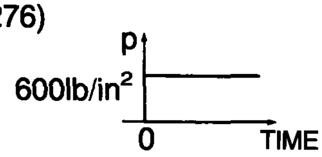

Spherical cap nodes under uniform pressure loading

Slide 14-4

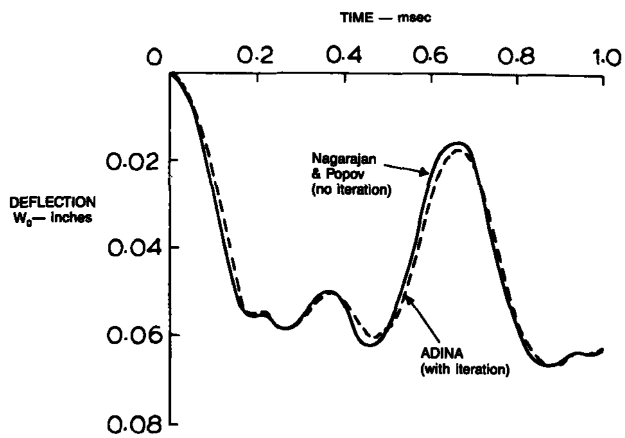

Dynamic elastic–plastic response of a spherical cap, p deformation independent

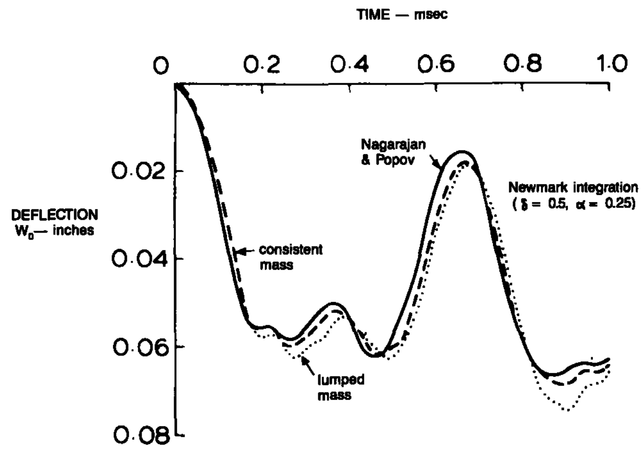

Response of the cap using consistent and lumped mass idealization

Slide 14-5

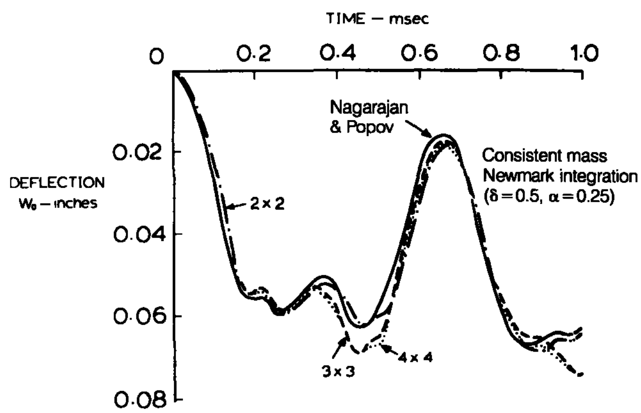

Effect of numbers of Gauss integration points on the cap response predicted

Slide 14-6

Slide 14-7

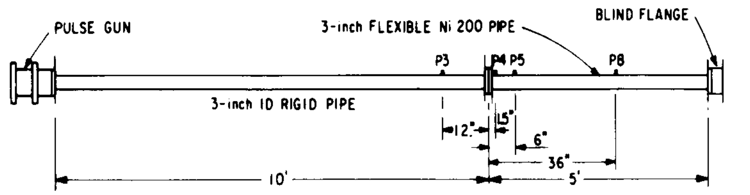

NICKEL 200

$E = 30 \times 10^6$ PSI

$E_T = 73.7 \times 10^4$ PSI

$\nu = 0.30$

$\rho = 8.31 \times 10^{-4} \frac{\text{SLUG-FT}}{\text{IN}^4}$

$\sigma_0 = 12.8 \times 10^3$ PSI

WATER

$\kappa = 32 \times 10^4$ PSI

$\rho = 9.36 \times 10^{-5} \frac{\text{SLUG-FT}}{\text{IN}^4}$

Analysis of fluid—structure interaction problem (pipe test)

Slide 14-8

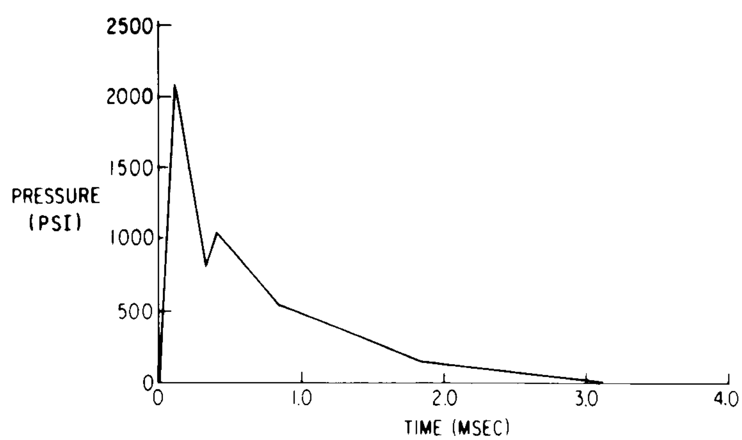

PRESSURE PULSE INPUT

Slide 14-9

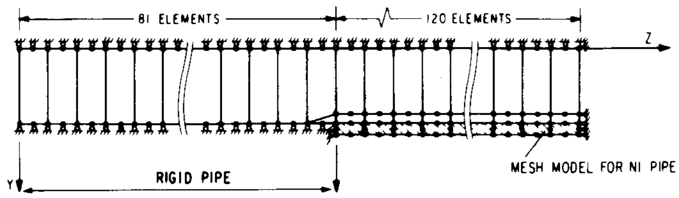

Finite element model

Slide 14-10

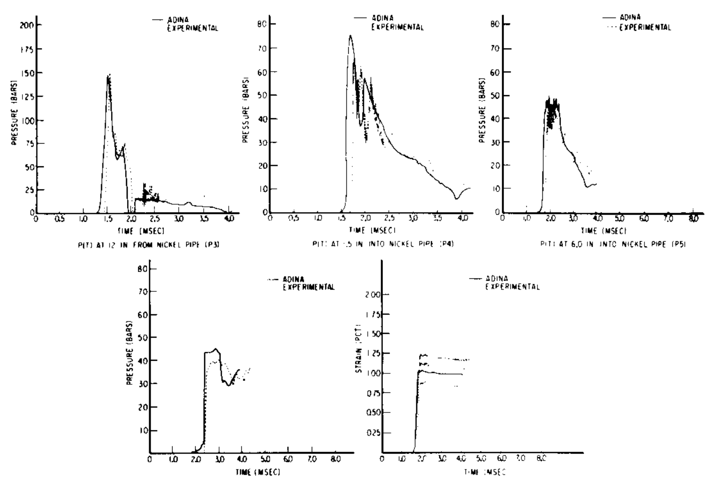

Topic 15

Use of Elastic Constitutive Relations in Total Lagrangian Formulation

Contents:

- **Basic considerations in modeling material response**
- **Linear and nonlinear elasticity**
- **Isotropic and orthotropic materials**
- **One-dimensional example, large strain conditions**
- **The case of large displacement/small strain analysis, discussion of effectiveness using the total Lagrangian formulation**
- **Hyperelastic material model (Mooney-Rivlin) for analysis of rubber-type materials**
- **Example analysis: Solution of a rubber tensile test specimen**
- **Example analysis: Solution of a rubber sheet with a hole**

Textbook: 6.4, 6.4.1

Reference: The solution of the rubber sheet with a hole is given in

Bathe, K. J., E. Ramm, and E. L. Wilson, "Finite Element Formulations for Large Deformation Dynamic Analysis," *International Journal for Numerical Methods in Engineering, 9,* 353–386, 1975.

USE OF CONSTITUTIVE RELATIONS

Transparency 15-1

- We developed quite general kinematic relations and finite element discretizations, applicable to small or large deformations.
- To use these finite element formulations, appropriate constitutive relations must be employed.
- Schematically

$$\underline{K} = \int_V \underline{B}^T \underline{C}\, \underline{B}\, dV, \qquad \underline{F} = \int_V \underline{B}^T \underline{\tau}\, dV$$

constitutive relations enter here

Transparency 15-2

For analysis, it is convenient to use the classifications regarding the magnitude of deformations introduced earlier:

- Infinitesimally small displacements
- Large displacements / large rotations, but small strains
- Large displacements / large rotations, and large strains

The applicability of material descriptions generally falls also into these categories.

Transparency 15-3

Recall:

- Materially-nonlinear-only (M.N.O.) analysis assumes (models only) infinitesimally small displacements.
- The total Lagrangian (T.L.) and updated Lagrangian (U.L.) formulations can be employed for analysis of infinitesimally small displacements, of large displacements and of large strains (considering the analysis of 2-D and 3-D solids).

→ All kinematic nonlinearities are fully included.

Transparency 15-4

We may use various material descriptions:

Material Model	Examples
Elastic	Almost all materials, for small enough stresses
Hyperelastic	Rubber
Hypoelastic	Concrete
Elastic-plastic	Metals, soils, rocks under high stresses
Creep	Metals at high temperatures
Viscoplastic	Polymers, metals

Transparency
15-5

ELASTIC MATERIAL BEHAVIOR:

In linear, infinitesimal displacement, small strain analysis, we are used to employing

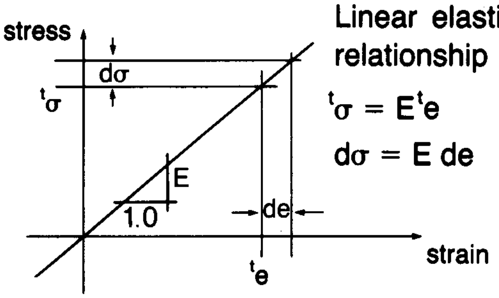

Linear elastic stress-strain relationship

$${}^t\sigma = E\,{}^te$$

$$d\sigma = E\,de$$

Transparency
15-6

For 1-D nonlinear analysis we can use

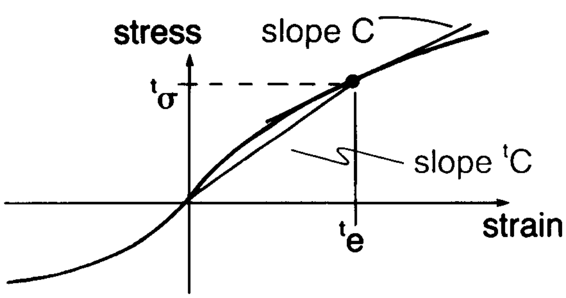

Nonlinear elastic stress-strain relationship

$${}^t\sigma = {}^tC\,{}^te$$

not constant

$$d\sigma = C\,de$$

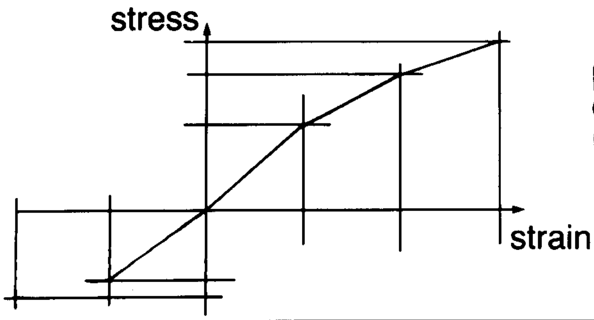

In practice, a piecewise linear description is used

Transparency 15-7

We can generalize the elastic material behavior using:

$$ {}_0^t S_{ij} = {}_0^t C_{ijrs}\, {}_0^t \varepsilon_{rs} $$

$$ d_0 S_{ij} = {}_0 C_{ijrs}\, d_0 \varepsilon_{rs} $$

This material description is frequently employed with

- the usual constant material moduli used in infinitesimal displacement analysis
- rubber-type materials

Transparency 15-8

Use of constant material moduli, for an isotropic material:

$$ {}_0^t C_{ijrs} = {}_0 C_{ijrs} = \lambda\, \delta_{ij}\, \delta_{rs} + \mu(\delta_{ir}\, \delta_{js} + \delta_{is}\, \delta_{jr}) $$

Lamé constants:

$$ \lambda = \frac{E\nu}{(1+\nu)(1-2\nu)}\ , \quad \mu = \frac{E}{2(1+\nu)} $$

Kronecker delta:

$$ \delta_{ij} = \begin{cases} 0; & i \neq j \\ 1; & i = j \end{cases} $$

Transparency 15-9

<u>Examples</u>:

2-D plane stress analysis:

$$
{}_0\underline{C} = \frac{E}{1-\nu^2}\left[\begin{array}{cc|c} 1 & \nu & 0 \\ \nu & 1 & 0 \\ \hline 0 & 0 & \dfrac{1-\nu}{2} \end{array}\right]
$$

corresponds to ${}^t_0S_{12} = \mu\,({}^t_0\varepsilon_{12} + {}^t_0\varepsilon_{21})$

Transparency 15-10

2-D axisymmetric analysis:

$$
\underline{C} = \frac{E(1-\nu)}{(1+\nu)(1-2\nu)}\begin{bmatrix} 1 & \dfrac{\nu}{1-\nu} & 0 & \dfrac{\nu}{1-\nu} \\ \dfrac{\nu}{1-\nu} & 1 & 0 & \dfrac{\nu}{1-\nu} \\ 0 & 0 & \dfrac{1-2\nu}{2(1-\nu)} & 0 \\ \dfrac{\nu}{1-\nu} & \dfrac{\nu}{1-\nu} & 0 & 1 \end{bmatrix}
$$

Transparency 15-11

For an orthotropic material, we also use the usual constant material moduli:

Example: 2-D plane stress analysis

local coordinate system a-b

$$ {}_{0}C_{\ell}^{-1} = \begin{bmatrix} \dfrac{1}{E_a} & -\dfrac{\nu_{ab}}{E_b} & 0 \\ & \dfrac{1}{E_b} & 0 \\ \text{sym.} & & \dfrac{1}{G_{ab}} \end{bmatrix} $$

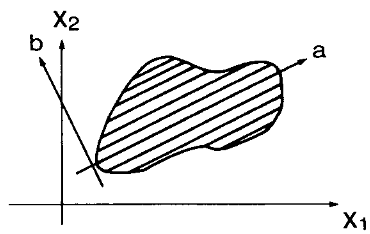

$E_a \neq E_b$

Transparency 15-12

Sample analysis: One-dimensional problem:

Material constants E, ν

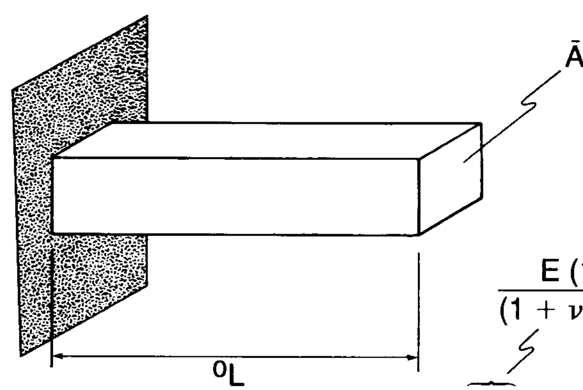

$$\frac{E\,(1-\nu)}{(1+\nu)(1-2\nu)}$$

Constitutive relation: ${}_{0}^{t}S_{11} = \tilde{E}\; {}_{0}^{t}\varepsilon_{11}$

Transparency 15-13

Sample analysis: One-dimensional problem:

Material constants E, ν

In tension:

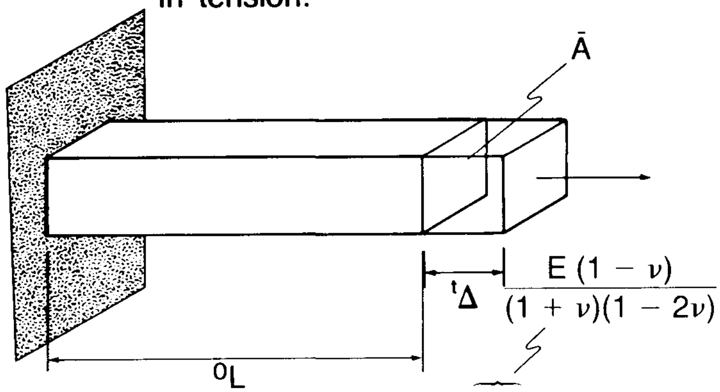

Constitutive relation: ${}_{0}^{t}S_{11} = \tilde{E}\ {}_{0}^{t}\varepsilon_{11}$

Transparency 15-14

Sample analysis: One-dimensional problem:

Material constants E, ν

In tension:

In compression:

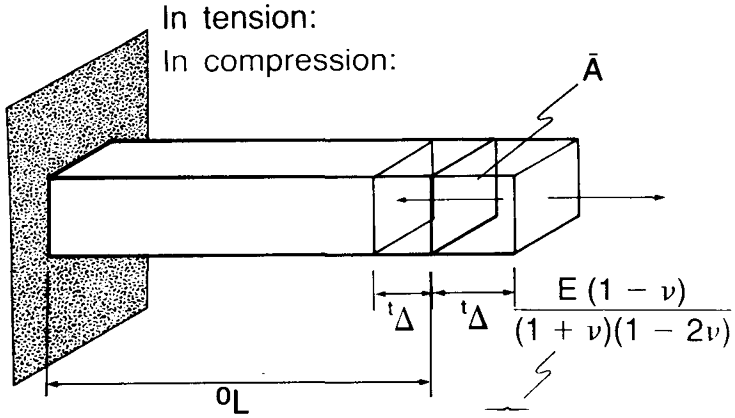

Constitutive relation: ${}_{0}^{t}S_{11} = \tilde{E}\ {}_{0}^{t}\varepsilon_{11}$

Transparency 15-15

We establish the force-displacement relationship:

$$ {}_0^t\varepsilon_{11} = \underbrace{{}_0^t u_{1,1}}_{\frac{{}^tL - {}^0L}{{}^0L}} + \frac{1}{2}\left({}_0^t u_{1,1}\right)^2 $$

$$ = \frac{1}{2}\left[\left(\frac{{}^tL}{{}^0L}\right)^2 - 1\right], $$

$$ {}_0^t S_{11} = \frac{{}^0\rho}{{}^t\rho}\, {}_t^0x_{1,1}\, {}^t\tau_{11}\, {}_t^0x_{1,1} $$

$$ = \frac{{}^tL}{{}^0L}\left(\frac{{}^0L}{{}^tL}\right)\frac{{}^tP}{\bar{A}}\left(\frac{{}^0L}{{}^tL}\right) = \frac{{}^0L}{{}^tL}\,\frac{{}^tP}{\bar{A}} $$

Transparency 15-16

Using ${}^tL = {}^0L + {}^t\Delta$, ${}_0^tS_{11} = \tilde{E}\,{}_0^t\varepsilon_{11}$, we find

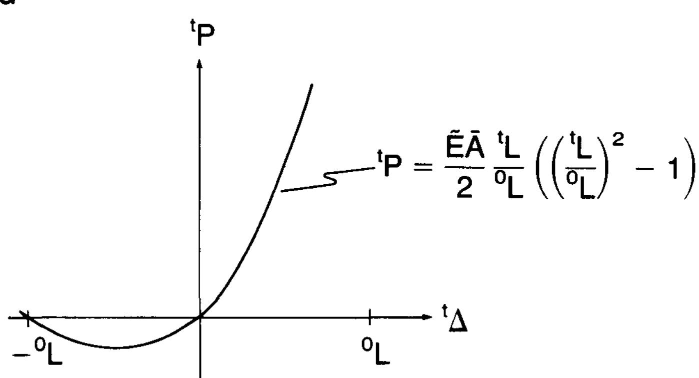

This is not a realistic material description for large strains.

- The usual isotropic and orthotropic material relationships (constant E, ν, E_a, etc.) are mostly employed in large displacement/large rotation, but small strain analysis.
- Recall that the components of the 2nd Piola-Kirchhoff stress tensor and of the Green-Lagrange strain tensor are invariant under a rigid body motion (rotation) of the material.

Transparency 15-17

— Hence only the actual straining increases the components of the Green-Lagrange strain tensor and, through the material relationship, the components of the 2nd Piola-Kirchhoff stress tensor.

— The effect of rotating the material is included in the T.L. formulation,

$$ {}_0^t\underline{F} = \int_{{}^0V} \underbrace{{}_0^t\underline{B}_L^T}_{\text{includes rotation}} \; \underbrace{{}_0^t\hat{\underline{S}}}_{\text{invariant under a rigid body rotation}} \, {}^0dV $$

Transparency 15-18

Transparency 15-19

Pictorially:

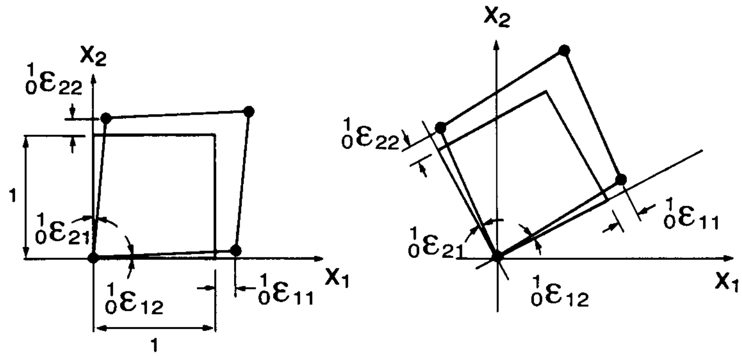

Deformation to state 1 (small strain situation) | Rigid rotation from state 1 to state 2

Transparency 15-20

For small strains,

$${}^1_0\varepsilon_{11}\ ,\ {}^1_0\varepsilon_{22}\ ,\ {}^1_0\varepsilon_{12} = {}^1_0\varepsilon_{21} << 1,$$

$${}^1_0S_{ij} = \underbrace{{}^1_0C_{ijrs}}_{\text{a function of } E,\ \nu}\ {}^1_0\varepsilon_{rs},$$

$${}^1_0S_{ij} \doteq {}^1\tau_{ij}$$

Also, since state 2 is reached by a rigid body rotation,

$${}^2_0\varepsilon_{ij} = {}^1_0\varepsilon_{ij}\ ,\ {}^2_0S_{ij} = {}^1_0S_{ij},$$

$${}^2\underline{\tau} = \underbrace{\underline{R}}_{\text{rotation matrix}}\ {}^1\underline{\tau}\ \underline{R}^T$$

Applications:

- Large displacement / large rotation but small strain analysis of beams, plates and shells. These can frequently be modeled using 2-D or 3-D elements. Actual beam and shell elements will be discussed later.
- Linearized buckling analysis of structures.

Transparency 15-21

Frame analysis:

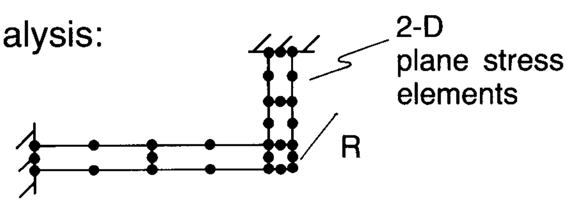

Axisymmetric shell:

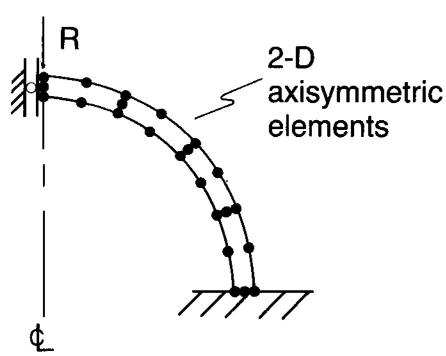

Transparency 15-22

Transparency 15-23

General shell:

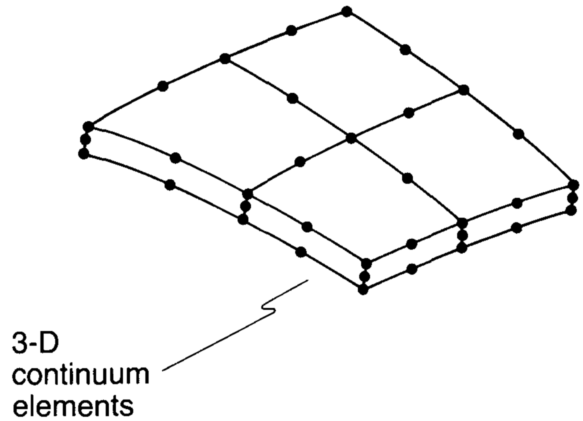

Transparency 15-24

Hyperelastic material model:
formulation of rubber-type materials

$$ {}^t_0S_{ij} = \underbrace{\frac{\partial\, {}^t_0W}{\partial\, {}^t_0\varepsilon_{ij}}}_{{}^t_0C_{ijrs}\,{}^t_0\varepsilon_{rs}} $$

$$ d_0S_{ij} = \underbrace{{}_0C_{ijrs}}_{\frac{\partial^2\, {}^t_0W}{\partial\, {}^t_0\varepsilon_{ij}\,\partial\, {}^t_0\varepsilon_{rs}}}\, d_0\varepsilon_{rs} $$

where

${}^t_0W$ = strain energy density function (per unit original volume)

Rubber is assumed to be an isotropic material, hence

$$ {}_0^tW = \text{function of } (I_1, I_2, I_3) $$

where the I_i's are the invariants of the Cauchy-Green deformation tensor (with components ${}_0^tC_{ij}$):

$$ I_1 = {}_0^tC_{ii} $$

$$ I_2 = \frac{1}{2}\left(I_1^2 - {}_0^tC_{ij}\,{}_0^tC_{ij}\right) $$

$$ I_3 = \det\left({}_0^t\underline{C}\right) $$

Transparency 15-25

Example: Mooney-Rivlin material law

$$ {}_0^tW = \underbrace{C_1}_{\text{material constants}}(I_1 - 3) + \underbrace{C_2}(I_2 - 3) $$

with

$$ I_3 = 1 \leftarrow \text{incompressibility constraint} $$

Note, in general, the displacement-based finite element formulations presented above should be extended to include the incompressibility constraint effectively. A special case, however, is the analysis of plane stress problems.

Transparency 15-26

Transparency 15-27

Special case of Mooney-Rivlin law: plane stress analysis

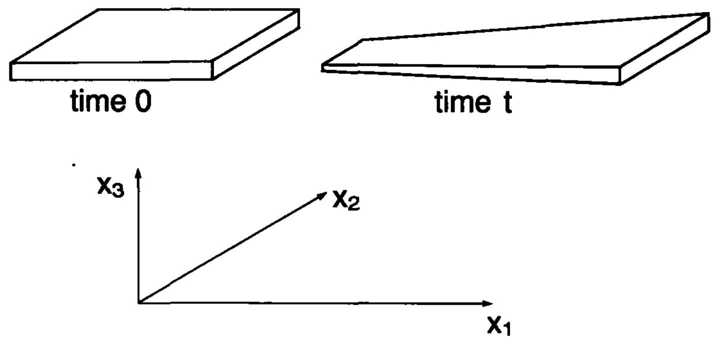

Transparency 15-28

For this (two-dimensional) problem,

$$
{}_0^t\underline{C} = \begin{bmatrix} {}_0^tC_{11} & {}_0^tC_{12} & 0 \\ {}_0^tC_{21} & {}_0^tC_{22} & 0 \\ 0 & 0 & {}_0^tC_{33} \end{bmatrix}
$$

Since the rubber is assumed to be incompressible, we set det $({}_0^t\underline{C})$ to 1 by choosing

$$
{}_0^tC_{33} = \frac{1}{({}_0^tC_{11}\,{}_0^tC_{22} - {}_0^tC_{12}\,{}_0^tC_{21})}
$$

We can now evaluate I_1, I_2:

$$I_1 = {}_0^tC_{11} + {}_0^tC_{22} + \frac{1}{({}_0^tC_{11}\,{}_0^tC_{22} - {}_0^tC_{12}\,{}_0^tC_{21})}$$

$$I_2 = {}_0^tC_{11}\,{}_0^tC_{22} + \frac{{}_0^tC_{11} + {}_0^tC_{22}}{({}_0^tC_{11}\,{}_0^tC_{22} - {}_0^tC_{12}\,{}_0^tC_{21})} - \frac{1}{2}({}_0^tC_{12})^2 - \frac{1}{2}({}_0^tC_{21})^2$$

Transparency 15-29

The 2nd Piola-Kirchhoff stresses are

$$ {}_0^tS_{ij} = \frac{\partial\,{}_0^tW}{\partial\,{}_0^t\varepsilon_{ij}} = 2\,\frac{\partial\,{}_0^tW}{\partial\,{}_0^tC_{ij}} \quad \left(\begin{array}{c}\text{remember}\\ {}_0^tC_{ij} = 2\,{}_0^t\varepsilon_{ij} + \delta_{ij}\end{array}\right)$$

$$= 2\,\frac{\partial}{\partial\,{}_0^tC_{ij}}\left[C_1\,(I_1 - 3) + C_2\,(I_2 - 3)\right]$$

$$= 2\,C_1\,\frac{\partial I_1}{\partial\,{}_0^tC_{ij}} + 2\,C_2\,\frac{\partial I_2}{\partial\,{}_0^tC_{ij}}$$

Transparency 15-30

Transparency 15-31

Performing the indicated differentiations gives

$$\begin{bmatrix} {}_0^tS_{11} \\ {}_0^tS_{22} \\ {}_0^tS_{12} \end{bmatrix} = 2\,C_1 \left\{ \begin{bmatrix} 1 \\ 1 \\ 0 \end{bmatrix} - ({}_0^tC_{33})^2 \begin{bmatrix} {}_0^tC_{22} \\ {}_0^tC_{11} \\ -{}_0^tC_{12} \end{bmatrix} \right\}$$

$$+\,2\,C_2 \left\{ {}_0^tC_{33} \begin{bmatrix} 1 \\ 1 \\ 0 \end{bmatrix} + \left[1 - ({}_0^tC_{33})^2\,({}_0^tC_{11} + {}_0^tC_{22})\right] \begin{bmatrix} {}_0^tC_{22} \\ {}_0^tC_{11} \\ -{}_0^tC_{12} \end{bmatrix} \right\}$$

This is the stress-strain relationship.

Transparency 15-32

We can also evaluate the tangent constitutive tensor ${}_0C_{ijrs}$ using

$$\begin{aligned} {}_0C_{ijrs} &= \frac{\partial^2\, {}_0^tW}{\partial\, {}_0^t\varepsilon_{ij}\, \partial\, {}_0^t\varepsilon_{rs}} \\ &= \underbrace{4\,C_1 \frac{\partial^2 I_1}{\partial\, {}_0^tC_{ij}\, \partial\, {}_0^tC_{rs}} + 4\,C_2 \frac{\partial^2 I_2}{\partial\, {}_0^tC_{ij}\, \partial\, {}_0^tC_{rs}}}_{\text{For the Mooney-Rivlin law}} \end{aligned}$$

etc.

Example: Analysis of a tensile test specimen:

Mooney-Rivlin constants:

$C_1 = .234\ N/mm^2$

$C_2 = .117\ N/mm^2$

thickness = 1 mm

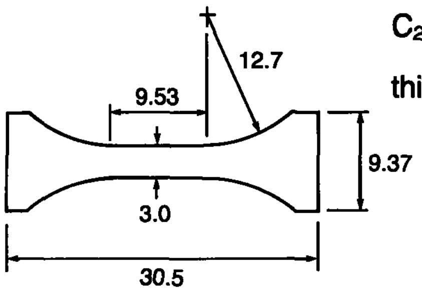

All dimensions in millimeters

Transparency 15-33

Finite element mesh: Fourteen 8-node elements

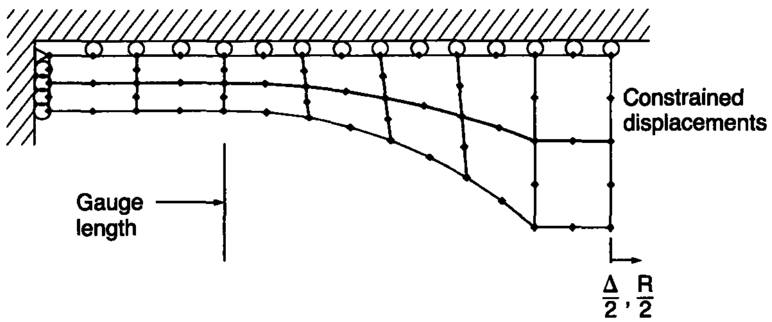

Transparency 15-34

Transparency 15-35

Results: Force – deflection curves

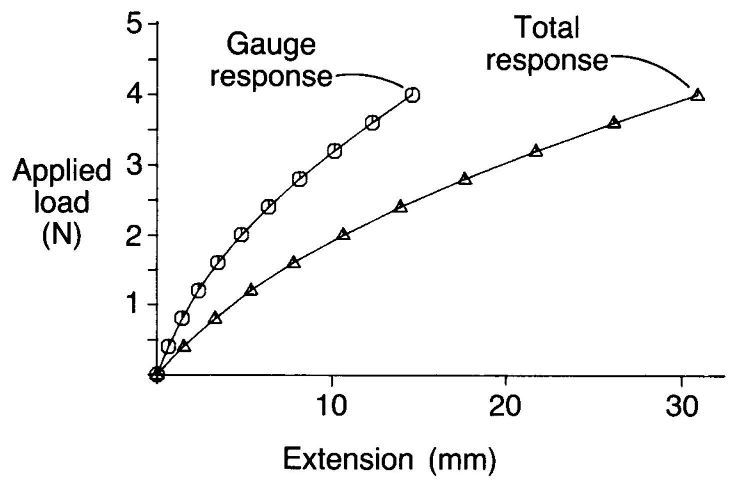

Transparency 15-36

Final deformed mesh (force = 4 N):

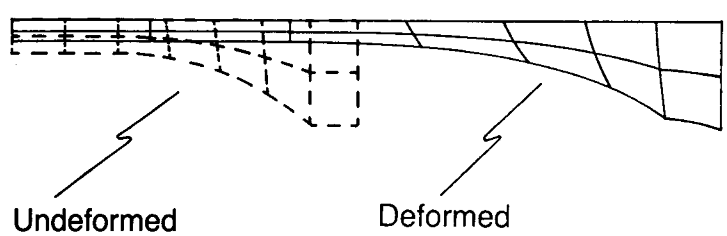

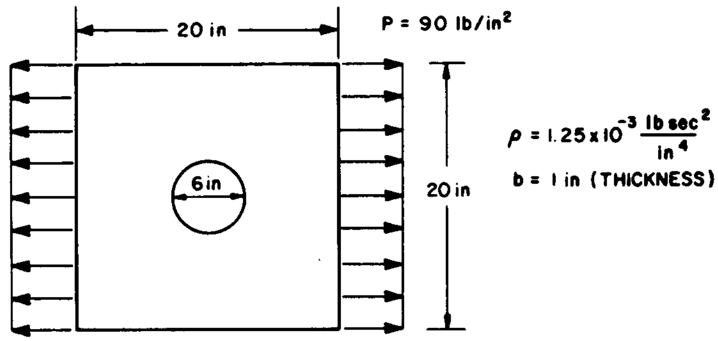

Analysis of rubber sheet with hole

Slide 15-1

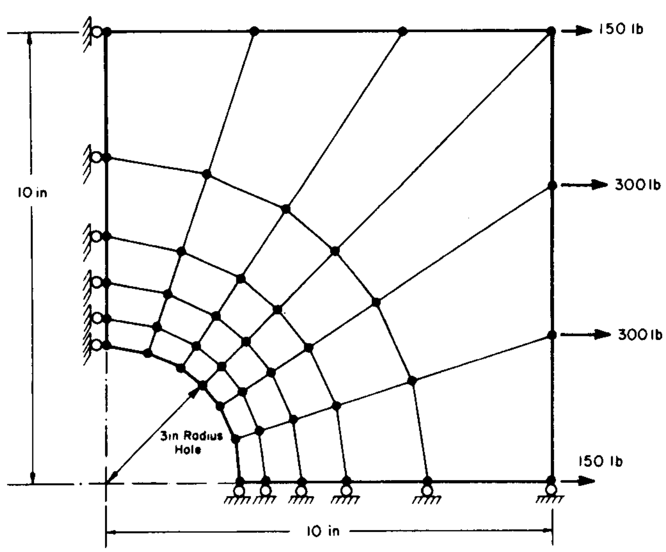

Finite element mesh

Slide 15-2

Slide 15-3

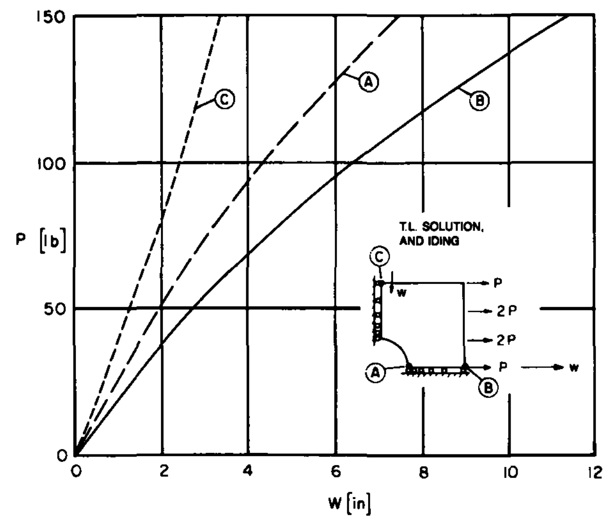

Static load-deflection curve for rubber sheet with hole

Slide 15-4

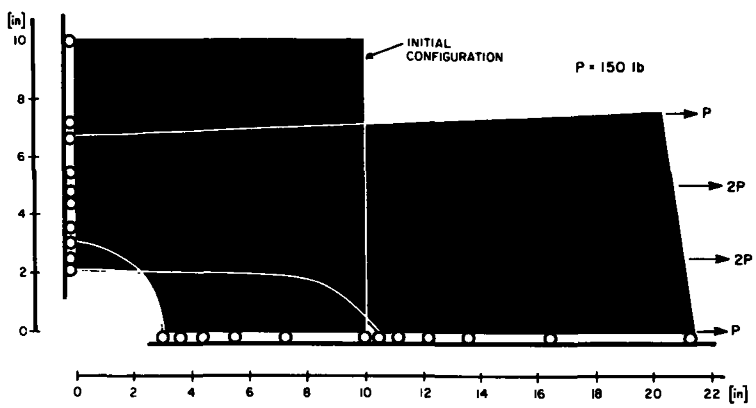

Deformed configuration drawn to scale of rubber sheet with hole (static analysis)

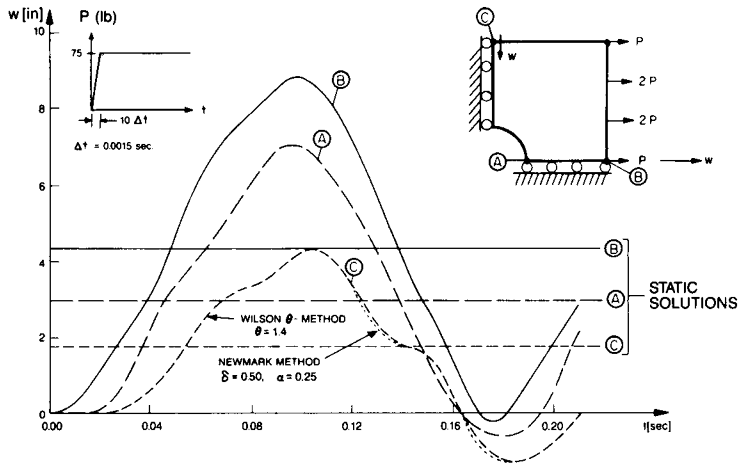

Displacements versus time for rubber sheet with hole, T.L. solution

Slide 15-5

Topic 16

Use of Elastic Constitutive Relations in Updated Lagrangian Formulation

Contents:

- **Use of updated Lagrangian (U.L.) formulation**
- **Detailed comparison of expressions used in total Lagrangian (T.L.) and U.L. formulations; strains, stresses, and constitutive relations**
- **Study of conditions to obtain in a general incremental analysis the same results as in the T.L. formulation, and vice versa**
- **The special case of elasticity**
- **The Almansi strain tensor**
- **One-dimensional example involving large strains**
- **Analysis of large displacement/small strain problems**
- **Example analysis: Large displacement solution of frame using updated and total Lagrangian formulations**

Textbook: 6.4, 6.4.1

Example: 6.19

Transparency 16-1

SO FAR THE USE OF
THE T.L. FORMULATION
WAS IMPLIED

Now suppose that we wish to use the U.L. formulation in the analysis. We ask

- Is it possible to obtain, using the U.L. formulation, identically the same numerical results (for each iteration) as are obtained using the T.L. formulation?

Transparency 16-2

In other words, the situation is

Program 1

- Only T.L. formulation is implemented
  — Constitutive relations are

$$\boxed{\begin{aligned} &{}^t_0S_{ij} = \text{function of displacements} \\ &d_0S_{ij} = {}_0C_{ijrs}\, d_0\varepsilon_{rs} \end{aligned}}$$

Information obtained from physical laboratory experiments.

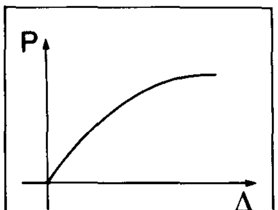

Program 1 results

Transparency 16-3

Program 2
• Only U.L. formulation is implemented – Constitutive relations are ${}^{t}\tau_{ij} = \cdots \rightarrow$ ① $d_t S_{ij} = \cdots \rightarrow$ ②

Question:

How can we obtain with program 2 identically the same results as are obtained from program 1?

Transparency 16-4

To answer, we consider the linearized equations of motion:

$$\left.\begin{aligned} &\int_{{}^0V} {}_0C_{ijrs}\, {}_0e_{rs}\, \delta {}_0e_{ij}\, {}^0dV + \int_{{}^0V} {}_0^tS_{ij}\, \delta {}_0\eta_{ij}\, {}^0dV \\ &\quad = {}^{t+\Delta t}\mathcal{R} - \int_{{}^0V} {}_0^tS_{ij}\, \delta {}_0e_{ij}\, {}^0dV \end{aligned}\right] \text{T.L.}$$

$$\left.\begin{aligned} &\int_{{}^tV} {}_tC_{ijrs}\, {}_te_{rs}\, \delta {}_te_{ij}\, {}^tdV + \int_{{}^tV} {}^t\tau_{ij}\, \delta {}_t\eta_{ij}\, {}^tdV \\ &\quad = {}^{t+\Delta t}\mathcal{R} - \int_{{}^tV} {}^t\tau_{ij}\, \delta {}_te_{ij}\, {}^tdV \end{aligned}\right] \text{U.L.}$$

Terms used in the formulations:

T.L. formulation	U.L. formulation	Transformation
$\int_{{}^0V} {}^0dV$	$\int_{{}^tV} {}^tdV$	${}^0dV = \frac{{}^t\rho}{{}^0\rho}\, {}^tdV$
${}_0e_{ij},\ {}_0\eta_{ij}$	${}_te_{ij},\ {}_t\eta_{ij}$	${}_0e_{ij} = {}^t_0x_{r,i}\ {}^t_0x_{s,j}\ {}_te_{rs}$ ${}_0\eta_{ij} = {}^t_0x_{r,i}\ {}^t_0x_{s,j}\ {}_t\eta_{rs}$
$\delta_0e_{ij},\ \delta_0\eta_{ij}$	$\delta_te_{ij},\ \delta_t\eta_{ij}$	$\delta_0e_{ij} = {}^t_0x_{r,i}\ {}^t_0x_{s,j}\ \delta_te_{rs}$ $\delta_0\eta_{ij} = {}^t_0x_{r,i}\ {}^t_0x_{s,j}\ \delta_t\eta_{rs}$

Transparency 16-5

Derivation of these kinematic relationships:

A fundamental property of ${}^t_0\varepsilon_{ij}$ is that

$$ {}^t_0\varepsilon_{ij}\, d{}^0x_i\, d{}^0x_j = \frac{1}{2}\left(({}^tds)^2 - ({}^0ds)^2\right) $$

Similarly,

$$ {}^{t+\Delta t}_{\ 0}\varepsilon_{ij}\, d{}^0x_i\, d{}^0x_j = \frac{1}{2}\left(({}^{t+\Delta t}ds)^2 - ({}^0ds)^2\right) $$

and

$$ {}_t\varepsilon_{rs}\, d{}^tx_r\, d{}^tx_s = \frac{1}{2}\left(({}^{t+\Delta t}ds)^2 - ({}^tds)^2\right) $$

Transparency 16-6

Transparency 16-7

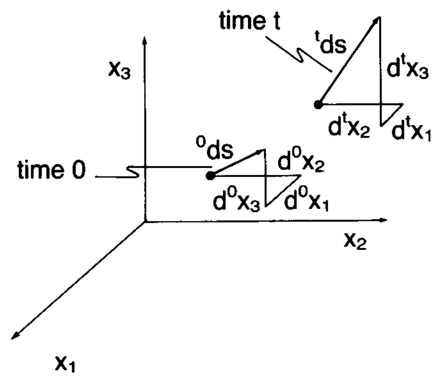

$$d^t\underline{x} = {}^t_0\underline{X}\, d^0\underline{x}$$

Fiber $d^0\underline{x}$ of length ${}^0ds$ moves to become $d^t\underline{x}$ of length ${}^tds$.

Transparency 16-8

Hence, by subtraction, we obtain

$${}_0\varepsilon_{ij}\, d^0x_i\, d^0x_j = {}_t\varepsilon_{rs}\, d^tx_r\, d^tx_s$$

Using $d^t\underline{x} = {}^t_0\underline{X}\, d^0\underline{x}$, we obtain

$${}_0\varepsilon_{ij}\, d^0x_i\, d^0x_j = {}_t\varepsilon_{rs}\, {}^t_0x_{r,i}\, {}^t_0x_{s,j}\, d^0x_i\, d^0x_j$$

Since this relationship holds for arbitrary material fibers, we have

$${}_0\varepsilon_{ij} = {}^t_0x_{r,i}\, {}^t_0x_{s,j}\, {}_t\varepsilon_{rs}$$

Transparency 16-9

Now we see that

$$ {}_0e_{ij} + {}_0\eta_{ij} = {}^t_0x_{r,i}\,{}^t_0x_{s,j}\,{}_te_{rs} + {}^t_0x_{r,i}\,{}^t_0x_{s,j}\,{}_t\eta_{rs} $$

Since the factors ${}^t_0x_{r,i}\,{}^t_0x_{s,j}$ do not contain the incremental displacements u_i, we have

$$ {}_0e_{ij} = {}^t_0x_{r,i}\,{}^t_0x_{s,j}\,{}_te_{rs} \leftarrow \text{linear in } u_i $$

$$ {}_0\eta_{ij} = {}^t_0x_{r,i}\,{}^t_0x_{s,j}\,{}_t\eta_{rs} \leftarrow \text{quadratic in } u_i $$

Transparency 16-10

In addition, we have

$$ \delta\,{}_0e_{ij} = {}^t_0x_{r,i}\,{}^t_0x_{s,j}\,\delta\,{}_te_{rs} $$

$$ \delta\,{}_0\eta_{ij} = {}^t_0x_{r,i}\,{}^t_0x_{s,j}\,\delta\,{}_t\eta_{rs} $$

These follow because the variation is taken on the configuration $t+\Delta t$ and hence the factors ${}^t_0x_{r,i}\,{}^t_0x_{s,j}$ are taken as constant during the variation.

Transparency 16-11

We also have

T.L. formulation	U.L. formulation	Transformation
${}_0^tS_{ij}$	${}^t\tau_{ij}$	${}_0^tS_{ij} = \frac{{}^0\rho}{{}^t\rho}\, {}_t^0x_{i,m}\, {}^t\tau_{mn}\, {}_t^0x_{j,n}$
${}_0C_{ijrs}$	${}_tC_{ijrs}$	${}_0C_{ijrs} = \frac{{}^0\rho}{{}^t\rho}\, {}_t^0x_{i,a}\, {}_t^0x_{j,b}\, {}_tC_{abpq}\, {}_t^0x_{r,p}\, {}_t^0x_{s,q}$ (To be derived below)

Transparency 16-12

Consider the tangent constitutive tensors ${}_0C_{ijrs}$ and ${}_tC_{ijrs}$:

Recall that

$$d_0S_{ij} = {}_0C_{ijrs}\, d_0\varepsilon_{rs}$$

$$d_tS_{ij} = {}_tC_{ijrs}\, d_t\varepsilon_{rs}$$

differential increments

Now we note that

$$d_0S_{ij} = \frac{{}^0\rho}{{}^t\rho}\, {}_t^0x_{i,a}\, {}_t^0x_{j,b}\, d_tS_{ab}$$

$$d_0\varepsilon_{rs} = {}_0^tx_{p,r}\, {}_0^tx_{q,s}\, d_t\varepsilon_{pq}$$

Transparency 16-13

Hence

$$\underbrace{\left(\frac{{}^{0}\rho}{{}^{t}\rho}\,{}^{0}_{t}x_{i,a}\,{}^{0}_{t}x_{j,b}\,d_{t}S_{ab}\right)}_{d_{0}S_{ij}} = {}_{0}C_{ijrs}\underbrace{\left({}^{t}_{0}x_{p,r}\,{}^{t}_{0}x_{q,s}\,d_{t}\varepsilon_{pq}\right)}_{d_{0}\varepsilon_{rs}}$$

Solving for d_tS_{ab} gives

$$d_{t}S_{ab} = \underbrace{\left(\frac{{}^{t}\rho}{{}^{0}\rho}\,{}^{t}_{0}x_{a,i}\,{}^{t}_{0}x_{b,j}\,{}_{0}C_{ijrs}\,{}^{t}_{0}x_{p,r}\,{}^{t}_{0}x_{q,s}\right)}_{{}_{t}C_{abpq}} d_{t}\varepsilon_{pq}$$

Transparency 16-14

And we therefore observe that the tangent material relationship to be used is

$${}_{t}C_{abpq} = \frac{{}^{t}\rho}{{}^{0}\rho}\,{}^{t}_{0}x_{a,i}\,{}^{t}_{0}x_{b,j}\,{}_{0}C_{ijrs}\,{}^{t}_{0}x_{p,r}\,{}^{t}_{0}x_{q,s}$$

Transparency 16-15

Now compare each of the integrals appearing in the T.L. and U.L. equations of motion:

$$1)\ \underbrace{\int_{^0V} {}^t_0S_{ij}\,\delta_0 e_{ij}\,{}^0dV = \int_{^tV} {}^t\tau_{ij}\,\delta_t e_{ij}\,{}^tdV}\qquad ?$$

True, as we verify by substituting the established transformations:

$$\int_{^0V} \underbrace{\left(\frac{{}^0\rho}{{}^t\rho}\,{}^0_t x_{i,m}\,{}^t\tau_{mn}\,{}^0_t x_{j,n}\right)}_{{}^t_0S_{ij}} \underbrace{\left({}^t_0x_{r,i}\,{}^t_0x_{s,j}\,\delta_t e_{rs}\right)}_{\delta_0 e_{ij}}\,{}^0dV$$

$$= \int_{^0V} {}^t\tau_{mn}\,\delta_t e_{rs}\,\underbrace{\left({}^0_t x_{i,m}\,{}^t_0x_{r,i}\right)}_{\delta_{mr}}\,\underbrace{\left({}^0_t x_{j,n}\,{}^t_0x_{s,j}\right)}_{\delta_{ns}}\,\underbrace{\frac{{}^0\rho}{{}^t\rho}\,{}^0dV}_{{}^tdV}$$

$$= \int_{^tV} {}^t\tau_{mn}\,\delta_t e_{mn}\,{}^tdV$$

Transparency 16-16

$$2)\ \underbrace{\int_{^0V} {}^t_0S_{ij}\,\delta_0 \eta_{ij}\,{}^0dV = \int_{^tV} {}^t\tau_{ij}\,\delta_t \eta_{ij}\,{}^tdV}\ ?$$

True, as we verify by substituting the established transformations:

$$\int_{^0V} \underbrace{\left(\frac{{}^0\rho}{{}^t\rho}\,{}^0_t x_{i,m}\,{}^t\tau_{mn}\,{}^0_t x_{j,n}\right)}_{{}^t_0S_{ij}} \underbrace{\left({}^t_0x_{r,i}\,{}^t_0x_{s,j}\,\delta_t \eta_{rs}\right)}_{\delta_0 \eta_{ij}}\,{}^0dV$$

$$= \int_{^0V} {}^t\tau_{mn}\,\delta_t \eta_{rs}\,\underbrace{\left({}^0_t x_{i,m}\,{}^t_0x_{r,i}\right)}_{\delta_{mr}}\underbrace{\left({}^0_t x_{j,n}\,{}^t_0x_{s,j}\right)}_{\delta_{ns}}\,\underbrace{\frac{{}^0\rho}{{}^t\rho}\,{}^0dV}_{{}^tdV}$$

$$= \int_{^tV} {}^t\tau_{mn}\,\delta_t \eta_{mn}\,{}^tdV$$

$$3)\ \underbrace{\int_{^0V} {}_0C_{ijrs}\, {}_0e_{rs}\, \delta_0 e_{ij}\, {}^0dV = \int_{^tV} {}_tC_{ijrs}\, {}_te_{rs}\, \delta_t e_{ij}\, {}^tdV\ ?}$$

True, as we verify by substituting the established transformations:

$$\int_{^0V} \underbrace{\left(\frac{{}^0\rho}{{}^t\rho}\, {}^0_t x_{i,a}\, {}^0_t x_{j,b}\, {}_tC_{abpq}\, {}^0_t x_{r,p}\, {}^0_t x_{s,q}\right)}_{{}_0C_{ijrs}} \times$$

$$\underbrace{({}^t_0 x_{k,r}\, {}^t_0 x_{\ell,s}\, {}_te_{k\ell})}_{{}_0e_{rs}}\ \underbrace{({}^t_0 x_{m,i}\, {}^t_0 x_{n,j}\, \delta_t e_{mn})}_{\delta_0 e_{ij}}\ {}^0dV$$

$$= \int_{^tV} {}_tC_{abpq}\, {}_te_{pq}\, \delta_t e_{ab}\, {}^tdV$$

Transparency 16-17

Provided the established transformations are used, the three integrals are identical. Therefore the resulting finite element discretizations will also be identical.

$$({}^t_0\underline{K}_L + {}^t_0\underline{K}_{NL})\,\Delta\underline{U} = {}^{t+\Delta t}\underline{R} - {}^t_0\underline{F}$$

$$({}^t_t\underline{K}_L + {}^t_t\underline{K}_{NL})\,\Delta\underline{U} = {}^{t+\Delta t}\underline{R} - {}^t_t\underline{F}$$

$$\boxed{\begin{aligned} {}^t_0\underline{K}_L &= {}^t_t\underline{K}_L \\ {}^t_0\underline{K}_{NL} &= {}^t_t\underline{K}_{NL} \\ {}^t_0\underline{F} &= {}^t_t\underline{F} \end{aligned}}$$

The same holds for each equilibrium iteration.

Transparency 16-18

Transparency 16-19

Hence, to summarize once more, program 2 gives the same results as program 1, provided

① → The Cauchy stresses are calculated from

$$ {}^{t}\tau_{ij} = \frac{{}^{t}\rho}{{}^{0}\rho}\, {}^{t}_{0}x_{i,m}\, {}^{t}_{0}S_{mn}\, {}^{t}_{0}x_{j,n} $$

② → The tangent stress-strain law is calculated from

$$ {}_{t}C_{ijrs} = \frac{{}^{t}\rho}{{}^{0}\rho}\, {}^{t}_{0}x_{i,a}\, {}^{t}_{0}x_{j,b}\, {}_{0}C_{abpq}\, {}^{t}_{0}x_{r,p}\, {}^{t}_{0}x_{s,q} $$

Transparency 16-20

Conversely, assume that the material relationships for program 2 are given, hence, from laboratory experimental information, ${}^{t}\tau_{ij}$ and ${}_{t}C_{ijrs}$ for the U.L. formulation are given.
Then we can show that, provided the appropriate transformations

$$ {}^{t}_{0}S_{ij} = \frac{{}^{0}\rho}{{}^{t}\rho}\, {}^{0}_{t}x_{i,m}\, {}^{t}\tau_{mn}\, {}^{0}_{t}x_{j,n} $$

$$ {}_{0}C_{ijrs} = \frac{{}^{0}\rho}{{}^{t}\rho}\, {}^{0}_{t}x_{i,a}\, {}^{0}_{t}x_{j,b}\, {}_{t}C_{abpq}\, {}^{0}_{t}x_{r,p}\, {}^{0}_{t}x_{s,q} $$

are used in program 1 with the T.L. formulation, again the same numerical results are generated.

Hence the choice of formulation (T.L. vs. U.L.) is based solely on the numerical effectiveness of the methods:

- The ${}^{t}_{t}\underline{B}_{L}$ matrix (U.L. formulation) contains less entries than the ${}^{t}_{0}\underline{B}_{L}$ matrix (T.L. formulation).
- The matrix product $\underline{B}^{T}\,\underline{C}\,\underline{B}$ is less expensive using the U.L. formulation.

Transparency 16-21

- If the stress-strain law is available in terms of ${}^{t}_{0}\underline{S}$, then the T.L. formulation will be in general most effective.
  - — Mooney-Rivlin material law
  - — Inelastic analysis allowing for large displacements / large rotations, but small strains

Transparency 16-22

Transparency 16-23

THE SPECIAL CASE OF ELASTICITY

Consider that the components ${}_0^tC_{ijrs}$ are given:

$${}_0^tS_{ij} = {}_0^tC_{ijrs}\, {}_0^t\varepsilon_{rs}$$

From the above discussion, to obtain the same numerical results with the U.L. formulation, we would employ

$${}^t\tau_{ij} = \frac{{}^t\rho}{{}^0\rho}\, {}_0^tx_{i,m}\, ({}_0^tC_{mnrs}\, {}_0^t\varepsilon_{rs})\, {}_0^tx_{j,n}$$

$${}_tC_{ijrs} = \frac{{}^t\rho}{{}^0\rho}\, {}_0^tx_{i,a}\, {}_0^tx_{j,b}\, {}_0C_{abpq}\, {}_0^tx_{r,p}\, {}_0^tx_{s,q}$$

Transparency 16-24

We see that in the above equation, the Cauchy stresses are related to the Green-Lagrange strains by a transformation acting only on the m and n components of ${}_0^tC_{mnrs}$.

However, we can write the total stress-strain law using a tensor, ${}_t^tC^a_{ijrs}$, by introducing another strain measure, namely the Almansi strain tensor,

$${}^t\tau_{ij} = {}_t^tC^a_{ijrs}\, \underbrace{{}_t^t\varepsilon^a_{rs}}\text{ Almansi strain tensor}$$

$${}_t^tC^a_{ijrs} = \frac{{}^t\rho}{{}^0\rho}\, {}_0^tx_{i,a}\, {}_0^tx_{j,b}\, {}_0^tC_{abpq}\, {}_0^tx_{r,p}\, {}_0^tx_{s,q}$$

Transparency 16-25

Definitions of the Almansi strain tensor:

$$ {}^t_t\varepsilon^a_{mn} = {}^0_t x_{i,m}\ {}^0_t x_{j,n}\ {}^t_0\varepsilon_{ij} $$

$$ {}^t_t\underline{\varepsilon}^a = \frac{1}{2}\left(\underline{I} - {}^0_t\underline{X}^T\ {}^0_t\underline{X}\right) $$

$$ {}^t_t\varepsilon^a_{ij} = \frac{1}{2}\left({}^t_t u_{i,j} + {}^t_t u_{j,i} - {}^t_t u_{k,i}\ \overbrace{{}^t_t u_{k,j}}^{\frac{\partial\, {}^t u_k}{\partial\, {}^t x_j}}\right) $$

Transparency 16-26

- A symmetric strain tensor, ${}^t_t\varepsilon^a_{ij} = {}^t_t\varepsilon^a_{ji}$
- The components of ${}^t_t\underline{\varepsilon}^a$ are not invariant under a rigid body rotation of the material.
- Hence, ${}^t_t\underline{\varepsilon}^a$ is not a very useful strain measure, but we wanted to introduce it here briefly.

Transparency 16-27

Example: Uniaxial strain

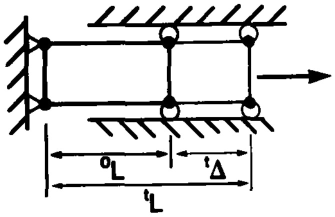

$$ {}^{t}_{0}\varepsilon_{11} = \frac{{}^{t}\Delta}{{}^{0}L} + \frac{1}{2}\left(\frac{{}^{t}\Delta}{{}^{0}L}\right)^2 $$

$$ {}^{t}_{t}\varepsilon^{a}_{11} = \frac{{}^{t}\Delta}{{}^{t}L} - \frac{1}{2}\left(\frac{{}^{t}\Delta}{{}^{t}L}\right)^2 $$

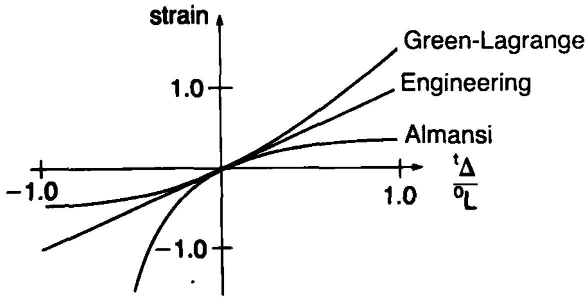

Transparency 16-28

It turns out that the use of ${}^{t}_{t}C^{a}_{ijrs}$ with the Almansi strain tensor is effective when the U.L. formulation is used with a linear isotropic material law for large displacement / large rotation but small strain analysis.

- In this case, ${}^t_tC^a_{ijrs}$ may be taken as

$$ {}^t_tC^a_{ijrs} = \underbrace{\lambda \delta_{ij} \delta_{rs} + \mu(\delta_{ir} \delta_{js} + \delta_{is} \delta_{jr})}_{\text{constants}} $$
$$ = {}_tC_{ijrs} $$

Practically the same response is calculated using the T.L. formulation with

$$ {}^t_0C_{ijrs} = \underbrace{\lambda\ \delta_{ij} \delta_{rs} + \mu(\delta_{ir} \delta_{js} + \delta_{is} \delta_{jr})}_{\text{constants}} $$
$$ = {}_0C_{ijrs} $$

Transparency 16-29

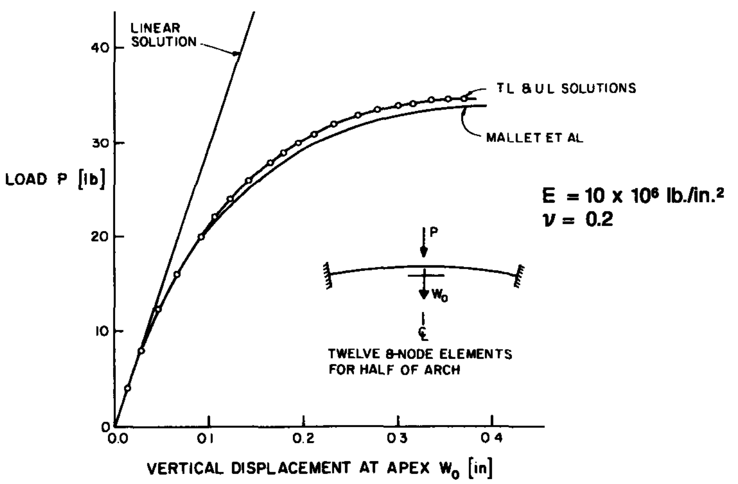

Load-deflection curve for a shallow arch under concentrated load

Slide 16-1

Transparency 16-30

The reason that practically the same response is calculated is that the required transformations to obtain exactly the same response reduce to mere rotations:

Namely, in the transformations from ${}^{t}_{t}C^{a}_{ijrs}$ to ${}^{t}_{0}C_{abpq}$, and in the relation between ${}_{0}C_{ijrs}$ and ${}_{t}C_{ijrs}$,

$$\frac{{}^{0}\rho}{{}^{t}\rho} \doteq 1, \quad [{}^{t}_{0}x_{i,j}] = {}^{t}_{0}\underline{X} = {}^{t}_{0}\underline{R}\,{}^{t}_{0}\underline{U} \doteq {}^{t}_{0}\underline{R}$$

Transparency 16-31

However, when using constant material moduli (E, ν) for large strain analysis, with

$${}^{t}\tau_{ij} = \underbrace{{}^{t}_{t}C^{a}_{ijrs}}\,{}^{t}_{t}\varepsilon^{a}_{rs}$$

and

$$= \lambda\, \delta_{ij}\, \delta_{rs} + \mu\, (\delta_{ir}\, \delta_{js} + \delta_{is}\, \delta_{jr})$$

$${}^{t}_{0}S_{ij} = \overbrace{{}^{t}_{0}C_{ijrs}}\,{}^{t}_{0}\varepsilon_{rs}$$

totally different results are obtained.

Consider the 1-D problem already solved earlier:

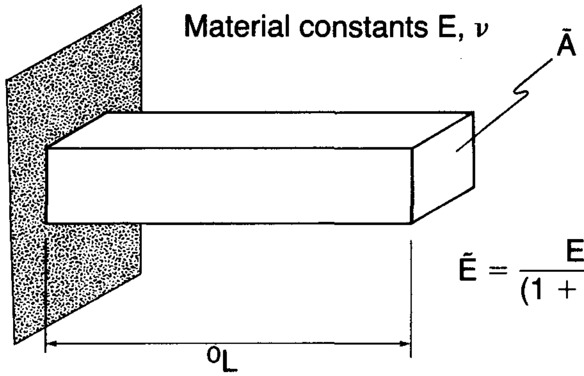

$$\tilde{E} = \frac{E\,(1-\nu)}{(1+\nu)\,(1-2\nu)}$$

Before, we used ${}_0^tS_{11} = \tilde{E}\ {}_0^t\varepsilon_{11}$.

Now, we consider ${}^t\tau_{11} = \tilde{E}\ {}_t^t\varepsilon_{11}^a$.

Transparency 16-32

Here, we have

$$ {}_t^t\varepsilon_{11}^a = \underbrace{{}_t^tu_{1,1}}_{\frac{{}^tL - {}^0L}{{}^tL}} - \frac{1}{2}\left({}_t^tu_{1,1}\right)^2 = \frac{1}{2}\left[1 - \left(\frac{{}^0L}{{}^tL}\right)^2\right] $$

$$ {}^t\tau_{11} = \frac{{}^tP}{\bar{A}} $$

Using ${}^tL = {}^0L + {}^t\Delta$, ${}^t\tau_{11} = \tilde{E}\ {}_t^t\varepsilon_{11}^a$, we obtain the force-displacement relationship.

Transparency 16-33

Transparency 16-34

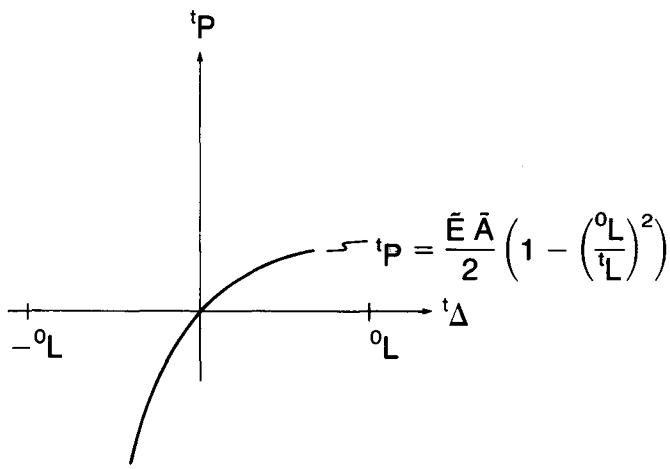

Transparency 16-35

<u>Example</u>: Corner under tip load

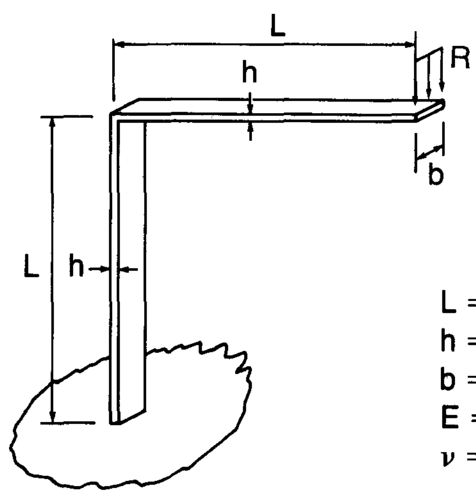

$$
\left.\begin{array}{l} L = 10.0\ \mathrm{m} \\ h = 0.2\ \mathrm{m} \end{array}\right\} \frac{h}{L} = \frac{1}{50}
$$

$b = 1.0\ \mathrm{m}$

$E = 207000\ \mathrm{MPa}$

$\nu = 0.3$

Finite element mesh: 51 two-dimensional 8-node elements

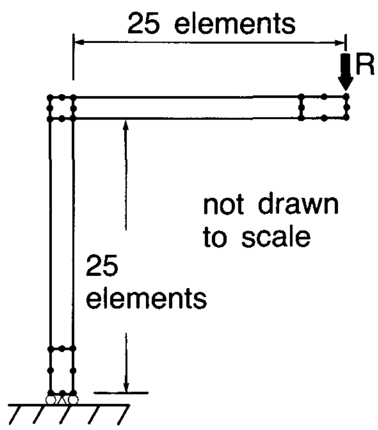

All elements are plane strain elements.

Transparency 16-36

Consider a nonlinear elastic analysis. For what loads will the T.L. and U.L. formulations give similar results?

Transparency 16-37

Transparency 16-38

— For large displacement/large rotation, but small strain conditions, the T.L. and U.L. formulations will give similar results.

— For large displacement/large rotation and large strain conditions, the T.L. and U.L. formulations will give different results, because different constitutive relations are assumed.

Transparency 16-39

Results: Force-deflection curve

- Over the range of loads shown, the T.L. and U.L. formulations give practically identical results
- The force-deflection curve obtained with two 4-node isoparametric beam elements is also shown.

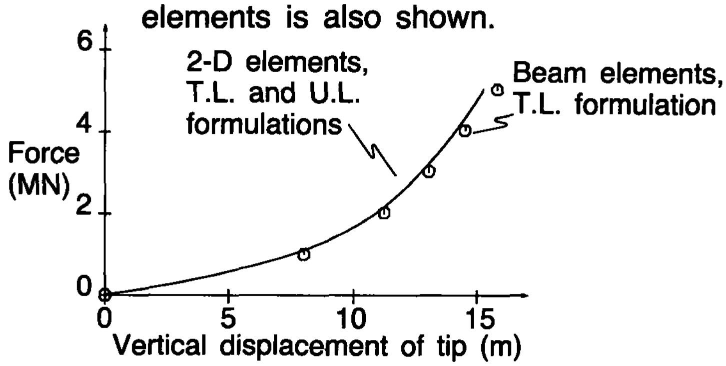

Deformed configuration for a load of 5 MN (2-D elements are used):

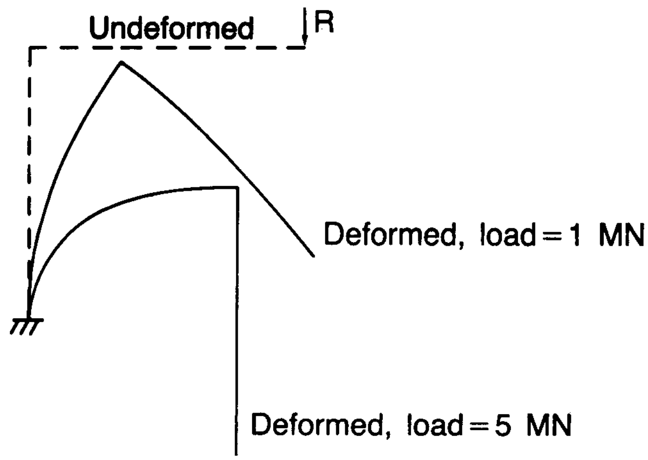

Transparency 16-40

Numerically, for a load of 5 MN, we have, using the 2-D elements,

	T.L. formulation	U.L. formulation
vertical tip displacement	15.289 m	15.282 m

The displacements and rotations are large. However, the strains are small – they can be estimated using strength of materials formulas:

$$\varepsilon_{base} = \frac{M(h/2)}{E\,I} \quad \text{where } M \doteq (5 \text{ MN})(7.5 \text{ m})$$

$$\doteq 3\%$$

Transparency 16-41

Topic 17

Modeling of Elasto-Plastic and Creep Response—Part I

Contents:

- **Basic considerations in modeling inelastic response**
- **A schematic review of laboratory test results, effects of stress level, temperature, strain rate**
- **One-dimensional stress-strain laws for elasto-plasticity, creep, and viscoplasticity**
- **Isotropic and kinematic hardening in plasticity**
- **General equations of multiaxial plasticity based on a yield condition, flow rule, and hardening rule**
- **Example of von Mises yield condition and isotropic hardening, evaluation of stress-strain law for general analysis**
- **Use of plastic work, effective stress, effective plastic strain**
- **Integration of stresses with subincrementation**
- **Example analysis: Plane strain punch problem**
- **Example analysis: Elasto-plastic response up to ultimate load of a plate with a hole**
- **Computer-plotted animation: Plate with a hole**

Textbook: Section 6.4.2

Example: 6.20

References: The plasticity computations are discussed in

Bathe, K. J., M. D. Snyder, A. P. Cimento, and W. D. Rolph III, "On Some Current Procedures and Difficulties in Finite Element Analysis of Elastic-Plastic Response," *Computers & Structures, 12,* 607–624, 1980.

References:
(continued)

Snyder, M. D., and K. J. Bathe, "A Solution Procedure for Thermo-Elastic-Plastic and Creep Problems," *Nuclear Engineering and Design, 64,* 49–80, 1981.

The plane strain punch problem is also considered in

Sussman, T., and K. J. Bathe, "Finite Elements Based on Mixed Interpolation for Incompressible Elastic and Inelastic Analysis," *Computers & Structures,* to appear.

- WE DISCUSSED IN THE PREVIOUS LECTURES THE MODELING OF ELASTIC MATERIALS
  - LINEAR STRESS-STRAIN LAW
  - NONLINEAR STRESS-STRAIN LAW

  THE T.L. AND U.L. FORMULATIONS

- WE NOW WANT TO DISCUSS THE MODELING OF INELASTIC MATERIALS
  - ELASTO-PLASTICITY AND CREEP

- WE PROCEED AS FOLLOWS:
  - WE DISCUSS BRIEFLY INELASTIC MATERIAL BEHAVIORS, AS OBSERVED IN LABORATORY TESTS
  - WE DISCUSS BRIEFLY MODELING OF SUCH RESPONSE IN 1-D ANALYSIS
  - WE GENERALIZE OUR MODELING CONSIDERATIONS TO 2-D AND 3-D STRESS SITUATIONS

Markerboard 17-1

Transparency 17-1

MODELING OF INELASTIC RESPONSE: ELASTO-PLASTICITY, CREEP AND VISCOPLASTICITY

- The total stress is not uniquely related to the current total strain. Hence, to calculate the response history, stress increments must be evaluated for each time (load) step and added to the previous total stress.

Transparency 17-2

- The differential stress increment is obtained as – assuming infinitesimally small displacement conditions –

$$d\sigma_{ij} = C^{E}_{ijrs}\,(de_{rs} - de^{IN}_{rs})$$

where

C^{E}_{ijrs} = components of the elasticity tensor

de_{rs} = total differential strain increment

de^{IN}_{rs} = inelastic differential strain increment

The inelastic response may occur rapidly or slowly in time, depending on the problem of nature considered.

Modeling:

- In plasticity, the model assumes that de^{IN}_{rs} occurs instantaneously with the load application.
- In creep, the model assumes that de^{IN}_{rs} occurs as a function of time.
- The actual response in nature can be modeled using plasticity and creep together, or alternatively using a viscoplastic material model.

Transparency 17-3

— In the following discussion we assume small strain conditions, hence

- we have either a materially-nonlinear-only analysis
- or a large displacement/large rotation but small strain analysis

Transparency 17-4

Transparency 17-5

- As pointed out earlier, for the large displacement solution we would use the total Lagrangian formulation and in the evaluation of the stress-strain laws simply use

  — Green-Lagrange strain component for the engineering strain components

  and

  — 2nd Piola-Kirchhoff stress components for the engineering stress components

Transparency 17-6

Consider a brief summary of some observations regarding material response measured in the laboratory

- We only consider schematically what approximate response is observed; no details are given.
- Note that, regarding the notation, no time, t, superscript is used on the stress and strain variables describing the material behavior.

MATERIAL BEHAVIOR, "INSTANTANEOUS" RESPONSE

Transparency 17-7

Tensile Test: Assume

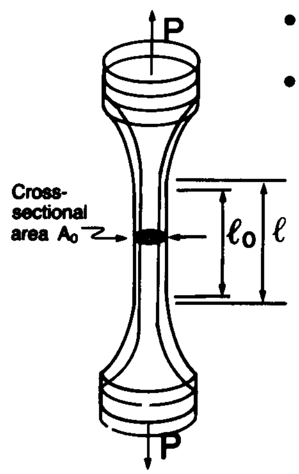

- small strain conditions
- behavior in compression is the same as in tension

Hence

$$e = \frac{\ell - \ell_0}{\ell_0}$$

$$\sigma = \frac{P}{A_0}$$

Transparency 17-8

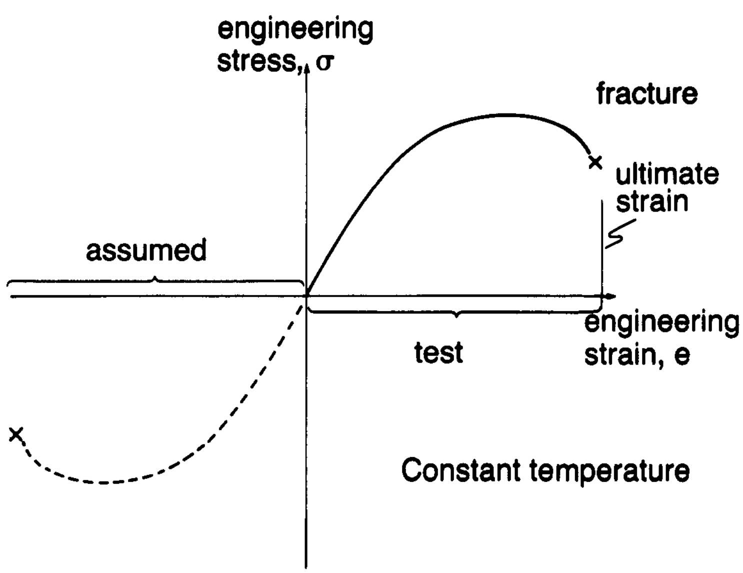

Transparency 17-9

Effect of strain rate:

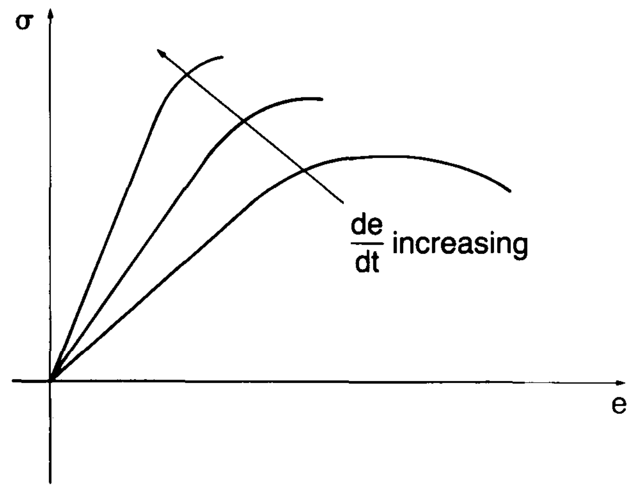

Transparency 17-10

Effect of temperature

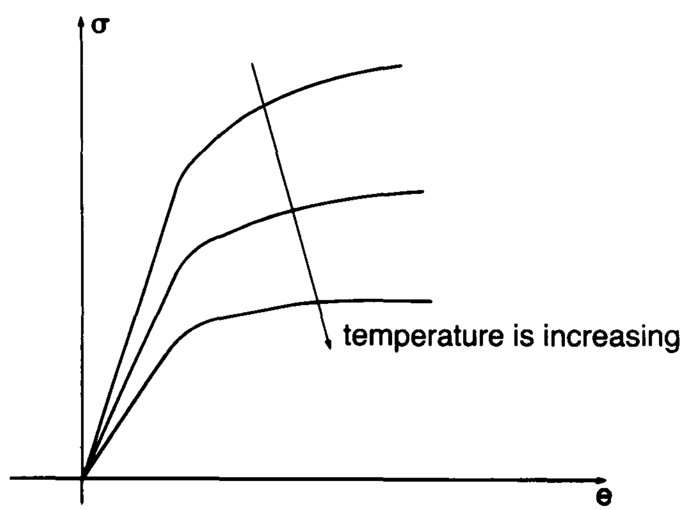

MATERIAL BEHAVIOR, TIME-DEPENDENT RESPONSE

- Now, at constant stress, inelastic strains develop.
- Important effect for materials when temperatures are high

Transparency 17-11

Typical creep curve

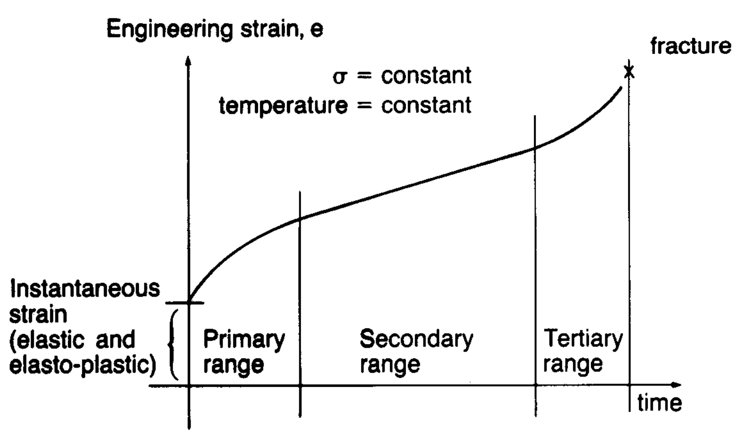

Transparency 17-12

Transparency 17-13

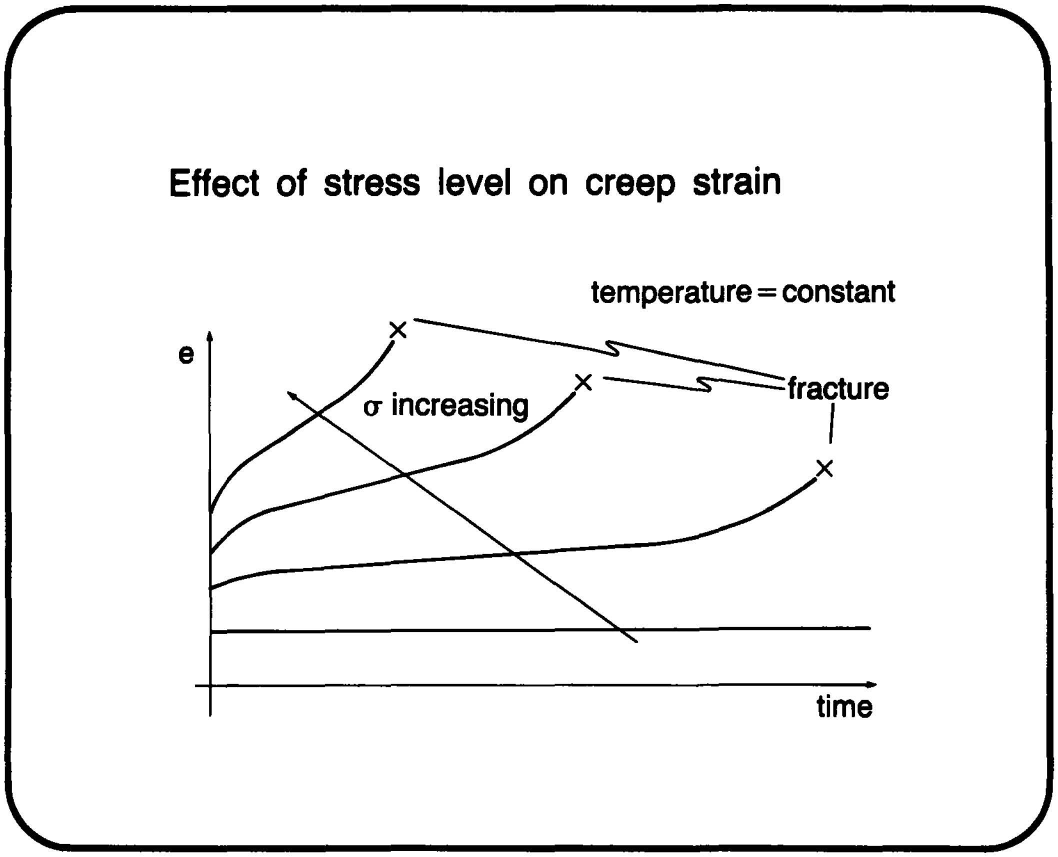

Transparency 17-14

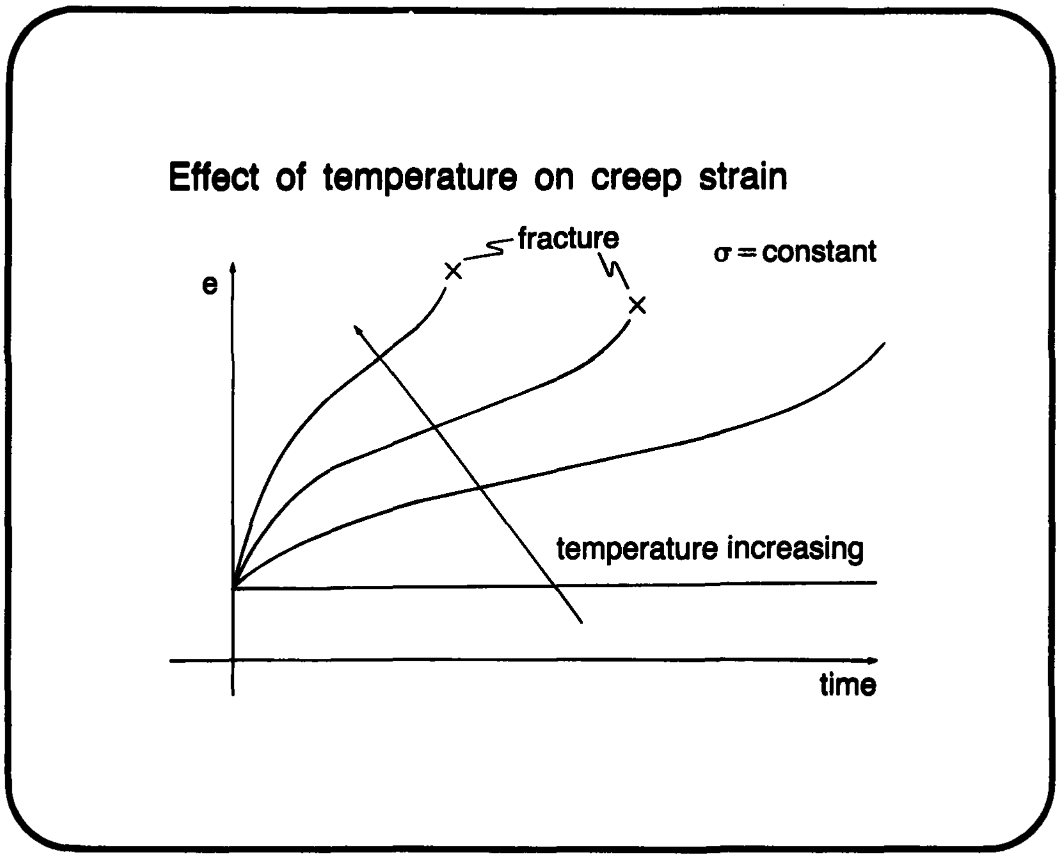

MODELING OF RESPONSE

Transparency 17-15

Consider a one-dimensional situation:

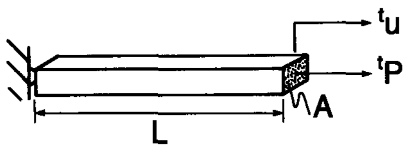

$$ {}^{t}\sigma = \frac{{}^{t}P}{A} $$

$$ {}^{t}e = \frac{{}^{t}u}{L} $$

- We assume that the load is increased monotonically to its final value, P*.
- We assume that the time is "long" so that inertia effects are negligible (static analysis).

Transparency 17-16

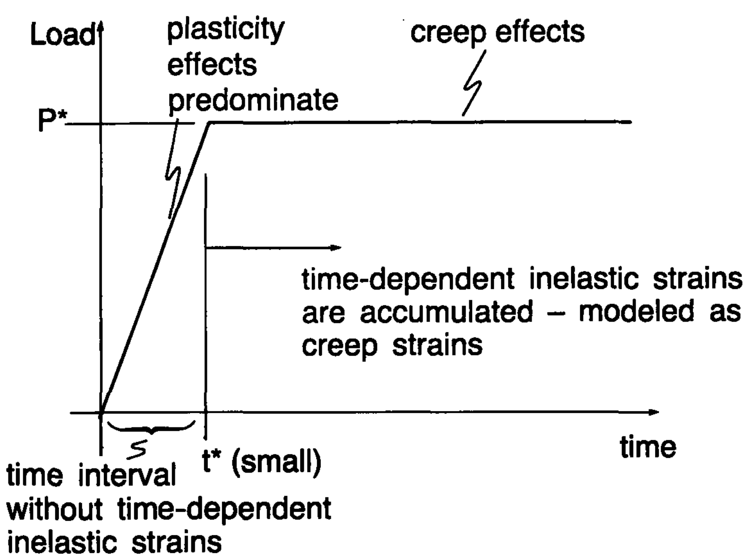

Transparency 17-17

Plasticity, uniaxial, bilinear material model

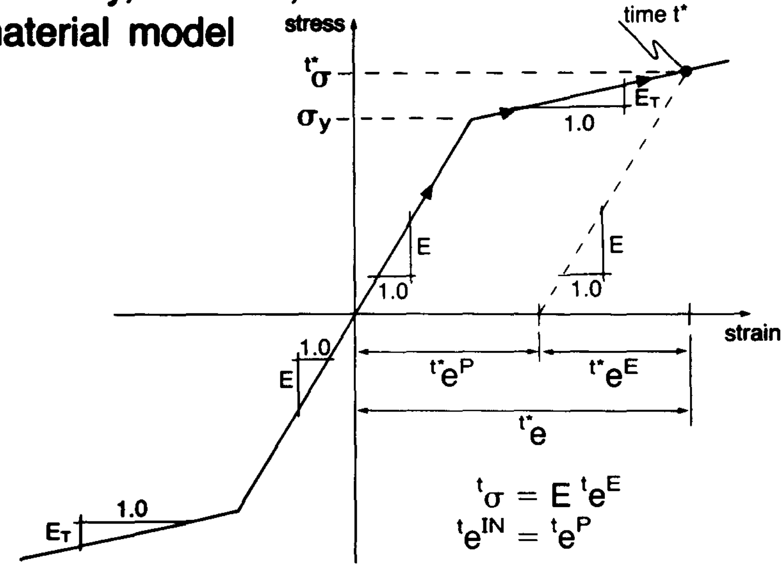

$$^t\sigma = E\,{}^te^E$$
$$^te^{IN} = {}^te^P$$

Transparency 17-18

Creep, power law material model:

$$e^C = a_0\,\sigma^{a_1}\,t^{a_2}$$

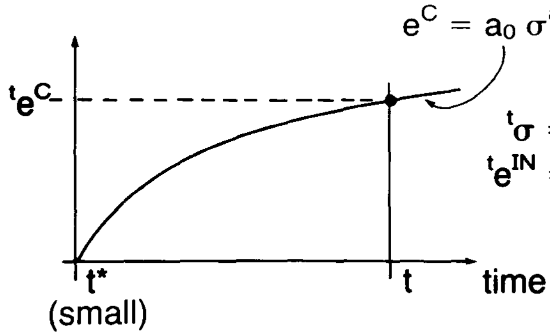

$$^t\sigma = E\,{}^te^E$$
$$^te^{IN} = {}^te^C + {}^te^P$$

- The elastic strain is the same as in the plastic analysis (this follows from equilibrium).
- The inelastic strain is time-dependent and time is now an actual variable.

Viscoplasticity:

- Time-dependent response is modeled using a fluidity parameter γ:

$$\dot{e} = \frac{\dot{\sigma}}{E} + \underbrace{\gamma \left\langle \frac{\sigma}{\sigma_y} - 1 \right\rangle}_{\dot{e}^{VP}}$$

where

$$\langle \sigma - \sigma_y \rangle = \begin{cases} 0 & , \sigma \le \sigma_y \\ \sigma - \sigma_y & , \sigma > \sigma_y \end{cases}$$

Transparency 17-19

Typical solutions (1-D specimen):

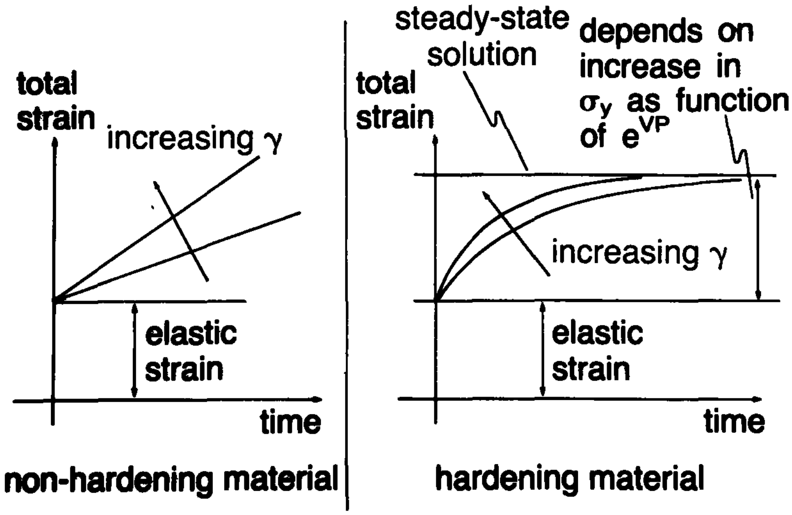

Transparency 17-20

Transparency 17-21

PLASTICITY

- So far we considered only loading conditions.
- Before we discuss more general multiaxial plasticity relations, consider unloading and cyclic loading assuming uniaxial stress conditions.

Transparency 17-22

- Consider that the load increases in tension, causes plastic deformation, reverses elastically, and again causes plastic deformation in compression.

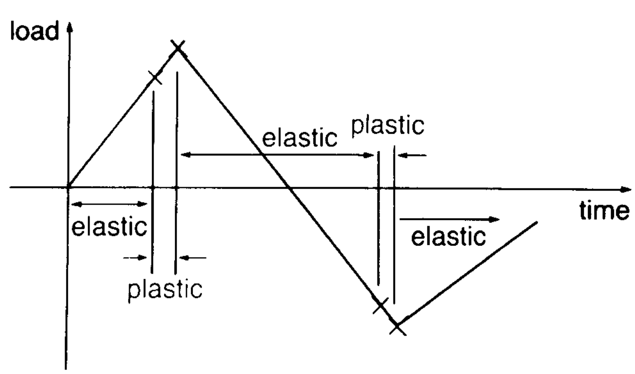

Bilinear material assumption, isotropic hardening

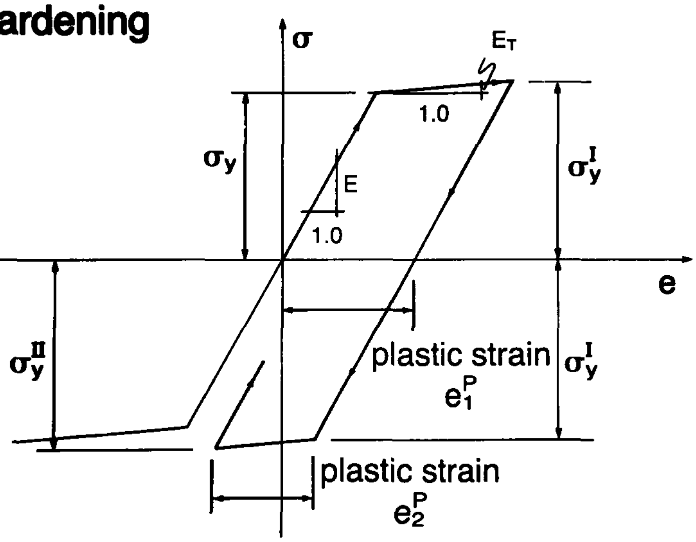

Transparency 17-23

Bilinear material assumption, kinematic hardening

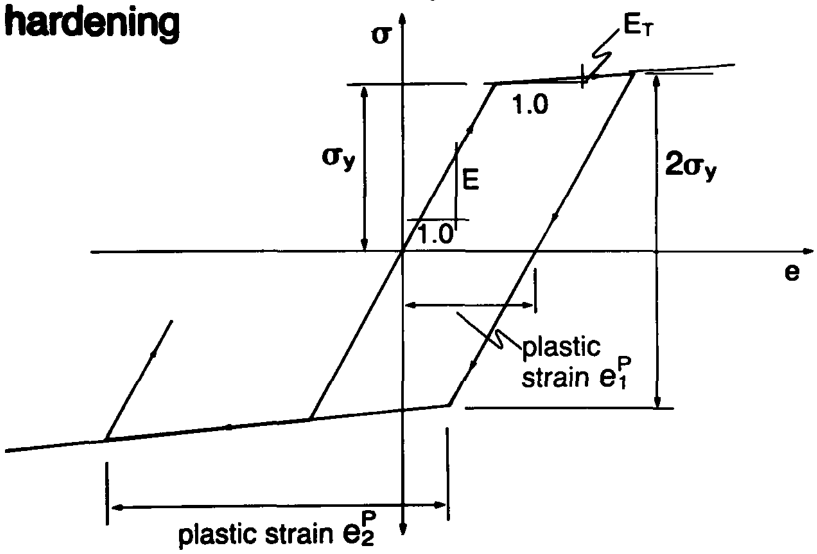

Transparency 17-24

Transparency 17-25

MULTIAXIAL PLASTICITY

To describe the plastic behavior in multiaxial stress conditions, we use

- A yield condition
- A flow rule
- A hardening rule

In the following, we consider isothermal (constant temperature) conditions.

Transparency 17-26

These conditions are expressed using a stress function ${}^{t}F$.

Two widely used stress functions are the

von Mises function

Drucker-Prager function

von Mises

$$^{t}F = \frac{1}{2}\,{}^{t}s_{ij}\,{}^{t}s_{ij} - {}^{t}\kappa$$

$$^{t}s_{ij} = {}^{t}\sigma_{ij} - \frac{^{t}\sigma_{mm}}{3}\,\delta_{ij}\;;\quad {}^{t}\kappa = \frac{1}{3}\,{}^{t}\sigma_{y}^{2}$$

Drucker-Prager

$$^{t}F = 3\alpha\,{}^{t}\sigma_{m} + {}^{t}\bar{\sigma} - k$$

$$^{t}\sigma_{m} = \frac{^{t}\sigma_{ii}}{3}\;;\quad {}^{t}\bar{\sigma} = \sqrt{\frac{1}{2}\,{}^{t}s_{ij}\,{}^{t}s_{ij}}$$

Transparency 17-27

We use both matrix notation and index notation:

$$d\underline{e}^{P} = \begin{bmatrix} de^{P}_{11} \\ de^{P}_{22} \\ de^{P}_{33} \\ de^{P}_{12} + \boxed{de^{P}_{21}} \\ de^{P}_{23} + de^{P}_{32} \\ de^{P}_{13} + de^{P}_{31} \end{bmatrix}, \quad d\underline{\sigma} = \begin{bmatrix} d\sigma_{11} \\ d\sigma_{22} \\ d\sigma_{33} \\ d\sigma_{12} \\ d\sigma_{23} \\ d\sigma_{31} \end{bmatrix}$$

matrix notation

note that both de^{P}_{12} and de^{P}_{21} are added

Transparency 17-28

Transparency 17-29

$$\left.\begin{array}{l} de^P_{ij} = \begin{bmatrix} de^P_{11} & de^P_{12} & de^P_{13} \\ de^P_{21} & de^P_{22} & de^P_{23} \\ de^P_{31} & de^P_{32} & de^P_{33} \end{bmatrix} \\ \\ d\sigma_{ij} = \begin{bmatrix} d\sigma_{11} & d\sigma_{12} & d\sigma_{13} \\ d\sigma_{21} & d\sigma_{22} & d\sigma_{23} \\ d\sigma_{31} & d\sigma_{32} & d\sigma_{33} \end{bmatrix} \end{array}\right\} \text{index notation}$$

Transparency 17-30

The basic equations are then (von Mises ${}^tF$):

1) Yield condition

$${}^tF\,({}^t\sigma_{ij},\ {}^t\kappa) = 0$$

current stresses   function of plastic strains

${}^tF$ is zero throughout the plastic response

- 1-D equivalent: $\frac{1}{3}\,({}^t\sigma^2 - {}^t\sigma_y^2) = 0$

  (uniaxial stress)

  current stresses   function of plastic strains.

2) Flow rule (associated rule):

$$de_{ij}^{P} = {}^{t}\lambda \frac{\partial\, {}^{t}F}{\partial\, {}^{t}\sigma_{ij}}$$

where ${}^{t}\lambda$ is a positive scalar.

- 1-D equivalent:

$$de_{11}^{P} = \frac{2}{3}\, {}^{t}\lambda\, {}^{t}\sigma$$

$$de_{22}^{P} = -\frac{1}{3}\, {}^{t}\lambda\, {}^{t}\sigma$$

$$de_{33}^{P} = -\frac{1}{3}\, {}^{t}\lambda\, {}^{t}\sigma$$

Transparency 17-31

3) Stress-strain relationship:

$$d\underline{\sigma} = \underline{C}^{E} (d\underline{e} - d\underline{e}^{P})$$

- 1-D equivalent:

$$d\sigma = E\,(de_{11} - de_{11}^{P})$$

Transparency 17-32

Transparency 17-33

Our goal is to determine $\underline{C}^{EP}$ such that

$$d\underline{\sigma} = \underbrace{\underline{C}^{EP}}_{\text{instantaneous elastic-plastic stress-strain matrix}} d\underline{e}$$

Transparency 17-34

General derivation of $\underline{C}^{EP}$:

<u>Define</u>

$$^{t}q_{ij} = \left. \frac{\partial\,^{t}F}{\partial\,^{t}\sigma_{ij}} \right|_{^{t}e_{ij}^{P} \text{ fixed}}$$

$$^{t}p_{ij} = - \left. \frac{\partial\,^{t}F}{\partial\,^{t}e_{ij}^{P}} \right|_{^{t}\sigma_{ij} \text{ fixed}}$$

Transparency 17-35

Using matrix notation,

results from our definition of the plastic strain and stress increment vectors

$${}^t\underline{q}^T = [{}^tq_{11} \vdots {}^tq_{22} \vdots {}^tq_{33} \vdots 2\,{}^tq_{12} \vdots 2\,{}^tq_{23} \vdots 2\,{}^tq_{31}]$$

$${}^t\underline{p}^T = [{}^tp_{11} \vdots {}^tp_{22} \vdots {}^tp_{33} \vdots {}^tp_{12} \vdots {}^tp_{23} \vdots {}^tp_{31}]$$

Transparency 17-36

We now determine ${}^t\lambda$ in terms of $d\underline{e}$:

Using ${}^tF = 0$ during plastic deformations,

$$d\,{}^tF = \frac{\partial\,{}^tF}{\partial\,{}^t\sigma_{ij}}\,d\sigma_{ij} + \frac{\partial\,{}^tF}{\partial\,{}^te^P_{ij}}\,de^P_{ij}$$

$$= {}^t\underline{q}^T\,d\underline{\sigma} - {}^t\underline{p}^T\,\underbrace{\cancel{d\underline{e}^P}}_{{}^t\lambda\,{}^t\underline{q}}$$

$$= 0$$

Transparency 17-37

Also

$$\underbrace{{}^t\underline{q}^T\, d\underline{\sigma}} = {}^t\underline{q}^T\, \underbrace{(\underline{C}^E\,(d\underline{e} - d\underline{e}^P))}$$

The flow rule assumption may be written as

$$d\underline{e}^P = {}^t\lambda\, {}^t\underline{q}$$

Hence

$$ {}^t\underline{q}^T\, d\underline{\sigma} = \boxed{{}^t\underline{q}^T\,(\underline{C}^E\,(d\underline{e} - {}^t\lambda\, {}^t\underline{q})) = \underbrace{{}^t\lambda\, {}^t\underline{p}^T\, {}^t\underline{q}}_{\text{from } d\,{}^tF = 0}}$$

Transparency 17-38

Solving the boxed equation for ${}^t\lambda$ gives

$${}^t\lambda = \frac{{}^t\underline{q}^T\,\underline{C}^E\,d\underline{e}}{{}^t\underline{p}^T\,{}^t\underline{q} + {}^t\underline{q}^T\,\underline{C}^E\,{}^t\underline{q}}$$

Hence we can determine the plastic strain increment from the total strain increment:

$$\underbrace{d\underline{e}^P}_{\text{plastic strain increment}} = \left(\frac{{}^t\underline{q}^T\,\underline{C}^E\,\overbrace{d\underline{e}}^{\text{total strain increment}}}{{}^t\underline{p}^T\,{}^t\underline{q} + {}^t\underline{q}^T\,\underline{C}^E\,{}^t\underline{q}}\right){}^t\underline{q}$$

Transparency 17-39

We can now solve for $\underline{C}^{EP}$:

$$d\underline{\sigma} = \underline{C}^{E}\,(d\underline{e} - d\underline{e}^{P})$$

function of $d\underline{e}$ from above

$$\underline{C}^{EP} = \underline{C}^{E} - \frac{\underline{C}^{E}\,{}^{t}\underline{q}\,(\underline{C}^{E}\,{}^{t}\underline{q})^{T}}{{}^{t}\underline{p}^{T}\,{}^{t}\underline{q} + {}^{t}\underline{q}^{T}\,\underline{C}^{E}\,{}^{t}\underline{q}}$$

Transparency 17-40

Example: Von Mises yield condition, isotropic hardening

Two equivalent equations:

$${}^{t}\sigma_{y} = \frac{\sqrt{2}}{2}\sqrt{({}^{t}\sigma_{1} - {}^{t}\sigma_{2})^{2} + ({}^{t}\sigma_{2} - {}^{t}\sigma_{3})^{2} + ({}^{t}\sigma_{3} - {}^{t}\sigma_{1})^{2}}$$

principal stresses

$${}^{t}F = \frac{1}{2}\,{}^{t}s_{ij}\,{}^{t}s_{ij} - {}^{t}\kappa \;;\quad {}^{t}\kappa = \frac{1}{3}\,{}^{t}\sigma_{y}^{2}$$

deviatoric stresses: ${}^{t}s_{ij} = {}^{t}\sigma_{ij} - \frac{{}^{t}\sigma_{mm}}{3}\,\delta_{ij}$

Transparency 17-41

Yield surface for plane stress

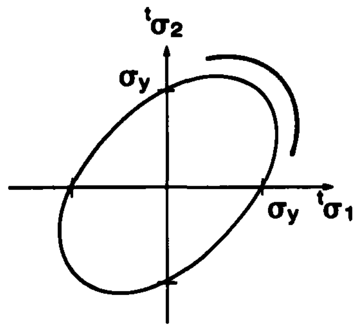

End view of yield surface

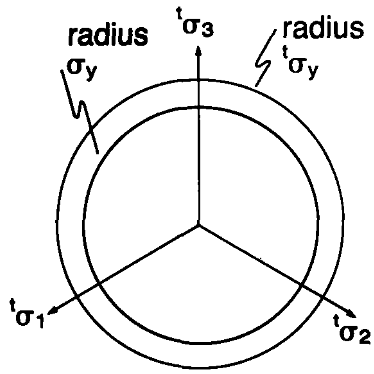

Transparency 17-42

We now compute the derivatives of the yield function.

First consider ${}^tp_{ij}$:

$$ {}^tp_{ij} = -\left.\frac{\partial\,{}^tF}{\partial\,{}^te^P_{ij}}\right|_{{}^t\sigma_{ij}\ \text{fixed}} = -\frac{\partial}{\partial\,{}^te^P_{ij}}\left(\frac{1}{2}\,{}^ts_{ij}\,{}^ts_{ij} - \frac{1}{3}\,{}^t\sigma_y^2\right) $$

$$ = \frac{2}{3}\,{}^t\sigma_y\,\frac{\partial\,{}^t\sigma_y}{\partial\,{}^te^P_{ij}} \qquad ({}^t\sigma_{ij}\ \text{fixed implies}\ {}^ts_{ij}\ \text{is fixed}) $$

Transparency 17-43

What is the relationship between ${}^t\sigma_y$ and the plastic strains?

We answer this question using the concept of "plastic work".

- The plastic work (per unit volume) is the amount of energy that is unrecoverable when the material is unloaded.
- This energy has been used in creating the plastic deformations within the material.

Transparency 17-44

- **Pictorially: 1-D example**

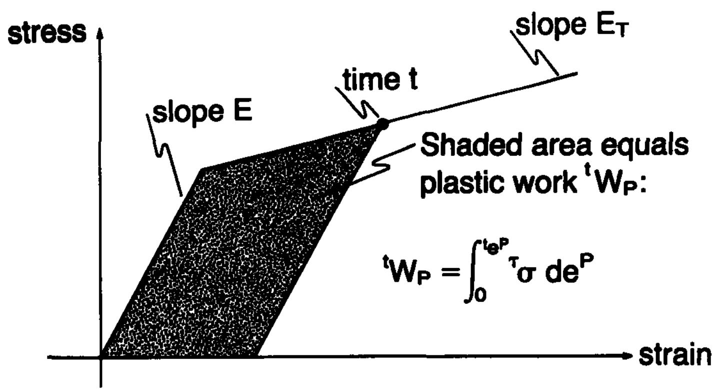

- **In general,** ${}^tW_P = \int_0^{{}^te^P_{ij}} {}^\tau\sigma_{ij} \, de^P_{ij}$

Transparency 17-45

Consider 1-D test results: the current yield stress may be written in terms of the plastic work.

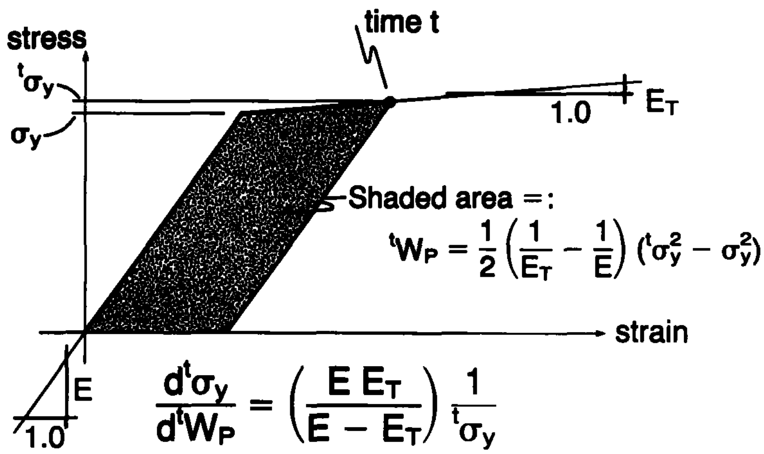

$$\frac{d\,{}^t\sigma_y}{d\,{}^tW_P} = \left(\frac{E\,E_T}{E - E_T}\right)\frac{1}{{}^t\sigma_y}$$

Transparency 17-46

We can now evaluate ${}^tp_{ij}$ – which corresponds to a generalization of the 1-D test results to multiaxial conditions.

$${}^tp_{ij} = \frac{2}{3}\,{}^t\sigma_y\,\underbrace{\left(\frac{d\,{}^t\sigma_y}{d\,{}^tW_P}\,\frac{\partial\,{}^tW_P}{\partial\,{}^te_{ij}^P}\right)}_{\frac{\partial\,{}^t\sigma_y}{\partial\,{}^te_{ij}^P}}$$

$$= \frac{2}{3}\,{}^t\sigma_y\left(\left(\frac{E\,E_T}{E - E_T}\right)\frac{1}{{}^t\sigma_y}\right)({}^t\sigma_{ij})$$

$$= \boxed{\frac{2}{3}\left(\frac{E\,E_T}{E - E_T}\right){}^t\sigma_{ij}}$$

Alternatively, we could have used that

$$d\,{}^t W_P = {}^t\bar{\sigma}\; d\,{}^t\bar{e}^P$$

where

$${}^t\bar{\sigma} = \sqrt{\frac{3}{2}\,{}^t s_{ij}\,{}^t s_{ij}} \quad \text{(effective stress)}$$

$$d\,{}^t\bar{e}^P = \sqrt{\frac{2}{3}\, de_{ij}^P\, de_{ij}^P}\,\Bigg|_t \quad \text{(increment in effective plastic strain)}$$

and then the same result is obtained using

$${}^t p_{ij} = \frac{2}{3}\,{}^t\sigma_y \left(\frac{d\,{}^t\sigma_y}{d\,{}^t\bar{e}^P}\,\frac{\partial\,{}^t\bar{e}^P}{\partial\,{}^t e_{ij}^P}\right)$$

Transparency 17-47

Next consider ${}^t q_{ij}$:

$${}^t q_{ij} = \frac{\partial\,{}^t F}{\partial\,{}^t\sigma_{ij}}\Bigg|_{{}^t e_{ij}^P \text{ fixed}} = \frac{\partial}{\partial\,{}^t\sigma_{ij}}\left(\frac{1}{2}\,{}^t s_{k\ell}\,{}^t s_{k\ell} - \frac{1}{3}\,{}^t\sigma_y^2\right)$$

$$= {}^t s_{k\ell}\,\frac{\partial\,{}^t s_{k\ell}}{\partial\,{}^t\sigma_{ij}} = {}^t s_{k\ell}\,\frac{\partial}{\partial\,{}^t\sigma_{ij}}\left({}^t\sigma_{k\ell} - \frac{{}^t\sigma_{mm}}{3}\,\delta_{k\ell}\right)$$

$$= {}^t s_{k\ell}\left(\delta_{ik}\,\delta_{j\ell} - \frac{\delta_{ij}\,\delta_{k\ell}}{3}\right)$$

$$= {}^t s_{ij} \quad \text{(note that } {}^t s_{k\ell}\,\delta_{k\ell} = {}^t s_{kk} = 0\text{)}$$

Transparency 17-48

Transparency 17-49

We can now evaluate $\underline{C}^{EP}$:

$$
\underline{C}^{EP} = \frac{E}{1+\nu}
\begin{array}{ccccc}
de_{11} & de_{22} & & 2\,de_{12} & \\
\end{array}
$$

$$
\left[
\begin{array}{ccccc}
\frac{1-\nu}{1-2\nu} - \beta({}^t s_{11})^2 & \frac{\nu}{1-2\nu} - \beta\, {}^t s_{11}\, {}^t s_{22} & \cdots & -\beta\, {}^t s_{11}\, {}^t s_{12} & \cdots \\
 & \frac{1-\nu}{1-2\nu} - \beta({}^t s_{22})^2 & \cdots & -\beta\, {}^t s_{22}\, {}^t s_{12} & \cdots \\
 & & \cdots & -\beta\, {}^t s_{33}\, {}^t s_{12} & \cdots \\
 \text{symmetric} & & & \frac{1}{2} - \beta({}^t s_{12})^2 & \cdots \\
 & & & & \cdots
\end{array}
\right]
$$

where $\beta = \frac{3}{2}\frac{1}{{}^t\sigma_y^2}\left(\frac{1}{1+\frac{2}{3}\frac{E\,E_T}{E-E_T}\frac{1+\nu}{E}}\right)$

Transparency 17-50

Evaluation of the stresses at time $t+\Delta t$:

$$
{}^{t+\Delta t}\underline{\sigma} = {}^t\underline{\sigma} + \int_t^{t+\Delta t} d\underline{\sigma}
$$

$$
= {}^t\underline{\sigma} + \int_{{}^t\underline{e}}^{{}^{t+\Delta t}\underline{e}} \underline{C}^{EP}\, d\underline{e}
$$

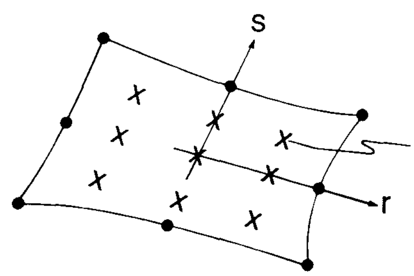

The stress integration must be performed at each Gauss integration point.

Transparency 17-51

We can approximate the evaluation of this integral using the Euler forward method.

- Without subincrementation:

$$\int_{{}^{t}\underline{e}}^{{}^{t+\Delta t}\underline{e}} \underline{C}^{EP}\, d\underline{e} \doteq \underline{C}^{EP}\Big|_{t} \underbrace{\Delta \underline{e}}_{{}^{t+\Delta t}\underline{e} - {}^{t}\underline{e}}$$

Transparency 17-52

- With n subincrements:

$$\int_{{}^{t}\underline{e}}^{{}^{t+\Delta t}\underline{e}} \underline{C}^{EP}\, d\underline{e} \doteq \underline{C}^{EP}\Big|_{t} \frac{\Delta \underline{e}}{n}$$

$$+ \underline{C}^{EP}\Big|_{t+\underbrace{\Delta\tau}_{\frac{\Delta t}{n}}} \frac{\Delta \underline{e}}{n}$$

$$+ \cdots$$

$$+ \underline{C}^{EP}\Big|_{t+(n-1)\Delta\tau} \frac{\Delta \underline{e}}{n}$$

Transparency 17-53

Pictorially:

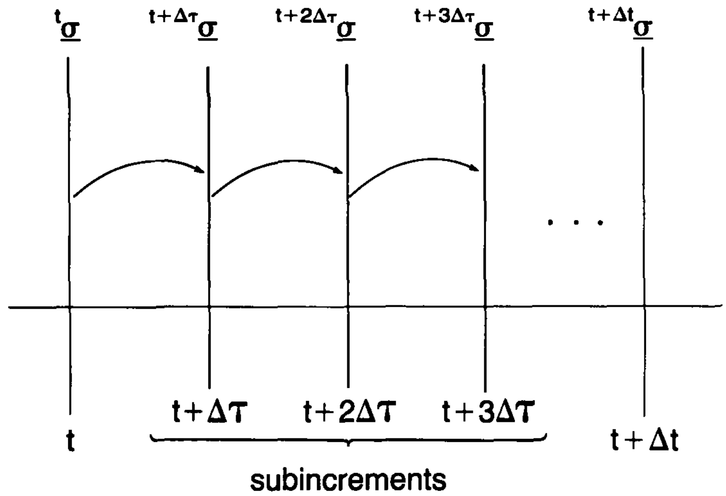

Transparency 17-54

Summary of the procedure used to calculate the total stresses at time $t+\Delta t$.

Given:

STRAIN = Total strains at time $t+\Delta t$

SIG = Total stresses at time t

EPS = Total strains at time t

(a) Calculate the strain increment DELEPS:

DELEPS = STRAIN − EPS

(b) Calculate the stress increment DELSIG, assuming elastic behavior:

$$\text{DELSIG} = C^E * \text{DELEPS}$$

(c) Calculate TAU, assuming elastic behavior:

$$\text{TAU} = \text{SIG} + \text{DELSIG}$$

(d) With TAU as the state of stress, calculate the value of the yield function F.

(e) If F(TAU) ≤ 0, the strain increment is elastic. In this case, TAU is correct; we return.

Transparency 17-55

(f) If the previous state of stress was plastic, set RATIO to zero and go to (g). Otherwise, there is a transition from elastic to plastic and RATIO (the portion of incremental strain taken elastically) has to be determined. RATIO is determined from

$$F\,(\text{SIG} + \text{RATIO} * \text{DELSIG}) = 0$$

since F = 0 signals the initiation of yielding.

Transparency 17-56

Transparency 17-57

(g) Redefine TAU as the stress at start of yield

$$\text{TAU} = \text{SIG} + \text{RATIO} * \text{DELSIG}$$

and calculate the elastic-plastic strain increment

$$\text{DEPS} = (1 - \text{RATIO}) * \text{DELEPS}$$

(h) Divide DEPS into subincrements DDEPS and calculate

$$\text{TAU} \leftarrow \text{TAU} + \underline{C}^{EP} * \text{DDEPS}$$

for all elastic-plastic strain subincrements.

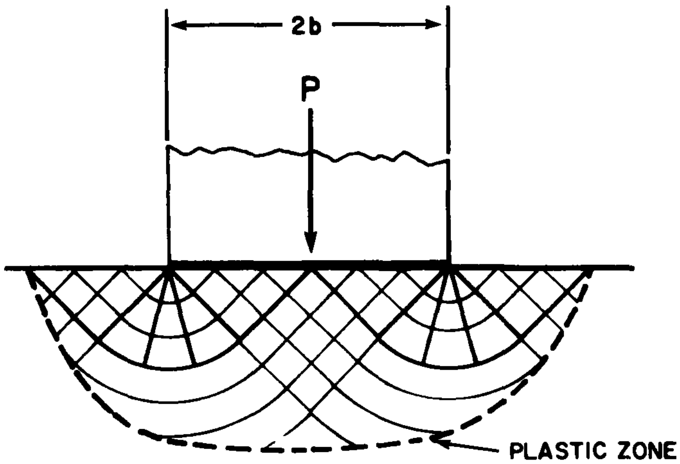

Plane strain punch problem

Slide 17-1

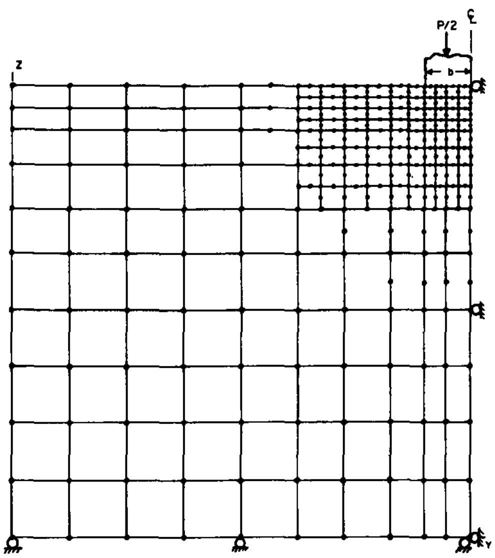

Finite element model of punch problem

Slide 17-2

Slide 17-3

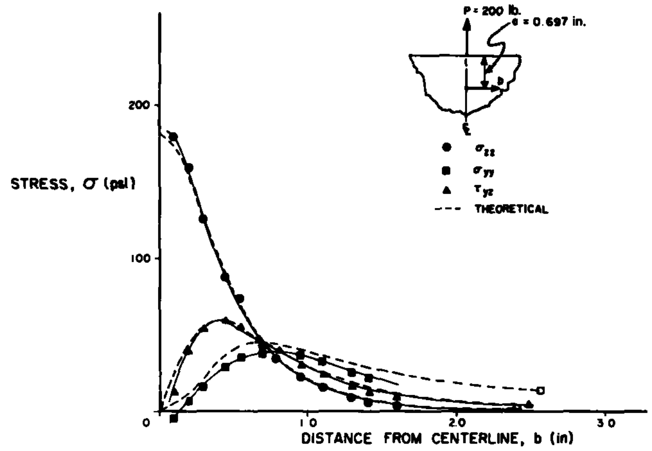

Solution of Boussinesq problem—2 pt. integration

Slide 17-4

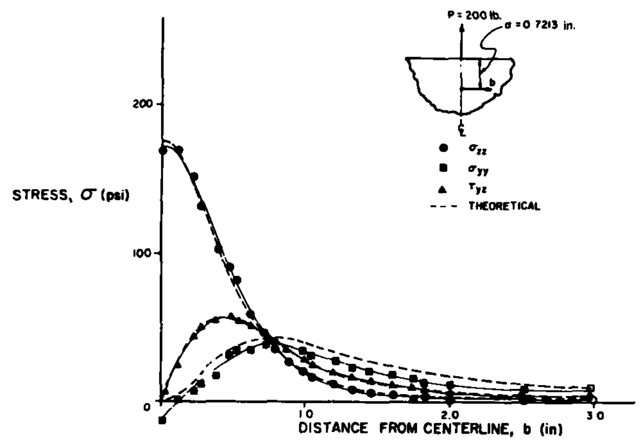

Solution of Boussinesq problem—3 pt. Integration

Slide 17-5

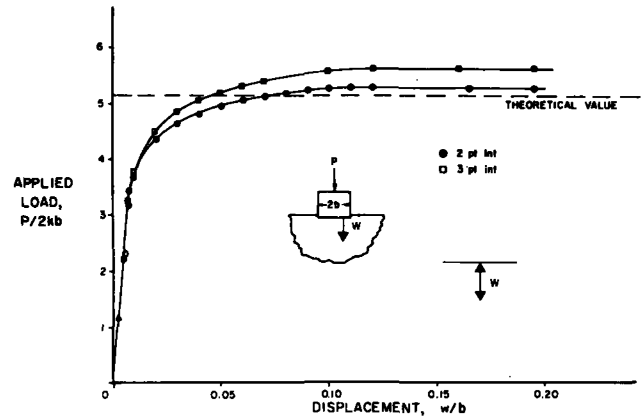

Load-displacement curves for punch problem

Transparency 17-58

Limit load calculations:

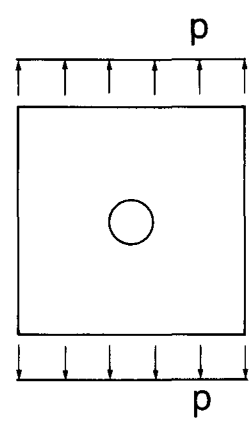

- Plate is elasto-plastic.

Transparency 17-59

Elasto-plastic analysis:

Material properties (steel)

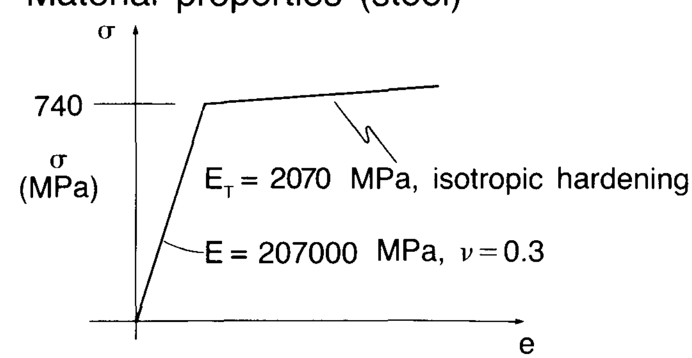

- This is an idealization, probably inaccurate for large strain conditions ($e > 2\%$).

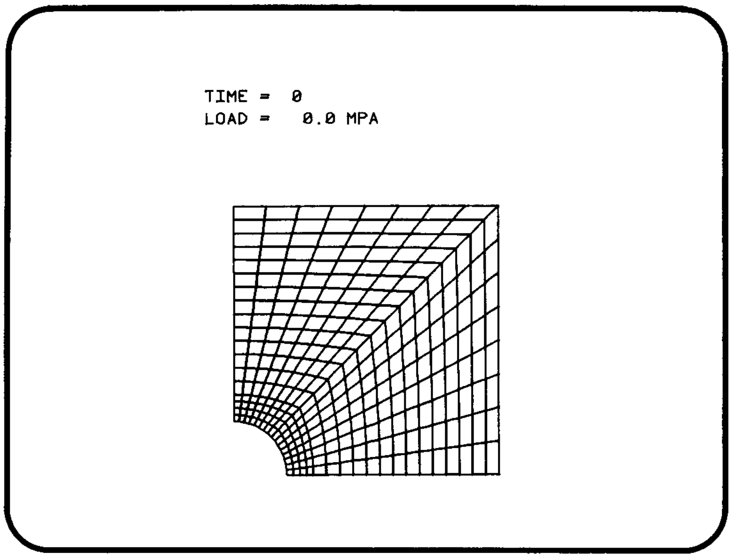

Computer Animation
Plate with hole

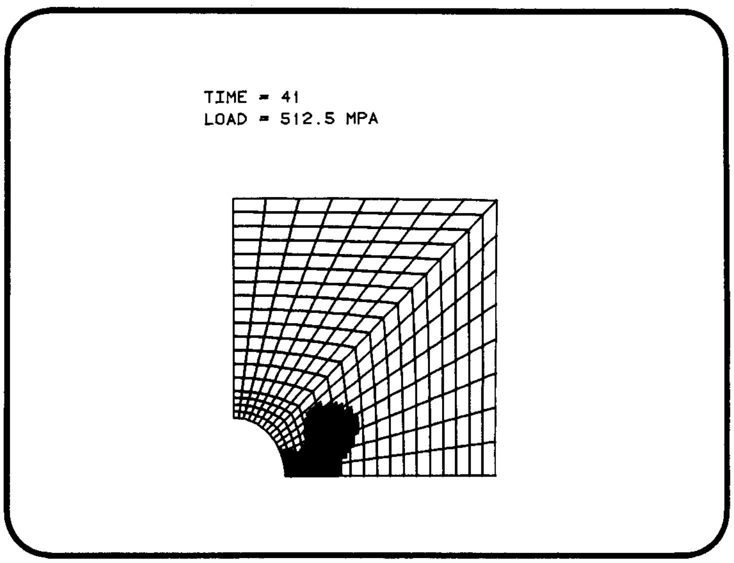

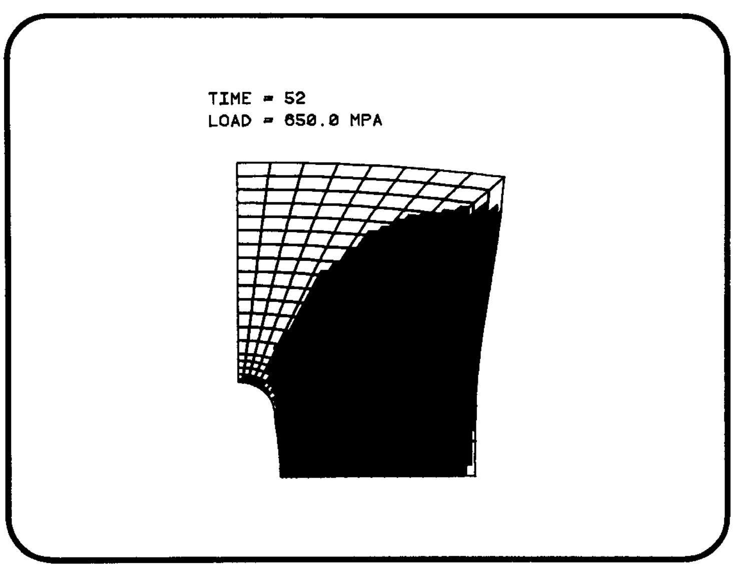

Topic 18

Modeling of Elasto-Plastic and Creep Response—Part II

Contents:

- **Strain formulas to model creep strains**
- **Assumption of creep strain hardening for varying stress situations**
- **Creep in multiaxial stress conditions, use of effective stress and effective creep strain**
- **Explicit and implicit integration of stress**
- **Selection of size of time step in stress integration**
- **Thermo-plasticity and creep, temperature-dependency of material constants**
- **Example analysis: Numerical uniaxial creep results**
- **Example analysis: Collapse analysis of a column with offset load**
- **Example analysis: Analysis of cylinder subjected to heat treatment**

Textbook: Section 6.4.2

References: The computations in thermo-elasto-plastic-creep analysis are described in

Snyder, M. D., and K. J. Bathe, "A Solution Procedure for Thermo-Elastic-Plastic and Creep Problems," *Nuclear Engineering and Design, 64*, 49–80, 1981.

Cesar, F., and K. J. Bathe, "A Finite Element Analysis of Quenching Processes," in *Numerical Methods for Non-Linear Problems*, (Taylor, C., et al. eds.), Pineridge Press, 1984.

References:
(continued)

The effective-stress-function algorithm is presented in

Bathe, K. J., M. Kojić, and R. Slavković, "On Large Strain Elasto-Plastic and Creep Analysis," in *Finite Element Methods for Nonlinear Problems* (Bergan, P. G., K. J. Bathe, and W. Wunderlich, eds.), Springer-Verlag, 1986.

The cylinder subjected to heat treatment is considered in

Rammerstorfer, F. G., D. F. Fischer, W. Mitter, K. J. Bathe, and M. D. Snyder, "On Thermo-Elastic-Plastic Analysis of Heat-Treatment Processes Including Creep and Phase Changes," *Computers & Structures, 13*, 771–779, 1981.

Transparency 18-1

CREEP

We considered already uniaxial constant stress conditions. A typical creep law used is the power creep law $e^C = a_0 \sigma^{a_1} t^{a_2}$.

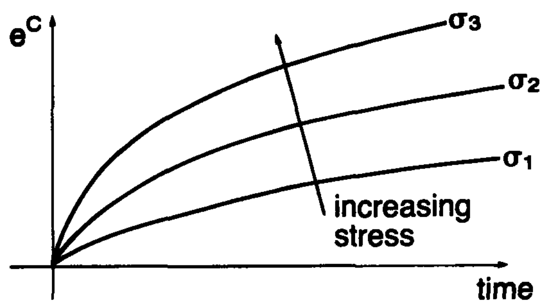

Transparency 18-2

Aside: other possible choices for the creep law are

- $e^C = a_0 \exp(a_1 \sigma)\left[1 - \exp\left(-a_2\left(\frac{\sigma}{a_3}\right)^{a_4} t\right)\right] + a_5\, t \exp(a_6\, \sigma)$
- $e^C = (a_0\, (\sigma)^{a_1})\, (t^{a_2} + a_3 t^{a_4} + a_5 t^{a_6}) \exp\left(\frac{-a_7}{\underbrace{{}^t\theta}_{\text{temperature, in degrees C}} + 273.16}\right)$

We will not discuss these choices further.

Transparency 18-3

The creep strain formula $e^C = a_0\, \sigma^{a_1}\, t^{a_2}$ cannot be directly applied to varying stress situations because the stress history does not enter directly into the formula.

Transparency 18-4

Example:

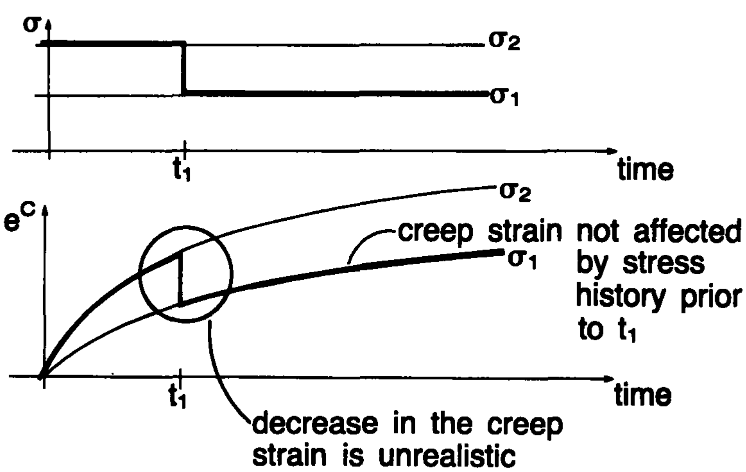

The assumption of strain hardening:

- The material creep behavior depends only on the current stress level and the accumulated total creep strain.
- To establish the ensuing creep strain, we solve for the "effective time" using the creep law:

$$ {}^{t}e^{C} = a_0 \, {}^{t}\sigma^{a_1} \, \bar{t}^{a_2} $$

totally unrelated to the physical time

(solve for $\bar{t}$)

Transparency 18-5

The effective time is now used in the creep strain rate formula:

$$ {}^{t}\dot{e}^{C} = a_0 \, {}^{t}\sigma^{a_1} \, a_2 \, \bar{t}^{a_2-1} $$

$$ = a_0^{1/a_2} \, a_2 \, ({}^{t}\sigma)^{a_1/a_2} \, ({}^{t}e^{C})^{\frac{a_2-1}{a_2}} $$

Now the creep strain rate depends on the current stress level and on the accumulated total creep strain.

Transparency 18-6

Transparency 18-7

Pictorially:

• Decrease in stress

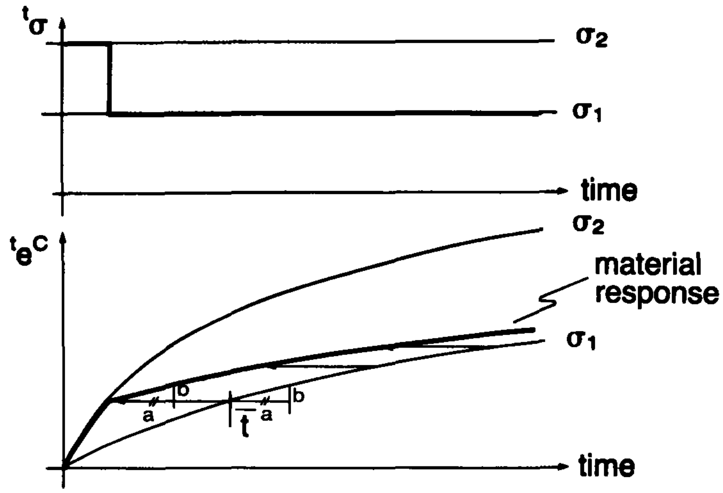

Transparency 18-8

• Increase in stress

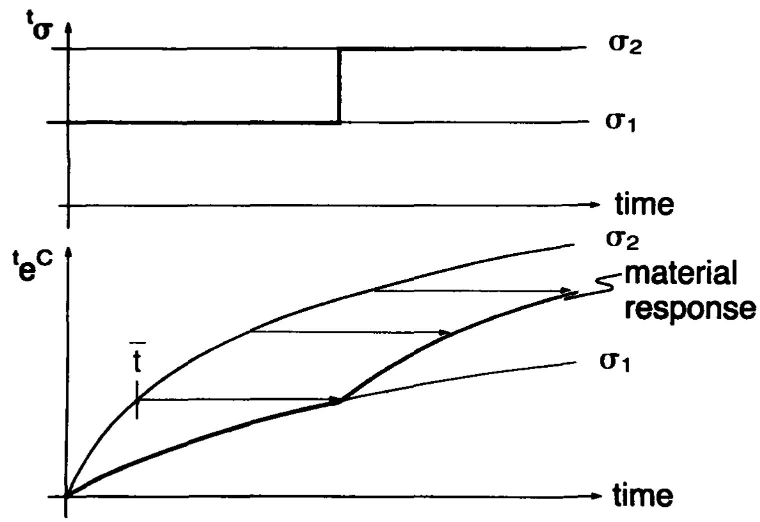

- Reverse in stress (cyclic conditions)

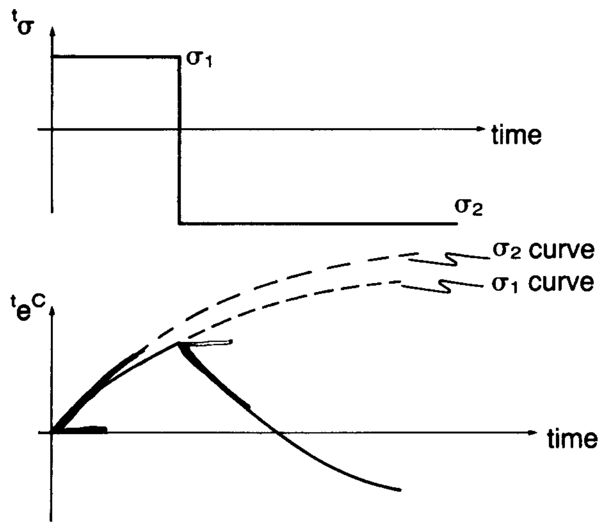

Transparency 18-9

MULTIAXIAL CREEP

The response is now obtained using

$$^{t+\Delta t}\underline{\sigma} = {}^{t}\underline{\sigma} + \int_{^{t}\underline{e}}^{^{t+\Delta t}\underline{e}} \underline{C}^{E}\, d\,(\underline{e} - \underline{e}^{C})$$

As in plasticity, the creep strains in multiaxial conditions are obtained by a generalization of the 1-D test results.

Transparency 18-10

Transparency 18-11

We define

$$^{t}\bar{\sigma} = \sqrt{\frac{3}{2}\,{}^{t}s_{ij}\,{}^{t}s_{ij}} \qquad \text{(effective stress)}$$

$$^{t}\bar{e}^{C} = \sqrt{\frac{2}{3}\,{}^{t}e^{C}_{ij}\,{}^{t}e^{C}_{ij}} \qquad \text{(effective strain)}$$

and use these in the uniaxial creep law:

$$\bar{e}^{C} = a_0\,\bar{\sigma}^{a_1}\,\bar{t}^{a_2}$$

Transparency 18-12

The assumption that the creep strain rates are proportional to the current deviatoric stresses gives

$$^{t}\dot{e}^{C}_{ij} = {}^{t}\gamma\,{}^{t}s_{ij} \quad \text{(as in von Mises plasticity)}$$

$^{t}\gamma$ is evaluated in terms of the effective stress and effective creep strain rate:

$$^{t}\gamma = \frac{3}{2}\frac{^{t}\dot{\bar{e}}^{C}}{^{t}\bar{\sigma}}$$

$$({}^{t}\dot{\bar{e}}^{C} = a_0\,a_2\,({}^{t}\bar{\sigma})^{a_1}\,(\bar{t})^{a_2-1})$$

Using matrix notation,

$$d\underline{e}^C = ({}^t\gamma)\,\underbrace{(\underline{D}\,{}^t\underline{\sigma})}_{\substack{\text{deviatoric}\\ \text{stresses}}}\,dt$$

For 3-D analysis,

$$\underline{D} = \begin{bmatrix} \frac{2}{3} & -\frac{1}{3} & -\frac{1}{3} & & & \\ & \frac{2}{3} & -\frac{1}{3} & & & \\ & & \frac{2}{3} & & & \\ & & & 1 & & \\ & \text{symmetric} & & & 1 & \\ & & & & & 1 \end{bmatrix}$$

Transparency 18-13

- In creep problems, the time integration is difficult due to the high exponent on the stress.
- Solution instability arises if the Euler forward integration is used and the time step Δt is too large.
  — Rule of thumb:

$$\Delta\bar{\underline{e}}^C \leq \frac{1}{10}\,({}^t\bar{\underline{e}}^E)$$

- Alternatively, we can use implicit integration, using the α-method:

$${}^{t+\alpha\Delta t}\underline{\sigma} = (1-\alpha)\,{}^t\underline{\sigma} + \alpha\,{}^{t+\Delta t}\underline{\sigma}$$

Transparency 18-14

Transparency 18-15

Iteration algorithm:

$$^{t+\Delta t}\underline{\sigma}_{(k)}^{(i-1)} = {}^{t}\underline{\sigma} + \underline{C}^{E}\left[\underline{e}^{(i-1)} - \Delta t\ {}^{t+\alpha\Delta t}\gamma_{(k-1)}^{(i-1)}\ (\underline{D}\ {}^{t+\alpha\Delta t}\underline{\sigma}_{(k-1)}^{(i-1)})\right]$$

k = iteration counter at each integration point

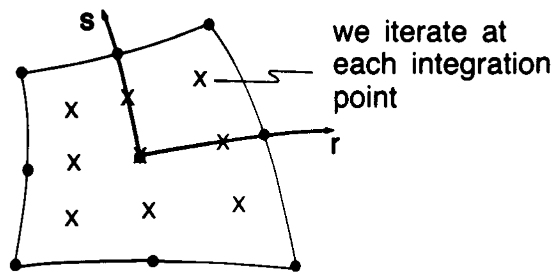

Transparency 18-16

- $\alpha \geq \frac{1}{2}$ gives a stable integration algorithm. We use largely $\alpha = 1.0$.
- In practice, a form of Newton-Raphson iteration to accelerate convergence of the iteration can be used.

Transparency 18-17

- Choice of time step Δt is now governed by need to converge in the iteration and accuracy considerations.
- Subincrementation can be employed.
- Relatively large time steps can be used with the effective-stress-function algorithm.

Transparency 18-18

THERMO-PLASTICITY-CREEP

Plasticity:

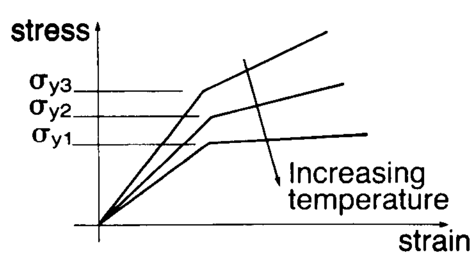

Creep:

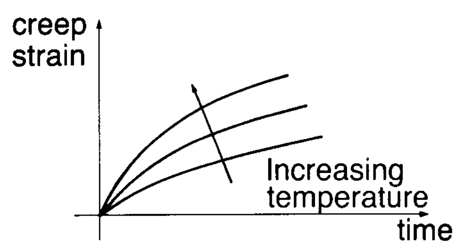

Transparency 18-19

Now we evaluate the stresses using

$$^{t+\Delta t}\underline{\sigma} = {}^{t}\underline{\sigma} + \int_{^{t}\underline{e}}^{^{t+\Delta t}\underline{e}} {}^{\tau}\underline{C}^{E}\, d(\underline{e} - \underline{e}^{P} - \underline{e}^{C} - \underbrace{\underline{e}^{TH}}_{\text{thermal strains}})$$

Using the α-method,

$$^{t+\Delta t}\underline{\sigma} = {}^{t+\Delta t}\underline{C}^{E}\{[\underline{e} - \underline{e}^{P} - \underline{e}^{C} - \underline{e}^{TH}] + [{}^{t}\underline{e} - {}^{t}\underline{e}^{P} - {}^{t}\underline{e}^{C} - {}^{t}\underline{e}^{TH}]\}$$

where

$$\underline{e} = {}^{t+\Delta t}\underline{e} - {}^{t}\underline{e}$$

Transparency 18-20

and

$$\underline{e}^{P} = \Delta t\, ({}^{t+\alpha\Delta t}\bar{\lambda})\, (\underline{D}\; {}^{t+\alpha\Delta t}\underline{\sigma})$$

$$\underline{e}^{C} = \Delta t\, ({}^{t+\alpha\Delta t}\gamma)\, (\underline{D}\; {}^{t+\alpha\Delta t}\underline{\sigma})$$

$$e_{ij}^{TH} = ({}^{t+\Delta t}\alpha\; {}^{t+\Delta t}\theta - {}^{t}\alpha\; {}^{t}\theta)\, \delta_{ij}$$

where

${}^{t}\alpha$ = coefficient of thermal expansion at time t

${}^{t}\theta$ = temperature at time t

Transparency 18-21

The final iterative equation is

$$
\begin{aligned}
{}^{t+\Delta t}\underline{\sigma}^{(i-1)}_{(k)} = \underline{C}^{E}\Big|_{t+\Delta t} \Big[& {}^{t+\Delta t}\underline{e}^{(i-1)} - {}^{t}\underline{e}^{P} - {}^{t}\underline{e}^{C} - {}^{t}\underline{e}^{TH} \\
& - \Delta t \left({}^{t+\alpha\Delta t}\bar{\lambda}^{(i-1)}_{(k-1)}\right) \left(\underline{D}\ {}^{t+\alpha\Delta t}\underline{\sigma}^{(i-1)}_{(k-1)}\right) \\
& - \Delta t \left({}^{t+\alpha\Delta t}\gamma^{(i-1)}_{(k-1)}\right) \left(\underline{D}\ {}^{t+\alpha\Delta t}\underline{\sigma}^{(i-1)}_{(k-1)}\right) \\
& - \underline{e}^{TH} \Big]
\end{aligned}
$$

and subincrementation may also be used.

Transparency 18-22

Numerical uniaxial creep results:

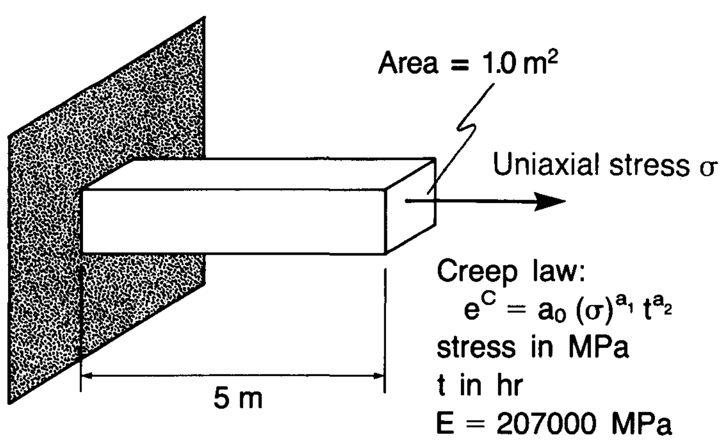

Creep law:

$e^C = a_0 (\sigma)^{a_1} t^{a_2}$

stress in MPa

t in hr

E = 207000 MPa

$\nu = 0.3$

Transparency 18-23

The results are obtained using two solution algorithms:

- $\alpha = 0$, (no subincrementation)
- $\alpha = 1$, effective-stress-function procedure

In all cases, the MNO formulation is employed. Full Newton iterations without line searches are used with

ETOL = 0.001
RTOL = 0.01
RNORM = 1.0 MN

Transparency 18-24

1) Constant load of 100 MPa

$$e^C = 4.1 \times 10^{-11} (\sigma)^{3.15} t^{0.8}$$

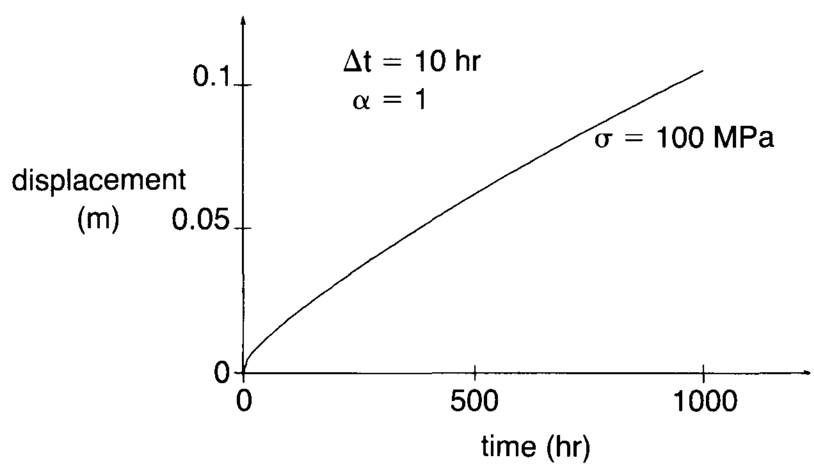

2) Stress increase from 100 MPa to 200 MPa

$$e^C = 4.1 \times 10^{-11} (\sigma)^{3.15} t^{0.8}$$

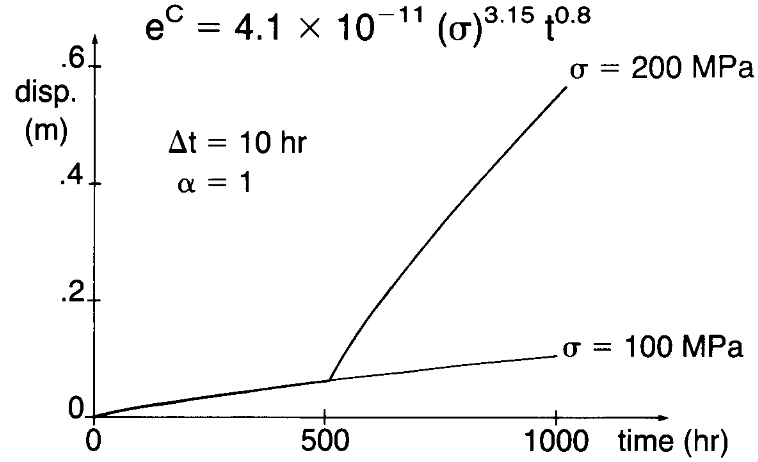

Transparency 18-25

Load function employed:

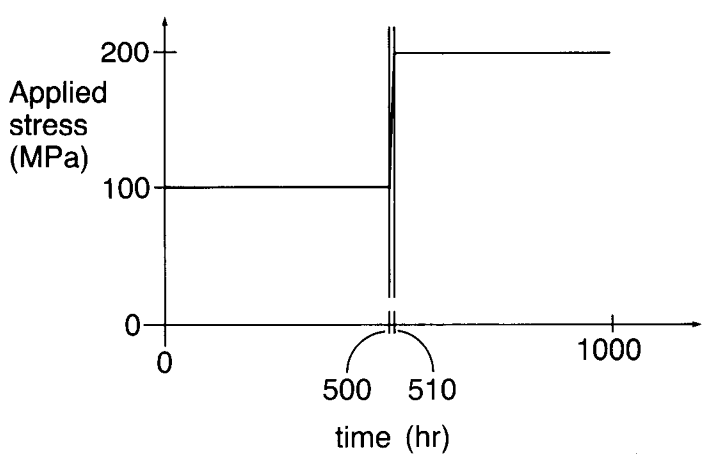

Transparency 18-26

Transparency 18-27

3) Stress reversal from 100 MPa to −100 MPa

$$e^C = 4.1 \times 10^{-11} (\sigma)^{3.15} t^{0.8}$$

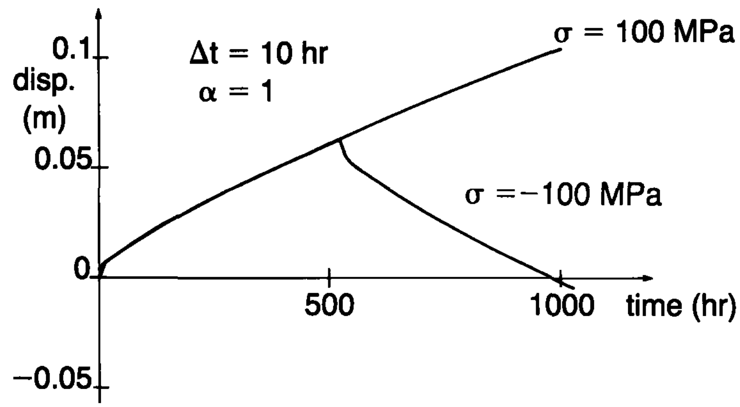

Transparency 18-28

4) Constant load of 100 MPa

$$e^C = 4.1 \times 10^{-11} (\sigma)^{3.15} t^{0.4}$$

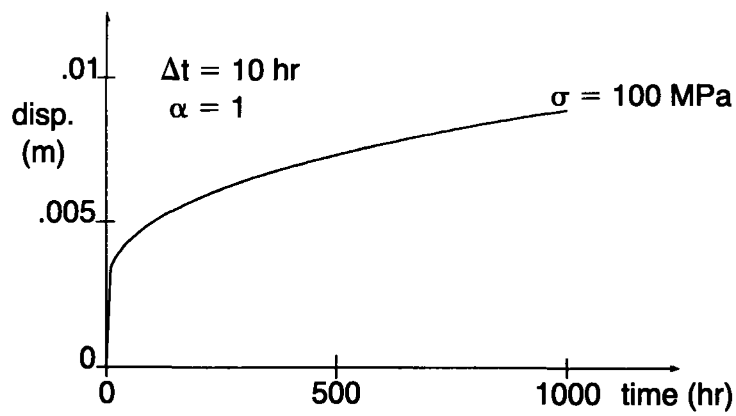

5) Stress increase from 100 MPa to 200 MPa

$$e^C = 4.1 \times 10^{-11} (\sigma)^{3.15} t^{0.4}$$

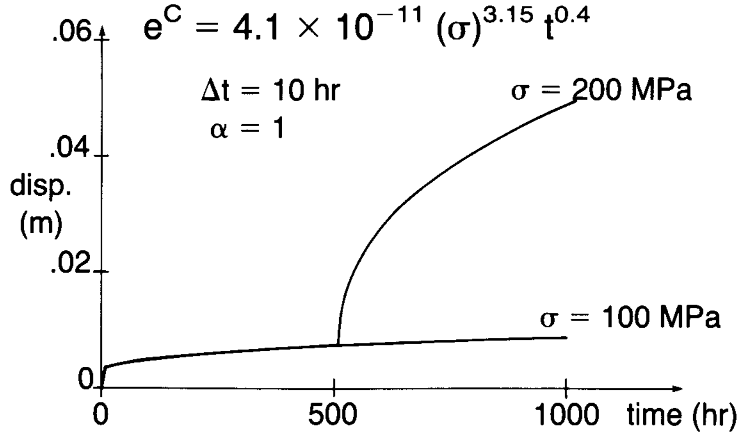

Transparency 18-29

6) Stress reversal from 100 MPa to −100 MPa

$$e^C = 4.1 \times 10^{-11} (\sigma)^{3.15} t^{0.4}$$

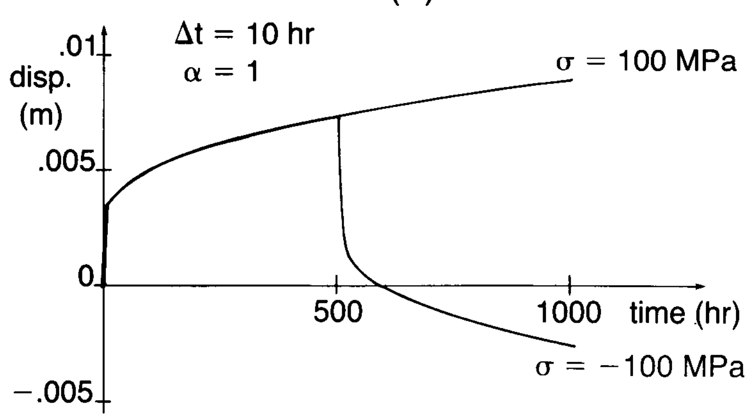

Transparency 18-30

Transparency 18-31

Consider the use of $\alpha = 0$ for the "stress increase from 100 MPa to 200 MPa" problem solved earlier (case #5):

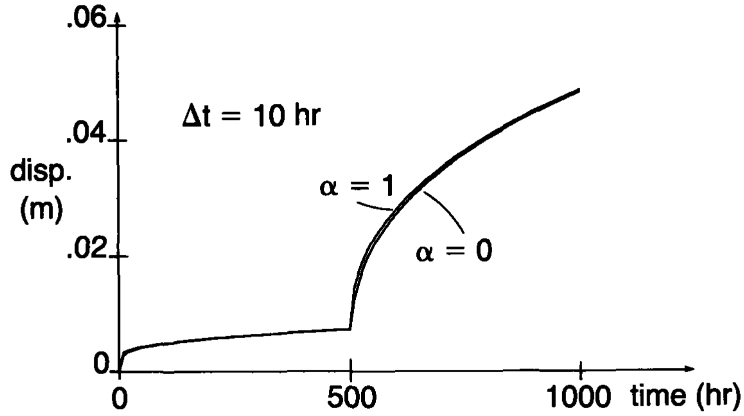

Transparency 18-32

Using $\Delta t = 50$ hr, both algorithms converge, although the solution becomes less accurate for $\alpha = 0$.

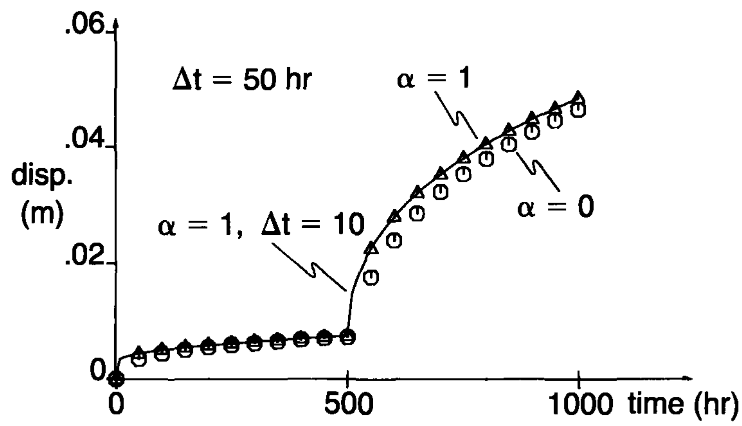

Using $\Delta t = 100$ hr, $\alpha = 0$ does not converge at $t = 600$ hr. $\alpha = 1$ still gives good results.

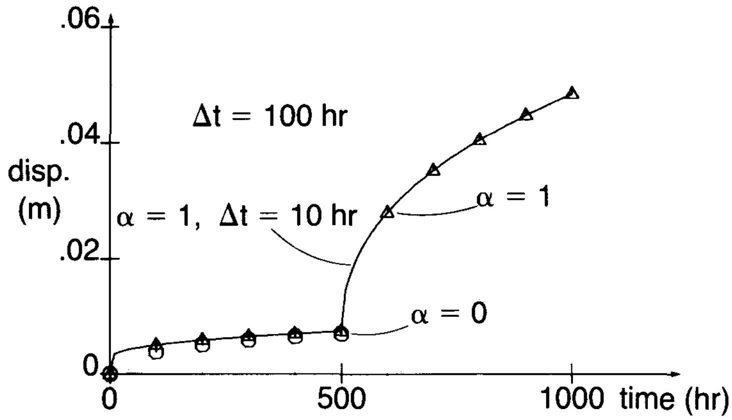

Transparency 18-33

Example: Column with offset load

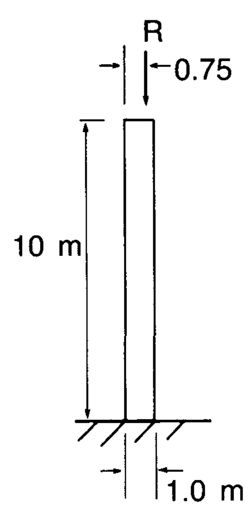

$E = 2 \times 10^6$ KPa
$\nu = 0.0$
plane stress
thickness = 1.0 m

Euler buckling load = 4100 KN

Transparency 18-34

Transparency 18-35

Goal: Determine the collapse response for different material assumptions:

— Elastic

— Elasto-plastic

— Creep

The total Lagrangian formulation is employed for all analyses.

Transparency 18-36

Solution procedure:

- The full Newton method without line searches is employed with

  ETOL = 0.001

  RTOL = 0.01

  RNORM = 1000 KN

Mesh used: Ten 8-node quadrilateral elements

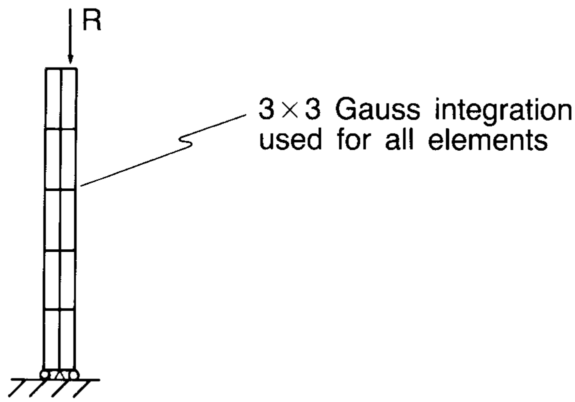

Transparency 18-37

Elastic response: We assume that the material law is approximated by

$${}_0^tS_{ij} = {}_0^tC_{ijrs}\ {}_0^t\varepsilon_{rs}$$

where the components ${}_0^tC_{ijrs}$ are constants determined by E and ν (as previously described).

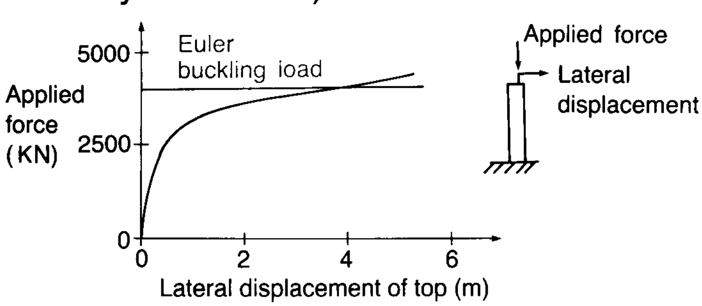

Transparency 18-38

Transparency 18-39

Elasto-plastic response: Here we use

$E_T = 0$

$\sigma_y = 3000$ KPa (von Mises yield criterion)

and

$$ {}^{t+\Delta t}_{0}\underline{S} = {}^{t}_{0}\underline{S} + \int_{{}^{t}_{0}\underline{\varepsilon}}^{{}^{t+\Delta t}_{0}\underline{\varepsilon}} {}_{0}\underline{C}^{EP}\, d_0\underline{\varepsilon} $$

where ${}_{0}\underline{C}^{EP}$ is the incremental elasto-plastic constitutive matrix.

Transparency 18-40

Plastic buckling is observed.

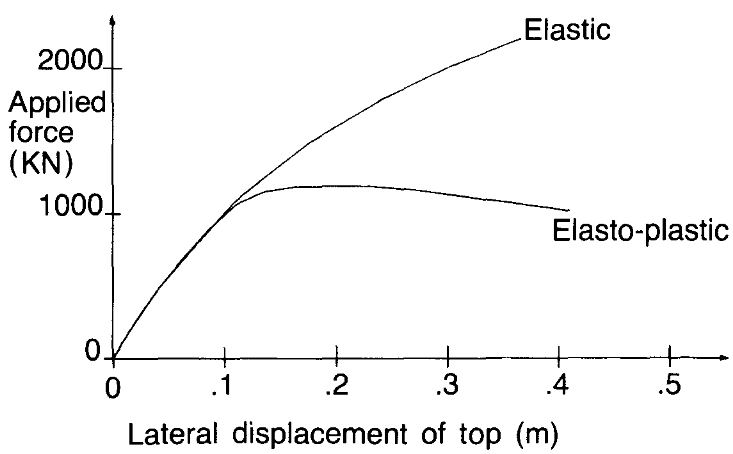

Creep response:

- Creep law: $\bar{e}^C = 10^{-16}(\bar{\sigma})^3 t$ (t in hours)
  No plasticity effects are included.
- We apply a constant load of 2000 KN and determine the time history of the column.
- For the purposes of this problem, the column is considered to have collapsed when a lateral displacement of 2 meters is reached. This corresponds to a total strain of about 2 percent at the base of the column.

Transparency 18-41

We investigate the effect of different time integration procedures on the obtained solution:

- Vary Δt ($\Delta t = .5, 1, 2, 5$ hr.)
- Vary α ($\alpha = 0, 0.5, 1$)

Transparency 18-42

Transparency 18-43

Collapse times: The table below lists the first time (in hours) for which the lateral displacement of the column exceeds 2 meters.

	$\alpha=0$	$\alpha=.5$	$\alpha=1$
$\Delta t=.5$	100.0	100.0	98.5
$\Delta t=1$	101	101	98
$\Delta t=2$	102	102	96
$\Delta t=5$	105	105	90

Transparency 18-44

Pictorially, using $\Delta t=0.5$ hr., $\alpha=0.5$, we have

Time = 1 hr (negligible creep effects)	Time = 50 hr (some creep effects)	Time = 100 hr (collapse)

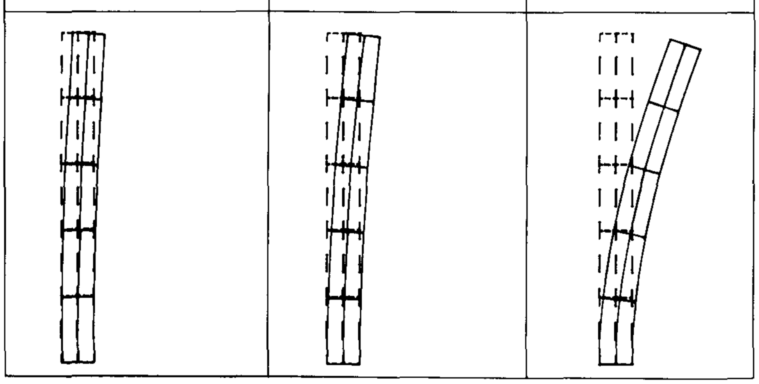

Choose $\Delta t = 0.5$ hr.
— All solution points are connected with straight lines.

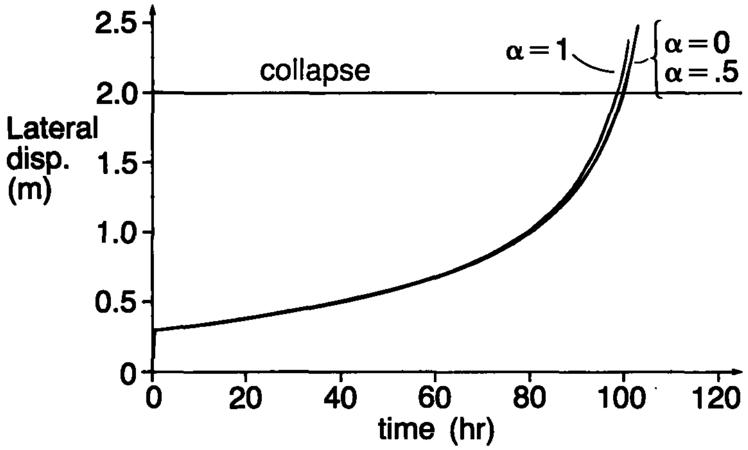

Transparency 18-45

Effect of α: Choose $\Delta t = 5$ hr.
— All solution points are connected with straight lines.

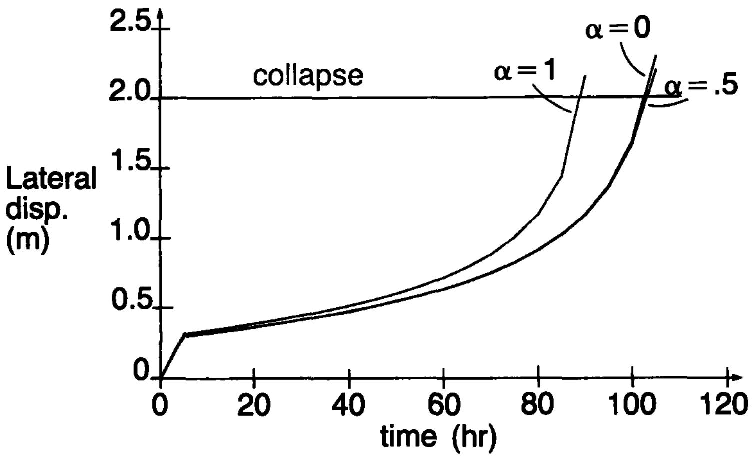

Transparency 18-46

Transparency 18-47

We conclude for this problem:

- As the time step is reduced, the collapse times given by $\alpha=0$, $\alpha=.5$, $\alpha=1$ become closer. For $\Delta t=.5$, the difference in collapse times is less than 2 hours.
- For a reasonable choice of time step, solution instability is not a problem.

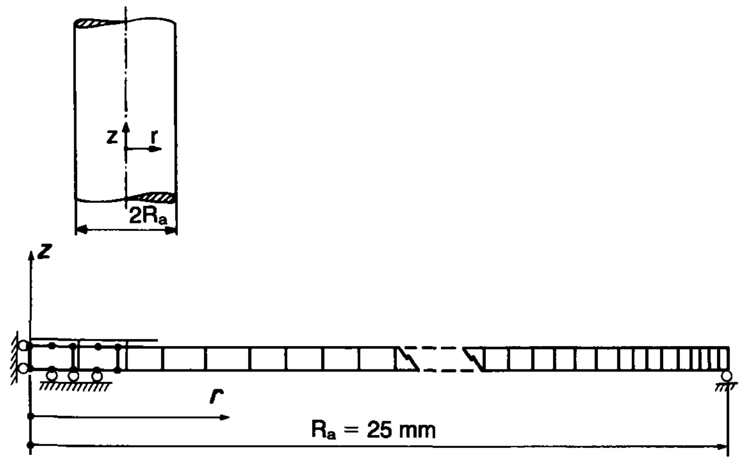

Analysis of a cylinder subjected to heat treatment

Slide 18-1

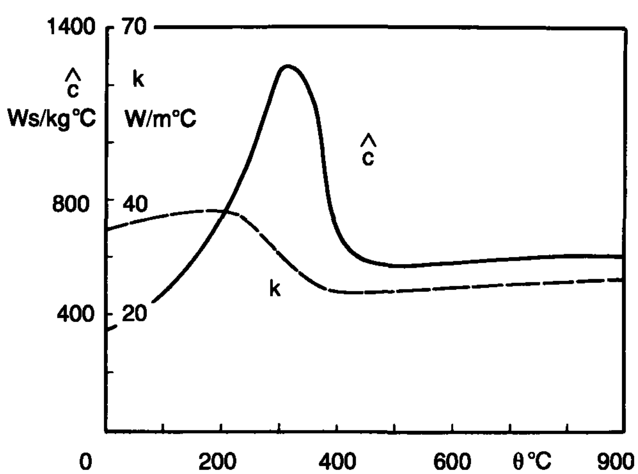

Temperature-dependence of the specific heat, $\hat{c}$, and the heat conduction coefficient, k.

Slide 18-2

Slide 18-3

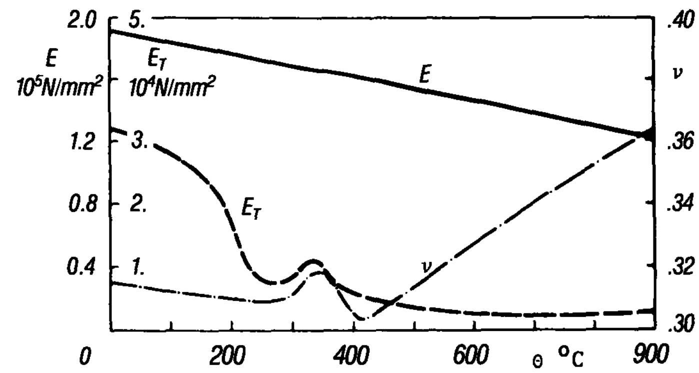

Temperature-dependence of the Young's modulus, E, Poisson's ratio, ν, and hardening modulus, E_T

Slide 18-4

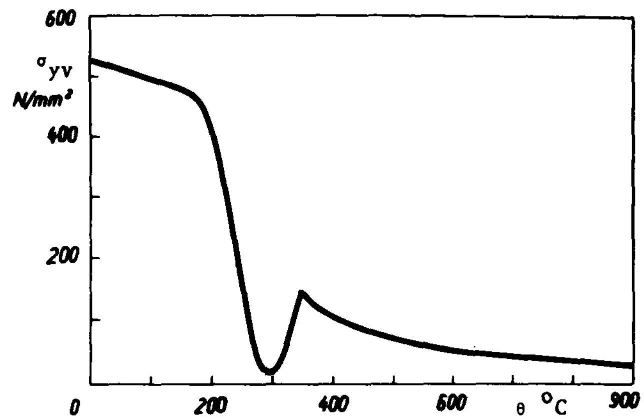

Temperature-dependence of the material yield stress

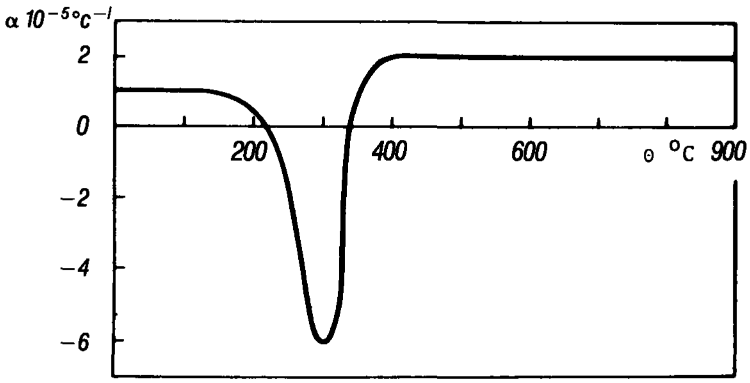

Temperature-dependence of the instantaneous coefficient of thermal expansion (including volume change due to phase transformation), α

Slide 18-5

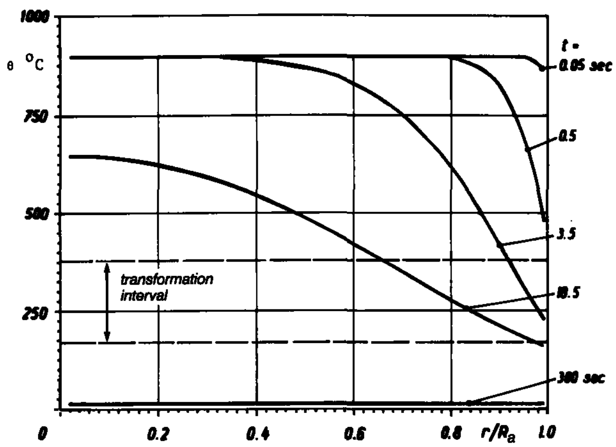

The calculated transient temperature field

Slide 18-6

Slide 18-7

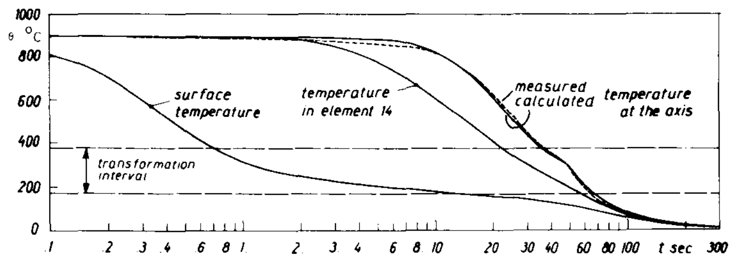

Surface and core temperature; comparison between measured and calculated results

Slide 18-8

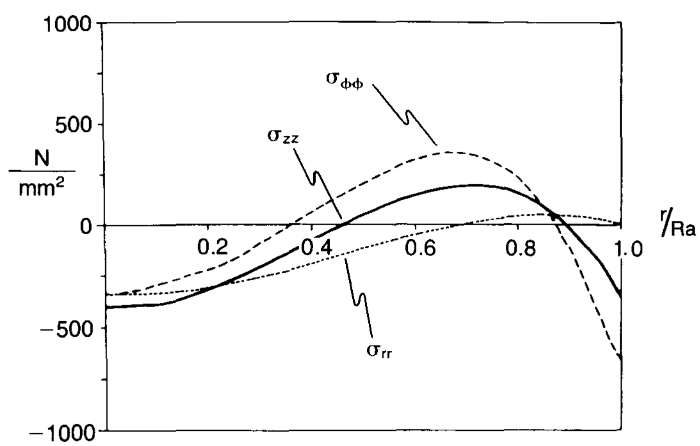

Measured residual stress field

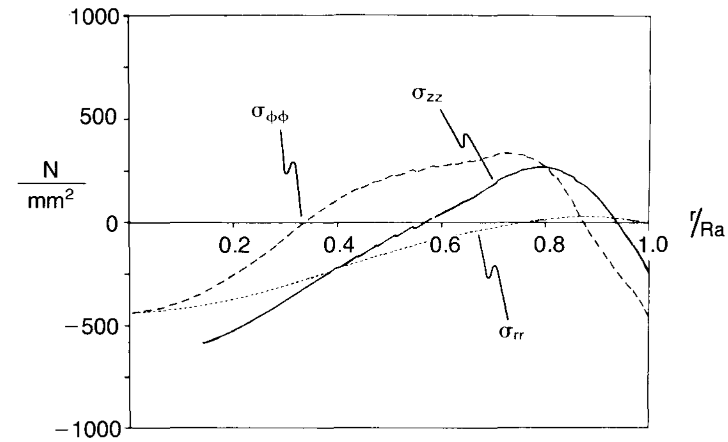

Calculated residual stress field

Slide 18-9

Topic 19

Beam, Plate, and Shell Elements—Part I

Contents:

- **Brief review of major formulation approaches**
- **The degeneration of a three-dimensional continuum to beam and shell behavior**
- **Basic kinematic and static assumptions used**
- **Formulation of isoparametric (degenerate) general shell elements of variable thickness for large displacements and rotations**
- **Geometry and displacement interpolations**
- **The nodal director vectors**
- **Use of five or six nodal point degrees of freedom, theoretical considerations and practical use**
- **The stress-strain law in shell analysis, transformations used at shell element integration points**
- **Shell transition elements, modeling of transition zones between solids and shells, shell intersections**

Textbook: Sections 6.3.4, 6.3.5

References:

The (degenerate) isoparametric shell and beam elements, including the transition elements, are presented and evaluated in

Bathe, K. J., and S. Bolourchi, "A Geometric and Material Nonlinear Plate and Shell Element," *Computers & Structures, 11*, 23–48, 1980.

Bathe, K. J., and L. W. Ho, "Some Results in the Analysis of Thin Shell Structures," in *Nonlinear Finite Element Analysis in Structural Mechanics*, (Wunderlich, W., et al., eds.), Springer-Verlag, 1981.

Bathe, K. J., E. Dvorkin, and L. W. Ho, "Our Discrete Kirchhoff and Isoparametric Shell Elements for Nonlinear Analysis—An Assessment," *Computers & Structures, 16*, 89–98, 1983.

References:
(continued)

The triangular flat plate/shell element is presented and also studied in

Bathe, K. J., and L. W. Ho, "A Simple and Effective Element for Analysis of General Shell Structures," *Computers & Structures, 13*, 673–681, 1981.

STRUCTURAL ELEMENTS

- Beams
- Plates
- Shells

We note that in geometrically nonlinear analysis, a plate (initially "flat shell") develops shell action, and is analyzed as a shell.

Transparency 19-1

Various solution approaches have been proposed:

- Use of general beam and shell theories that include the desired nonlinearities.
  - — With the governing differential equations known, variational formulations can be derived and discretized using finite element procedures.
  - — Elegant approach, but difficulties arise in finite element formulations:
    - Lack of generality
    - Large number of nodal degrees of freedom

Transparency 19-2

Transparency 19-3

- Use of simple elements, but a large number of elements can model complex beam and shell structures.
  - — An example is the use of 3-node triangular flat plate/membrane elements to model complex shells.
  - — Coupling between membrane and bending action is only introduced at the element nodes.
  - — Membrane action is not very well modeled.

Transparency 19-4

Example:

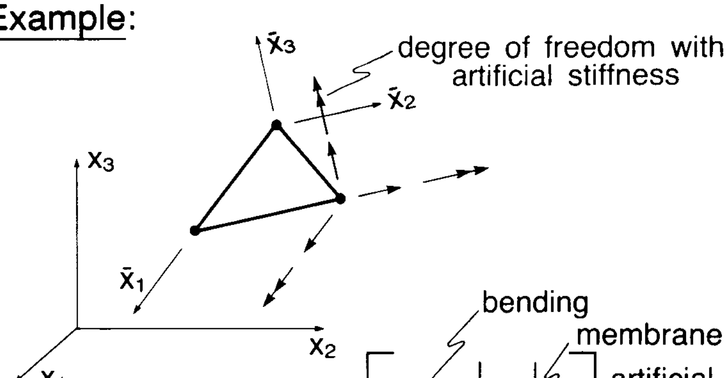

Stiffness matrix in local coordinate system ($\bar{x}_i$).

$$\underline{K}_\ell = \begin{bmatrix} \underline{K}_B & & \\ & \underline{K}_M & \\ & & \underline{k}_a \end{bmatrix}$$

- Isoparametric (degenerate) beam and shell elements.
  - These are derived from the 3-D continuum mechanics equations that we discussed earlier, but the basic assumptions of beam and shell behavior are imposed.
  - The resulting elements can be used to model quite general beam and shell structures.

We will discuss this approach in some detail.

Transparency 19-5

Basic approach:

- Use the total and updated Lagrangian formulations developed earlier.

Transparency 19-6

Transparency 19-7

We recall, for the T.L. formulation,

$$\int_{^0V} {}^{t+\Delta t}_{\ 0}S_{ij}\, \delta\, {}^{t+\Delta t}_{\ 0}\varepsilon_{ij}\, {}^0dV = {}^{t+\Delta t}\mathcal{R}$$

$$\Big\downarrow \text{Linearization}$$

$$\int_{^0V} {}_0C_{ijrs}\, {}_0e_{rs}\, \delta_0 e_{ij}\, {}^0dV + \int_{^0V} {}^t_0S_{ij}\, \delta_0\eta_{ij}\, {}^0dV$$

$$= {}^{t+\Delta t}\mathcal{R} - \int_{^0V} {}^t_0S_{ij}\, \delta_0 e_{ij}\, {}^0dV$$

Transparency 19-8

Also, for the U.L. formulation,

$$\int_{^tV} {}^{t+\Delta t}_{\ t}S_{ij}\, \delta\, {}^{t+\Delta t}_{\ t}\varepsilon_{ij}\, {}^tdV = {}^{t+\Delta t}\mathcal{R}$$

$$\Big\downarrow \text{Linearization}$$

$$\int_{^tV} {}_tC_{ijrs}\, {}_te_{rs}\, \delta_t e_{ij}\, {}^tdV + \int_{^tV} {}^t\tau_{ij}\, \delta_t\eta_{ij}\, {}^tdV$$

$$= {}^{t+\Delta t}\mathcal{R} - \int_{^tV} {}^t\tau_{ij}\, \delta_t e_{ij}\, {}^tdV$$

- Impose on these equations the basic assumptions of beam and shell action:
  1) Material particles originally on a straight line normal to the mid-surface of the beam (or shell) remain on that straight line throughout the response history.

Transparency 19-9

For beams, "plane sections initially normal to the mid-surface remain plane sections during the response history".

The effect of transverse shear deformations is included, and hence the lines initially normal to the mid-surface do not remain normal to the mid-surface during the deformations.

Transparency 19-10

Transparency 19-11

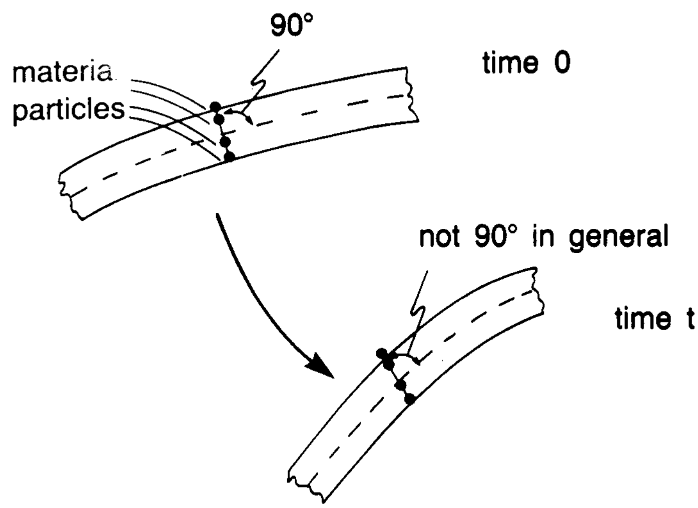

Transparency 19-12

2) The stress in the direction "normal" to the beam (or shell) mid-surface is zero throughout the response history.

   Note that here the stress along the material fiber that is initially normal to the mid-surface is considered; because of shear deformations, this material fiber does not remain exactly normal to the mid-surface.

3) The thickness of the beam (or shell) remains constant (we assume small strain conditions but allow for large displacements and rotations).

FORMULATION OF ISOPARAMETRIC (DEGENERATE) SHELL ELEMENTS

- To incorporate the geometric assumptions of "straight lines normal to the mid-surface remain straight", and of "the shell thickness remains constant" we use the appropriate geometric and displacement interpolations.
- To incorporate the condition of "zero stress normal to the mid-surface" we use the appropriate stress-strain law.

Transparency 19-13

Shell element geometry

Example: 9-node element

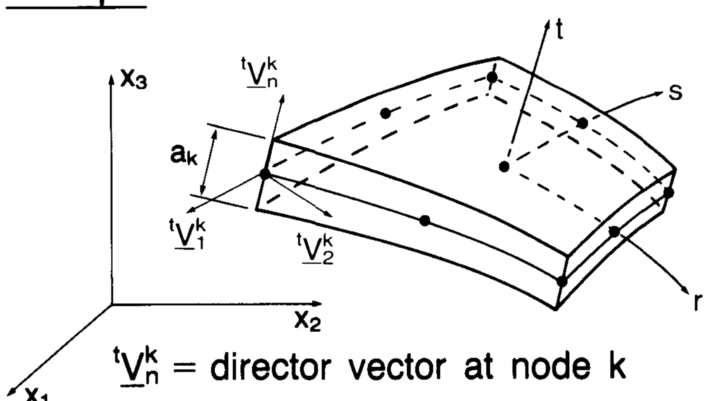

${}^t\underline{V}_n^k$ = director vector at node k

a_k = shell thickness at node k (measured into direction of ${}^t\underline{V}_n^k$)

Transparency 19-14

Transparency
19-15

Element geometry definition:

- Input mid-surface nodal point coordinates.
- Input all nodal director vectors at time 0.
- Input thicknesses at nodes.

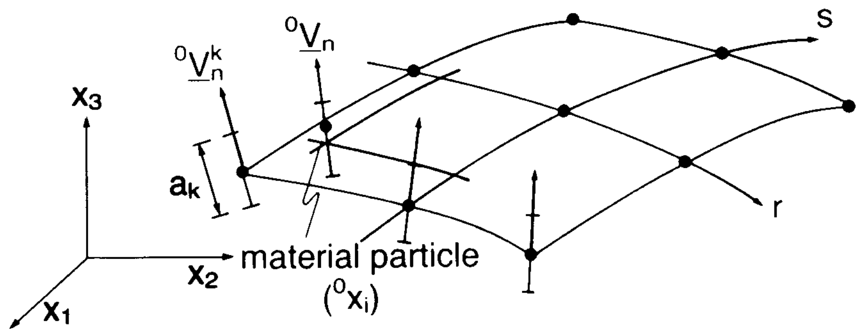

Transparency
19-16

- Isoparametric coordinate system (r, s, t):
  - — The coordinates r and s are measured in the mid-surface defined by the nodal point coordinates (as for a curved membrane element).
  - — The coordinate t is measured in the direction of the director vector at every point in the shell.

Interpolation of geometry at time 0:

$$\underbrace{{}^{0}x_i}_{\substack{\text{material}\\\text{particle}\\\text{with isoparametric}\\\text{coordinates }(r,\,s,\,t)}} = \underbrace{\sum_{k=1}^{N} h_k\, {}^{0}x_i^k}_{\substack{\text{mid-surface}\\\text{only}}} + \underbrace{\frac{t}{2}\sum_{k=1}^{N} a_k\, h_k\, {}^{0}V_{ni}^k}_{\substack{\text{effect of shell}\\\text{thickness}}}$$

h_k = 2-D interpolation functions (as for 2-D plane stress, plane strain and axisymmetric elements)

${}^{0}x_i^k$ = nodal point coordinates

${}^{0}V_{ni}^k$ = components of ${}^{0}\underline{V}_n^k$

Transparency 19-17

Similarly, at time t,

t-coordinate

$$ {}^{t}x_i = \sum_{k=1}^{N} h_k\, {}^{t}x_i^k + \frac{t}{2}\sum_{k=1}^{N} a_k\, h_k\, {}^{t}V_{ni}^k $$

The nodal point coordinates and director vectors have changed.

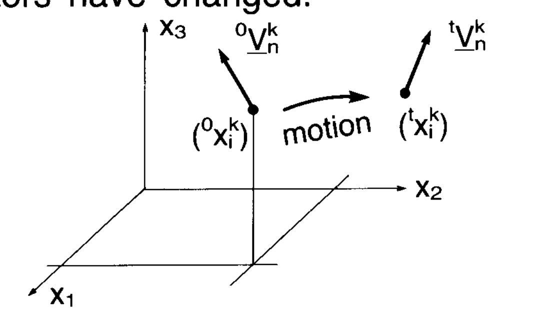

Transparency 19-18

Transparency 19-19

To obtain the displacements of any material particle,

$$^{t}u_i = {}^{t}x_i - {}^{0}x_i$$

Hence

$$^{t}u_i = \sum_{k=1}^{N} h_k \, {}^{t}u_i^k + \frac{t}{2} \sum_{k=1}^{N} a_k \, h_k \, ({}^{t}V_{ni}^k - {}^{0}V_{ni}^k)$$

where

$$^{t}u_i^k = {}^{t}x_i^k - {}^{0}x_i^k \qquad \text{(disp. of nodal point k)}$$

$^{t}V_{ni}^k - {}^{0}V_{ni}^k$ = change in direction cosines of director vector at node k

Transparency 19-20

The incremental displacements from time t to time $t+\Delta t$ are, similarly, for any material particle in the shell element,

$$u_i = {}^{t+\Delta t}x_i - {}^{t}x_i$$

$$= \sum_{k=1}^{N} h_k \, u_i^k + \frac{t}{2} \sum_{k=1}^{N} a_k \, h_k \, V_{ni}^k$$

where

u_i^k = incremental nodal point displacements

$V_{ni}^k = {}^{t+\Delta t}V_{ni}^k - {}^{t}V_{ni}^k$ = incremental change in direction cosines of director vector from time t to time $t+\Delta t$

Transparency 19-21

To develop the strain-displacement transformation matrices for the T.L. and U.L. formulations, we need

— the coordinate interpolations for the material particles (${}^0x_i$, ${}^tx_i$).

— the interpolation of incremental displacements from the incremental nodal point displacements and rotations.

Hence, express the V_{ni}^k in terms of nodal point rotations.

Transparency 19-22

We define at each nodal point k the vectors ${}^0\underline{V}_1^k$ and ${}^0\underline{V}_2^k$:

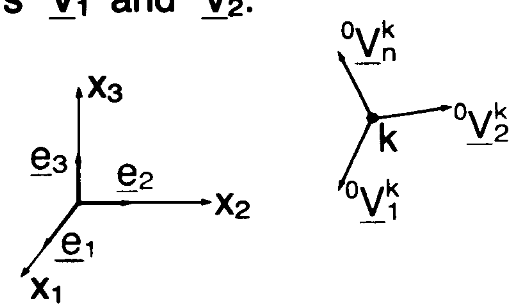

$$ {}^0\underline{V}_1^k = \frac{\underline{e}_2 \times {}^0\underline{V}_n^k}{\|\underline{e}_2 \times {}^0\underline{V}_n^k\|_2} \quad , \quad {}^0\underline{V}_2^k = {}^0\underline{V}_n^k \times {}^0\underline{V}_1^k $$

The vectors ${}^0\underline{V}_1^k$, ${}^0\underline{V}_2^k$ and ${}^0\underline{V}_n^k$ are therefore mutually perpendicular.

Transparency 19-23

Then let α_k and β_k be the rotations about ${}^t\underline{V}_1^k$ and ${}^t\underline{V}_2^k$. We have, for small α_k, β_k,

$$\underline{V}_n^k = -\,{}^t\underline{V}_2^k\,\alpha_k + {}^t\underline{V}_1^k\,\beta_k$$

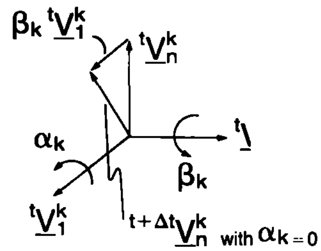

Transparency 19-24

Hence, the incremental displacements of any material point in the shell element are given in terms of incremental nodal point displacements and rotations

$$u_i = \sum_{k=1}^{N} h_k\, u_i^k + \frac{t}{2}\sum_{k=1}^{N} a_k\, h_k\,[-{}^tV_{2i}^k\,\alpha_k + {}^tV_{1i}^k\,\beta_k]$$

Transparency 19-25

Once the incremental nodal point displacements and rotations have been calculated from the solution of the finite element system equilibrium equations, we calculate the new director vectors using

$$ {}^{t+\Delta t}\underline{V}_n^k = {}^{t}\underline{V}_n^k + \int_{\alpha_k,\beta_k} \left(-{}^{\tau}\underline{V}_2^k \, d\alpha_k + {}^{\tau}\underline{V}_1^k \, d\beta_k\right) $$

→ and normalize length

Transparency 19-26

Nodal point degrees of freedom:

- We have only five degrees of freedom per node:
  - — three translations in the Cartesian coordinate directions
  - — two rotations referred to the local nodal point vectors ${}^{t}\underline{V}_1^k$, ${}^{t}\underline{V}_2^k$
- The nodal point vectors ${}^{t}\underline{V}_1^k$, ${}^{t}\underline{V}_2^k$ change directions in a geometrically nonlinear solution.

Transparency 19-27

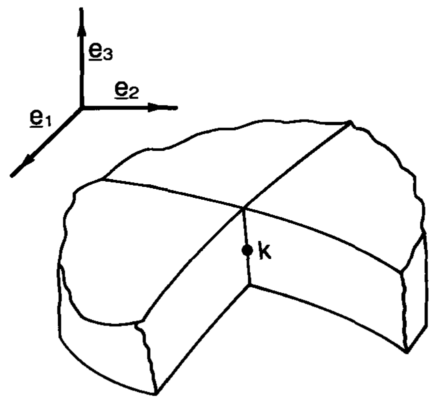

— Node k is shared by four shell elements

Transparency 19-28

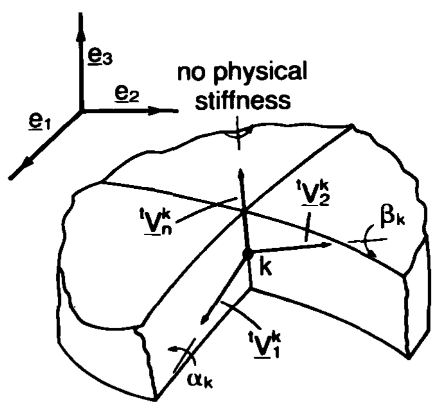

— Node k is shared by four shell elements
— One director vector ${}^t\underline{V}_n^k$ at node k
— No physical stiffness corresponding to rotation about ${}^t\underline{V}_n^k$.

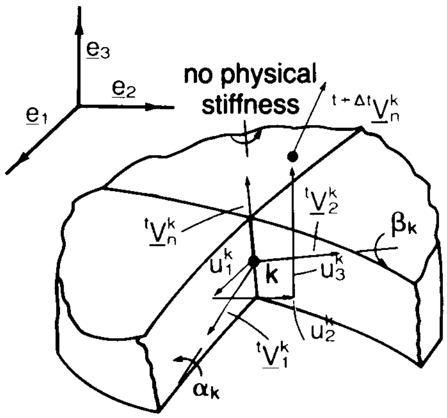

— Node k is shared by four shell elements

— One director vector ${}^t\underline{V}_n^k$ at node k

— No physical stiffness corresponding to rotation about ${}^t\underline{V}_n^k$.

Transparency 19-29

- If only shell elements connect to node k, and the node is not subjected to boundary prescribed rotations, we only assign five local degrees of freedom to that node.
- We transform the two nodal rotations to the three Cartesian axes in order to
  - — connect a beam element (three rotational degrees of freedom) or
  - — impose a boundary rotation (other than α_k or β_k) at that node.

Transparency 19-30

Transparency 19-31

- The above interpolations of ${}^0x_i$, ${}^tx_i$, u_i are employed to establish the strain-displacement transformation matrices corresponding to the Cartesian strain components, as in the analysis of 3-D solids.

Transparency 19-32

- Using the expression ${}_0e_{ij}$ derived earlier the exact linear strain-displacement matrix ${}^t_0\underline{B}_L$ is obtained.

  However, using $\frac{1}{2}\, {}_0u_{k,i}\, {}_0u_{k,j}$ to develop the nonlinear strain-displacement matrix ${}^t_0\underline{B}_{NL}$, only an approximation to the exact second-order strain-displacement rotation expression is obtained because the internal element displacements depend nonlinearly on the nodal point rotations.

  The same conclusion holds for the U.L. formulation.

Transparency 19-33

- We still need to impose the condition that the stress in the direction "normal" to the shell mid-surface is zero.

  We use the direction of the director vector as the "normal direction."

Transparency 19-34

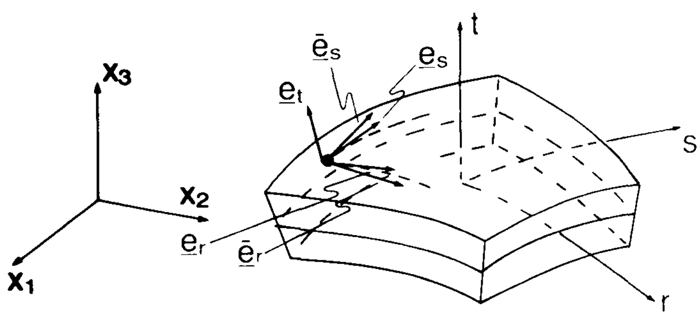

$$\underline{\bar{e}}_r = \frac{\underline{e}_s \times \underline{e}_t}{\|\underline{e}_s \times \underline{e}_t\|_2} \quad , \quad \underline{\bar{e}}_s = \underline{e}_t \times \underline{\bar{e}}_r$$

We note: $\underline{e}_r$, $\underline{e}_s$, $\underline{e}_t$ are not mutually perpendicular in general.

$\underline{\bar{e}}_r$, $\underline{\bar{e}}_s$, $\underline{e}_t$ are constructed to be mutually perpendicular.

Transparency 19-35

Then the stress-strain law used is, for a linear elastic material,

$$\underline{C}_{sh} = \underline{Q}_{sh}^{T}\left(\frac{E}{1-\nu^2}\begin{bmatrix} 1 & \nu & 0 & 0 & 0 & 0 \\ & 1 & 0 & 0 & 0 & 0 \\ & & 0 & 0 & 0 & 0 \\ & & & \frac{1-\nu}{2} & 0 & 0 \\ & & & & k\left(\frac{1-\nu}{2}\right) & 0 \\ \text{symmetric} & & & & & k\left(\frac{1-\nu}{2}\right) \end{bmatrix}\right)\underline{Q}_{sh}$$

k = shear correction factor

Transparency 19-36

where

$$\begin{array}{l} \text{row 1} \\ \\ \underline{Q}_{sh} = \\ \text{row 4} \\ \\ \end{array}\begin{bmatrix} (\ell_1)^2 & (m_1)^2 & (n_1)^2 & \ell_1 m_1 & m_1 n_1 & n_1 \ell_1 \\ \vdots & \vdots & \vdots & \vdots & \vdots & \vdots \\ 2\ell_1\ell_2 & 2m_1m_2 & 2n_1n_2 & \ell_1 m_2 + \ell_2 m_1 & m_1 n_2 + m_2 n_1 & n_1\ell_2 + n_2\ell_1 \\ \vdots & \vdots & \vdots & \vdots & \vdots & \vdots \end{bmatrix}$$

using

$$\begin{array}{l|l|l} \ell_1 = \cos(\underline{e}_1, \bar{\underline{e}}_r) & m_1 = \cos(\underline{e}_2, \bar{\underline{e}}_r) & n_1 = \cos(\underline{e}_3, \bar{\underline{e}}_r) \\ \ell_2 = \cos(\underline{e}_1, \bar{\underline{e}}_s) & m_2 = \cos(\underline{e}_2, \bar{\underline{e}}_s) & n_2 = \cos(\underline{e}_3, \bar{\underline{e}}_s) \\ \ell_3 = \cos(\underline{e}_1, \underline{e}_t) & m_3 = \cos(\underline{e}_2, \underline{e}_t) & n_3 = \cos(\underline{e}_3, \underline{e}_t) \end{array}$$

Transparency 19-37

- The columns and rows 1 to 3 in $\underline{C}_{sh}$ reflect that the stress "normal" to the shell mid-surface is zero.
- The stress-strain matrix for plasticity and creep solutions is similarly obtained by calculating the stress-strain matrix as in the analysis of 3-D solids, and then imposing the condition that the stress "normal" to the mid-surface is zero.

Transparency 19-38

- Regarding the kinematic description of the shell element, transition elements can also be developed.
- Transition elements are elements with some mid-surface nodes (and associated director vectors and five degrees of freedom per node) and some top and bottom surface nodes (with three translational degrees of freedom per node). These elements are used
  - — to model shell-to-solid transitions
  - — to model shell intersections

Transparency 19-39

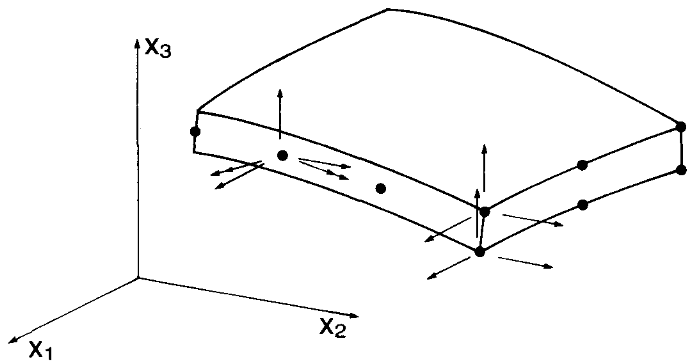

Transparency 19-40

a) Shell intersection

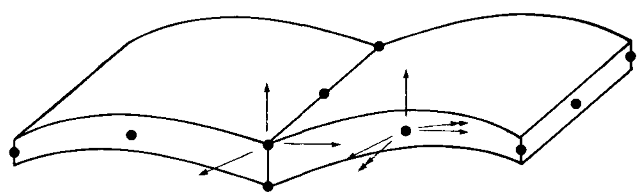

b) Solid-shell intersection

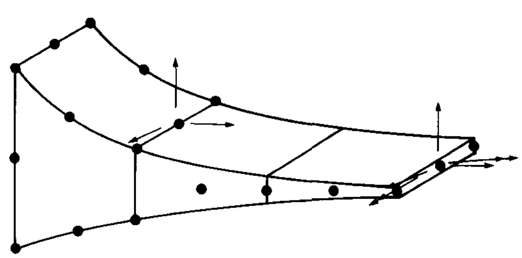

Topic 20

Beam, Plate, and Shell Elements—Part II

Contents:

- **Formulation of isoparametric (degenerate) beam elements for large displacements and rotations**
- **A rectangular cross-section beam element of variable thickness; coordinate and displacement interpolations**
- **Use of the nodal director vectors**
- **The stress-strain law**
- **Introduction of warping displacements**
- **Example analysis: 180 degrees, large displacement twisting of a ring**
- **Example analysis: Torsion of an elastic-plastic cross-section**
- **Recommendations for the use of isoparametric beam and shell elements**
- **The phenomena of shear and membrane locking as observed for certain elements**
- **Study of solutions of straight and curved cantilevers modeled using various elements**
- **An effective 4-node shell element (the MITC4 element) for analysis of general shells**
- **The patch test, theoretical and practical considerations**
- **Example analysis: Solution of a three-dimensional spherical shell**
- **Example analysis: Solution of an open box**
- **Example analysis: Solution of a square plate, including use of distorted elements**
- **Example analysis: Solution of a 30-degree skew plate**
- **Example analysis: Large displacement solution of a cantilever**

Contents: (continued)

- **Example analysis: Collapse analysis of an I-beam in torsion**
- **Example analysis: Collapse analysis of a cylindrical shell**

Textbook: Sections 6.3.4, 6.3.5

Example: 6.18

References:

The displacement functions to account for warping in the rectangular cross-section beam are introduced in

Bathe, K. J., and A. Chaudhary, "On the Displacement Formulation of Torsion of Shafts with Rectangular Cross-Sections," *International Journal for Numerical Methods in Engineering, 18,* 1565–1568, 1982.

The 4-node and 8-node shell elements based on mixed interpolation (i.e., the MITC4 and MITC8 elements) are developed and discussed in

Dvorkin, E., and K. J. Bathe, "A Continuum Mechanics Based Four-Node Shell Element for General Nonlinear Analysis," *Engineering Computations, 1,* 77–88, 1984.

Bathe, K. J., and E. Dvorkin, "A Four-Node Plate Bending Element Based on Mindlin/Reissner Plate Theory and a Mixed Interpolation," *International Journal for Numerical Methods in Engineering, 21,* 367–383, 1985.

Bathe, K. J., and E. Dvorkin, "A Formulation of General Shell Elements—The Use of Mixed Interpolation of Tensorial Components," *International Journal for Numerical Methods in Engineering,* in press.

The I-beam analysis is reported in

Bathe, K. J., and P. M. Wiener, "On Elastic-Plastic Analysis of I-Beams in Bending and Torsion," *Computers & Structures, 17,* 711–718, 1983.

The beam formulation is extended to a pipe element, including ovalization effects, in

Bathe, K. J., C. A. Almeida, and L. W. Ho, "A Simple and Effective Pipe Elbow Element—Some Nonlinear Capabilities," *Computers & Structures, 17,* 659–667, 1983.

FORMULATION OF ISOPARAMETRIC (DEGENERATE) BEAM ELEMENTS

- The usual Hermitian beam elements (cubic transverse displacements, linear longitudinal displacements) are usually most effective in the linear analysis of beam structures.
- When in the following discussion we refer to a "beam element" we always mean the "isoparametric beam element."

Transparency 20-1

- The isoparametric formulation can be effective for the analysis of
  - Curved beams
  - Geometrically nonlinear problems
  - Stiffened shell structures (isoparametric beam and shell elements are coupled compatibly)
- The formulation is analogous to the formulation of the isoparametric (degenerate) shell element.

Transparency 20-2

Transparency 20-3

Consider a beam element with a rectangular cross-section:

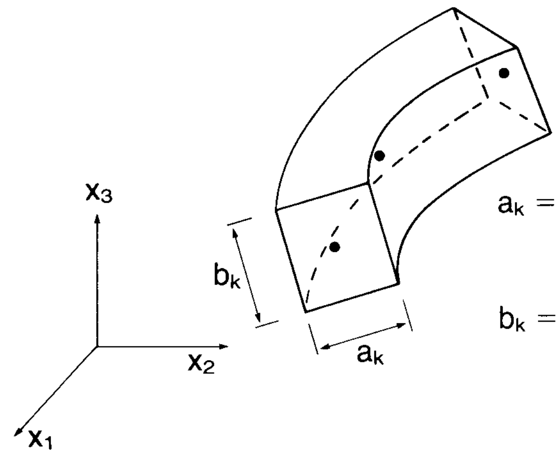

a_k = thickness at node k in t-direction

b_k = thickness at node k in s-direction

Transparency 20-4

Consider a beam element with a rectangular cross-section:

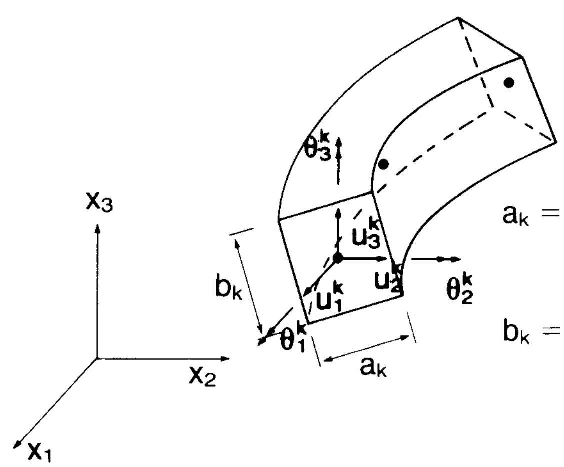

a_k = thickness at node k in t-direction

b_k = thickness at node k in s-direction

Consider a beam element with a rectangular cross-section:

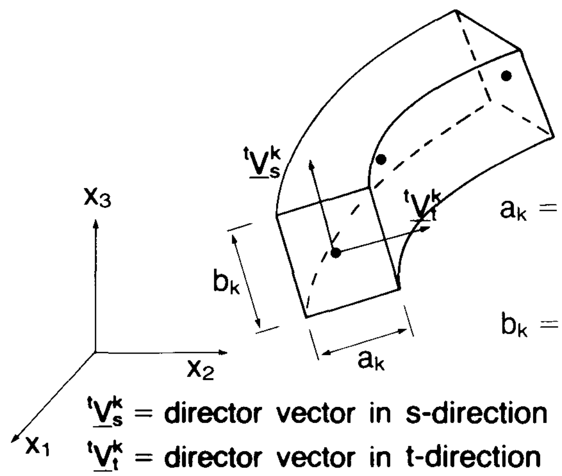

a_k = thickness at node k in t-direction

b_k = thickness at node k in s-direction

$^t\underline{V}_s^k$ = director vector in s-direction

$^t\underline{V}_t^k$ = director vector in t-direction

Transparency 20-5

Consider a beam element with a rectangular cross-section:

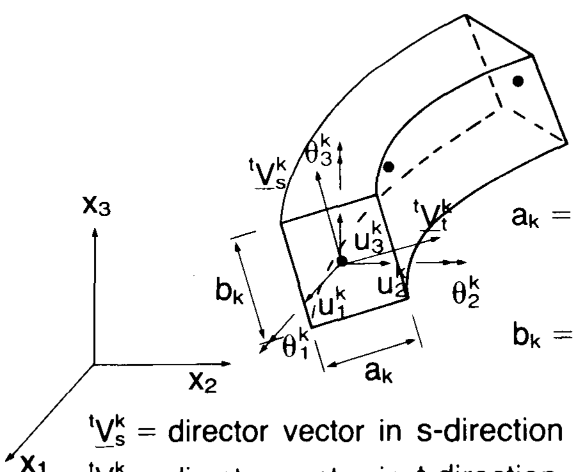

a_k = thickness at node k in t-direction

b_k = thickness at node k in s-direction

$^t\underline{V}_s^k$ = director vector in s-direction

$^t\underline{V}_t^k$ = director vector in t-direction

Transparency 20-6

Transparency 20-7

The coordinates of the material particles of the beam are interpolated as

$$^{t}x_i = \sum_{k=1}^{N} h_k\, {}^{t}x_i^k + \frac{t}{2}\sum_{k=1}^{N} a_k\, h_k\, {}^{t}V_{ti}^k + \frac{s}{2}\sum_{k=1}^{N} b_k\, h_k\, {}^{t}V_{si}^k$$

where

${}^{t}V_{ti}^k$ = direction cosines of the director vector in the t-direction, of node k at time t

${}^{t}V_{si}^k$ = direction cosines of the director vector in the s-direction, of node k at time t

Transparency 20-8

Since ${}^{t}u_i = {}^{t}x_i - {}^{0}x_i$, we have

$$^{t}u_i = \sum_{k=1}^{N} h_k\, {}^{t}u_i^k + \frac{t}{2}\sum_{k=1}^{N} a_k\, h_k\, ({}^{t}V_{ti}^k - {}^{0}V_{ti}^k) + \frac{s}{2}\sum_{k=1}^{N} b_k\, h_k\, ({}^{t}V_{si}^k - {}^{0}V_{si}^k)$$

The vectors ${}^{0}\underline{V}_t^k$ and ${}^{0}\underline{V}_s^k$ can be calculated automatically from the initial geometry of the beam element if the element is assumed to lie initially in a plane.

Also

$$u_i = {}^{t+\Delta t}x_i - {}^{t}x_i$$

$$= \sum_{k=1}^{N} h_k u_i^k + \frac{t}{2}\sum_{k=1}^{N} a_k h_k V_{ti}^k + \frac{s}{2}\sum_{k=1}^{N} b_k h_k V_{si}^k$$

where V_{ti}^k and V_{si}^k are increments in the direction cosines of the vectors ${}^{t}\underline{V}_t^k$ and ${}^{t}\underline{V}_s^k$. These increments are given in terms of the incremental rotations $\underline{\theta}_k$, about the Cartesian axes, as

$$\underline{V}_t^k = \underline{\theta}_k \times {}^{t}\underline{V}_t^k \; ; \; \underline{V}_s^k = \underline{\theta}_k \times {}^{t}\underline{V}_s^k$$

Transparency 20-9

- Using the above displacement and geometry interpolations, we can develop the strain-displacement matrices for the Cartesian strain components. A standard transformation yields the strain-displacement relations corresponding to the beam coordinates η, ξ, ζ.

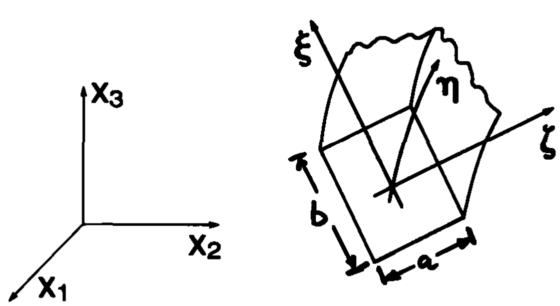

Transparency 20-10

Transparency 20-11

- The stress-strain relationship used for linear elastic material conditions is

$$\begin{array}{cc} & \begin{array}{ccc} \eta\eta & \eta\xi & \eta\zeta \leftarrow \text{components} \end{array} \\ \underline{C}_{beam} = & \begin{bmatrix} E & 0 & 0 \\ 0 & Gk & 0 \\ 0 & 0 & Gk \end{bmatrix} \end{array}$$

k = shear correction factor

since only the one normal and two transverse shear stresses are assumed to exist.

Transparency 20-12

- The material stress-strain matrix for analysis of elasto-plasticity or creep would be obtained using also the condition that only the stress components $(\eta\eta)$, $(\eta\zeta)$ and $(\eta\xi)$ are non-zero.

Transparency 20-13

- Note that the kinematic assumptions in the beam element do not allow – so far – for cross-sectional out-of-plane displacements (warping). In torsional loading, allowing for warping is important.
- We therefore amend the displacement assumptions by the following displacements:

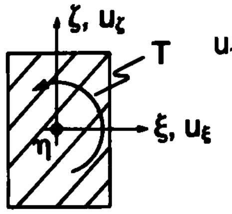

$$u_\eta = \alpha \underbrace{\xi\zeta}_{\substack{\text{exact warping}\\ \text{displacements}\\ \text{for infinitely}\\ \text{narrow section}}} + \beta \underbrace{\xi\zeta(\xi^2 - \zeta^2)}_{\substack{\text{exact warping}\\ \text{displacements}\\ \text{for square}\\ \text{section}}}$$

Transparency 20-14

Torsion constant k in formula,
$T = k\, G\theta\, a^3 b$

$\frac{b}{a}$	k: Analytical value (Timoshenko)	k: ADINA
1·0	0·141	0·141
2·0	0·229	0·230
4·0	0·281	0·289
10·0	0·312	0·323
100·0	0·333	0·333

Transparency 20-15

Example: Twisting of a ring

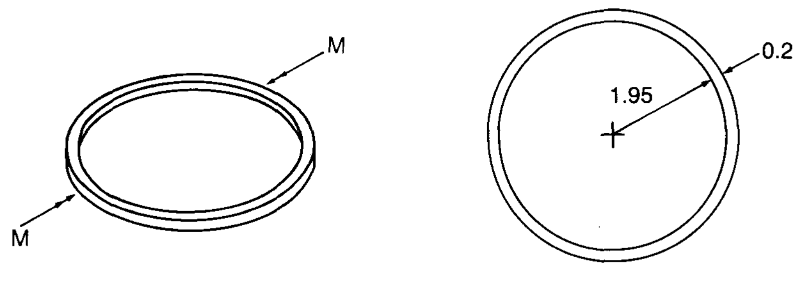

All dimensions in inches
thickness = 0.2
$E = 3 \times 10^5$ psi
$\nu = 0.3$

Transparency 20-16

Finite element mesh: Twelve 4-node iso-beam elements

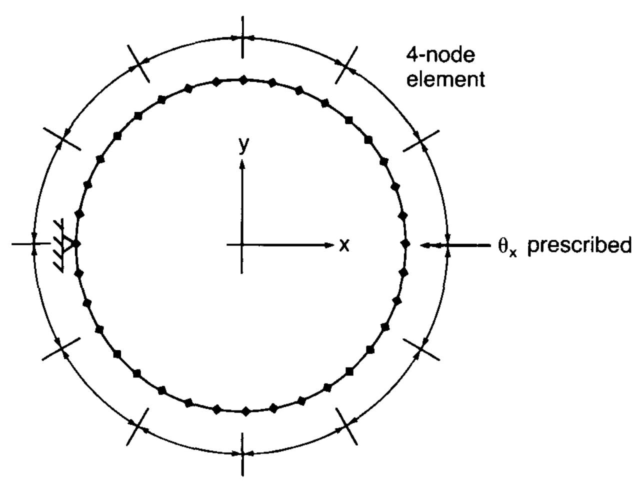

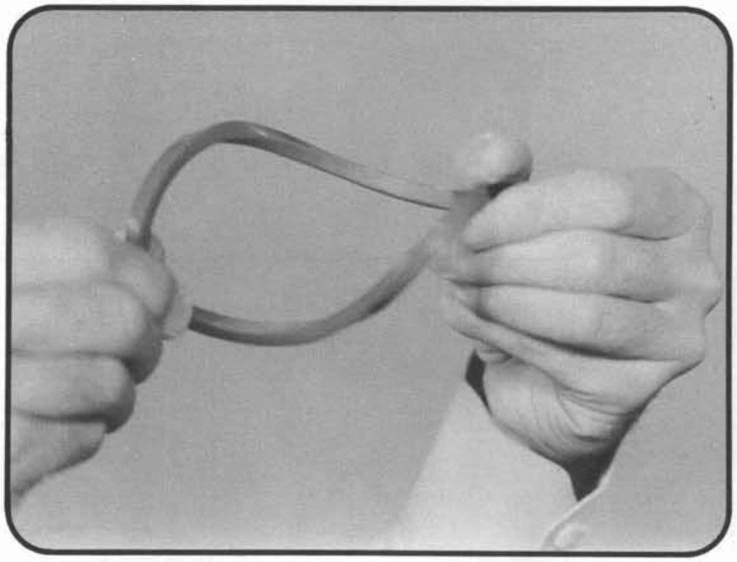

Demonstration Photograph 20-1
Close-up of ring deformations

Use the T.L. formulation to rotate the ring 180 degrees:

Force-deflection curve

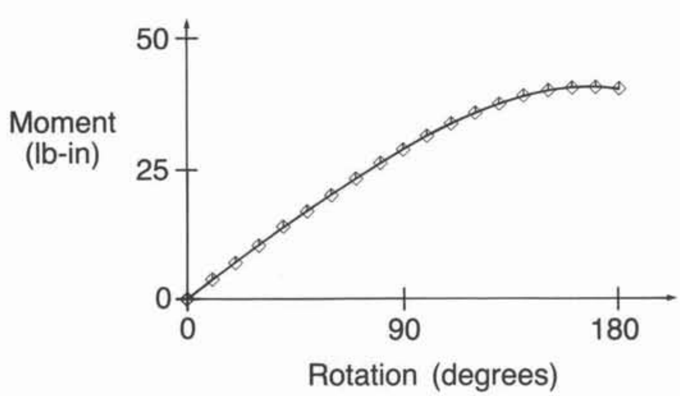

Transparency 20-17

Transparency 20-18

Pictorially, for a rotation of 180 degrees, we have

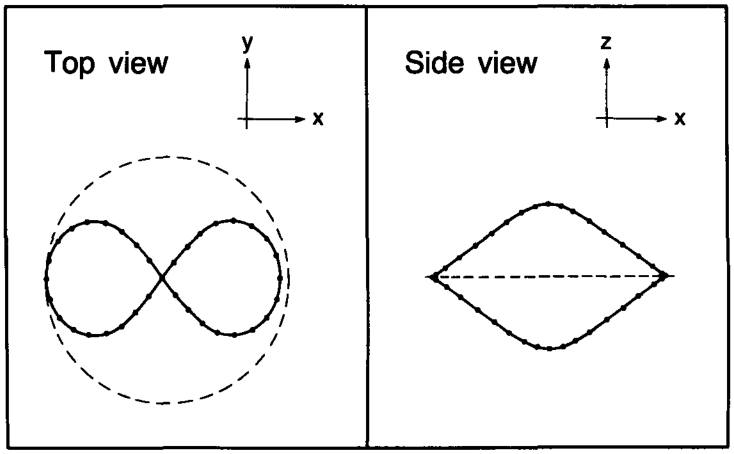

Slide 20-1

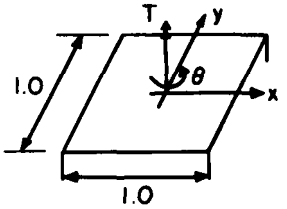

MATERIAL DATA:

GREENBERG et. al.

$$\varepsilon = \frac{\sigma}{E}\left[1 + \left(\frac{\sigma}{100}\right)^{2n}\right]$$

$E = 18{,}600;\ n = 9$

ADINA:

$E = 18{,}600;\ \nu = 0.0$

$\sigma_y = 93.33;\ E_T = 900$

Elastic–plastic analysis of torsion problem

Slide 20-2

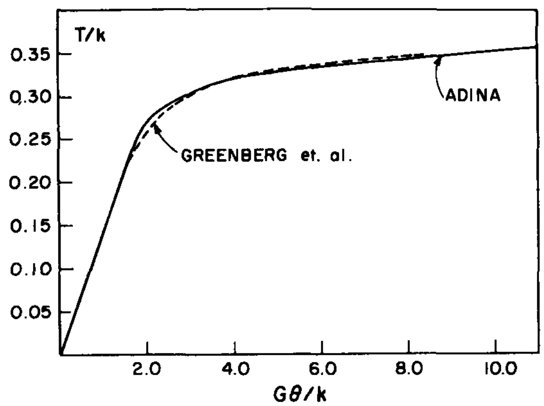

Solution of torsion problem
($k = 100/\sqrt{3}$, θ = rotation per unit length)

Transparency
20-19

Use of the isoparametric beam and shell elements

- The elements can be programmed for use with different numbers of nodes
  - For the beam,
    2, 3 or 4 nodes
  - For the shell,
    4, 8, 9, ···, 16 nodes
- The elements can be employed for analysis of moderately thick structures (shear deformations are approximately taken into account).

Transparency
20-20

- The elements can be used for analysis of thin structures – but then only certain elements of those mentioned above should be used.

For shells: Use only the 16-node element with 4 × 4 Gauss integration over the mid-surface.

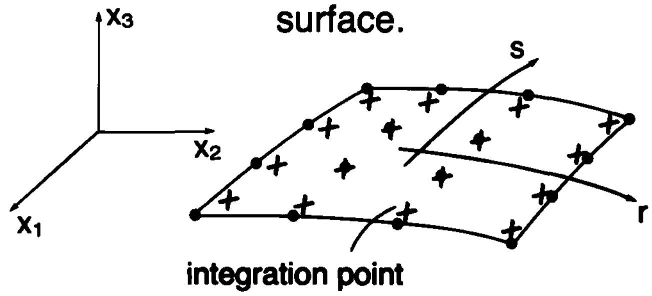

For beams:

Use 2-node beam element with 1-point Gauss integration along r-direction,

or

Use 3-node beam element with 2-point Gauss integration along r-direction,

or

Use 4-node beam element with 3-point Gauss integration along r-direction.

Transparency 20-21

The reason is that the other elements become overly (and artificially) stiff when used to model thin structures and curved structures.

Two phenomena occur:

- Shear locking
- Membrane locking

Transparency 20-22

Transparency 20-23

- The 2-, 3- and 4-node beam elements with 1-, 2- and 3-point Gauss integration along the beam axes do not display these phenomena.
- The 16-node shell element with 4×4 Gauss integration on the shell mid-surface is relatively immune to shear and membrane locking (the element should not be distorted for best predictive capability).

Transparency 20-24

- To explain shear locking, consider a 2-node beam element with exact integration (2-point Gauss integration corresponding to the r-direction).

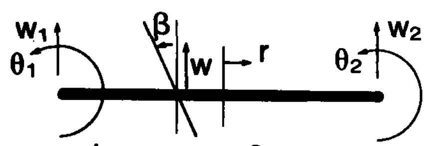

Transverse displacement:

$$w = \frac{1}{2}(1 - r)\, w_1 + \frac{1}{2}(1 + r)\, w_2$$

Section rotation:

$$\beta = \frac{1}{2}(1 - r)\, \theta_1 + \frac{1}{2}(1 + r)\, \theta_2$$

Hence the transverse shear deformations are given by

$$\gamma = \underbrace{\frac{2}{L}\frac{\partial w}{\partial r}}_{\frac{\partial w}{\partial x}} - \beta$$

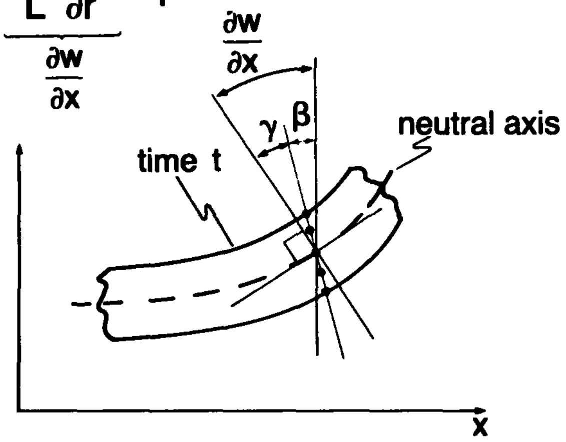

Transparency 20-25

Consider now the simple case of a cantilever subjected to a tip bending moment, modeled using one 2-node element:

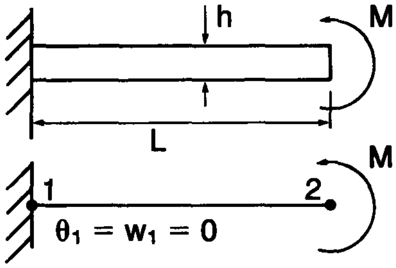

Here $\beta = \frac{1}{2}(1 + r)\,\theta_2$

$$\gamma = \frac{1}{L}w_2 - \frac{1}{2}(1 + r)\,\theta_2$$

Transparency 20-26

Transparency 20-27

We observe:

- Clearly, γ cannot be zero at all points along the beam, unless θ_2 and w_2 are zero. But then also β would be zero and there would be no bending of the beam.
- Since for the beam
  — bending strain energy $\propto h^3$
  — shear strain energy $\propto h$
  any error in the shear strains (due to the finite element interpolation functions) becomes increasingly more detrimental as h becomes small.

Transparency 20-28

- For the cantilever example, the shear strain energy should be zero. As h decreases, the relative error in the shear strain increases rapidly and in effect, introduces an artificial stiffness that makes the model "lock."

h/L L = 100	$\theta_{analytical}$	finite element solution (exact integration)
0.50	9.6×10^{-7}	3.2×10^{-7}
0.10	1.2×10^{-4}	2.4×10^{-6}
0.01	1.2×10^{-1}	2.4×10^{-5}

Transparency 20-29

- Although we considered only one element in the solution, the same conclusion of locking holds for an assemblage of elements.

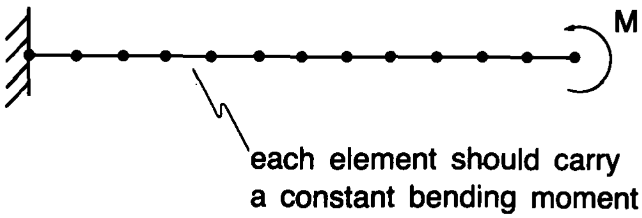

Transparency 20-30

Example: Beam locking study

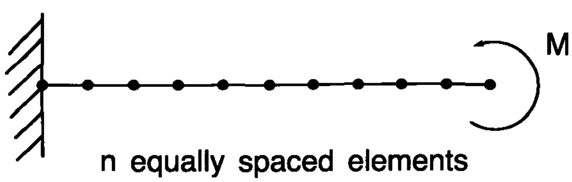

L = 10 m
Square cross-section, height = 0.1 m
Two-node beam elements,
full integration

Transparency 20-31

Plot tip deflection as a function of the number of elements:

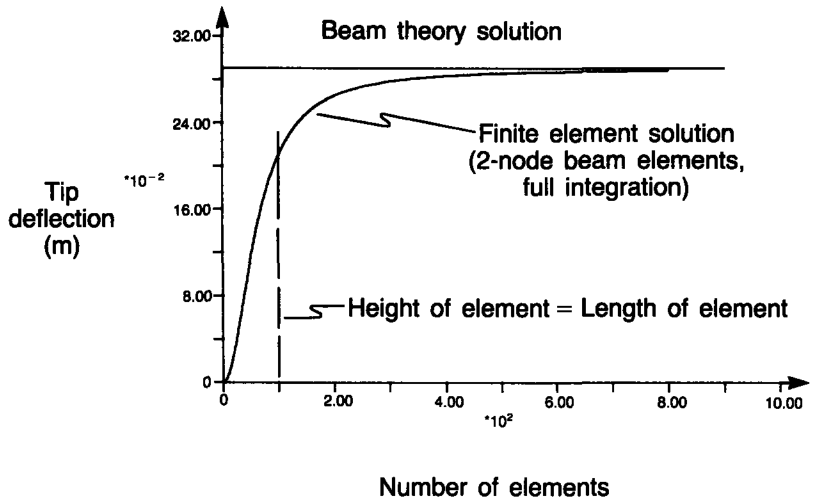

Transparency 20-32

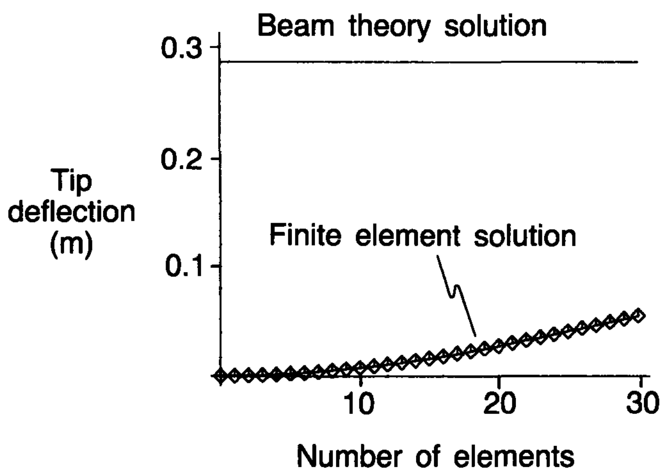

A remedy for the 2-node beam element is to use only 1-point Gauss integration (along the beam axis).

This corresponds to assuming a constant transverse shear strain, (since the shear strain is only evaluated at the mid-point of the beam).

The bending energy is still integrated accurately (since $\frac{\partial \beta}{\partial r}$ is correctly evaluated).

h/L L = 100	$\theta_{analytical}$	finite element solution (1-point integration)
0.50	9.6×10^{-7}	9.6×10^{-7}
0.10	1.2×10^{-4}	1.2×10^{-4}
0.01	1.2×10^{-1}	1.2×10^{-1}

Transparency 20-33

- The 3- and 4-node beam elements evaluated using 2- and 3-point integration are similarly effective.
- We should note that these beam elements based on "reduced" integration are reliable because they do not possess any spurious zero energy modes. (They have only 6 zero eigenvalues in 3-D analysis corresponding to the 6 physical rigid body modes).
- The formulation can be interpreted as a mixed interpolation of displacements and transverse shear strains.

Transparency 20-34

Transparency 20-35

- Regarding membrane-locking we note that in addition to not exhibiting erroneous shear strains, the beam model must also not contain erroneous mid-surface membrane strains in the analysis of curved structures.
- The beam elements with reduced integration also do not "membrane-lock."

Transparency 20-36

Consider the analysis of a curved cantilever:

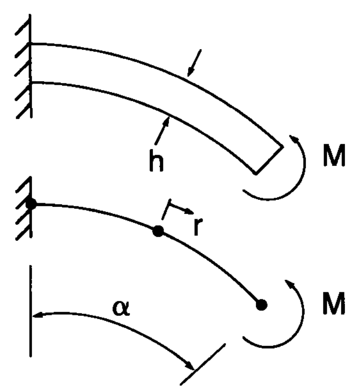

The exactly integrated 3-node beam element, when curved, does contain erroneous shear strains and erroneous mid-surface membrane strains. As a result, when h becomes small, the element becomes very stiff.

h/R R = 100	$\theta_{analytical}$ ($\alpha = 45°$)	finite element solution: 3-node element, 3-point integration	finite element solution: 3-node element, 2-point integration
0.50	7.5×10^{-7}	6.8×10^{-7}	7.4×10^{-7}
0.10	9.4×10^{-5}	2.9×10^{-5}	9.4×10^{-5}
0.01	9.4×10^{-2}	4.1×10^{-4}	9.4×10^{-2}

Transparency 20-37

- Similarly, we can study the use of the 4-node cubic beam element:

h/R R = 100	$\theta_{analytical}$ ($\alpha = 45°$)	finite element solution: 4-node element, 4-point integration	finite element solution: 4-node element, 3-point integration
0.50	7.5×10^{-7}	7.4×10^{-7}	7.4×10^{-7}
0.10	9.4×10^{-5}	9.4×10^{-5}	9.4×10^{-5}
0.01	9.4×10^{-2}	9.4×10^{-2}	9.4×10^{-2}

We note that the cubic beam element performs well even when using full integration.

Transparency 20-38

Transparency 20-39

Considering the analysis of shells, the phenomena of shear and membrane locking are also present, but the difficulty is that simple "reduced" integration (as used for the beam elements) cannot be recommended, because the resulting elements contain spurious zero energy modes.

For example, the 4-node shell element with 1-point integration contains 6 spurious zero energy modes (twelve zero eigenvalues instead of only six).

Transparency 20-40

Such spurious zero energy modes can lead to large errors in the solution that – unless a comparison with accurate results is possible – are not known and hence the analysis is unreliable.

Transparency 20-41

- For this reason, only the 16-node shell element with 4×4 Gauss integration on the shell mid-surface can be recommended.
- The 16-node element should, as much as possible, be used with the internal and boundary nodes placed at their $\frac{1}{3}$rd points (without internal element distortions). This way the element performs best.

Transparency 20-42

- Recently, we have developed elements based on the mixed interpolation of tensorial components.
- The elements do not lock, in shear or membrane action, and also do not contain spurious zero energy modes.
- We will use the 4-node element, referred to as the MITC4 element, in some of our demonstrative sample solutions.

Transparency 20-43

The MITC4 element:

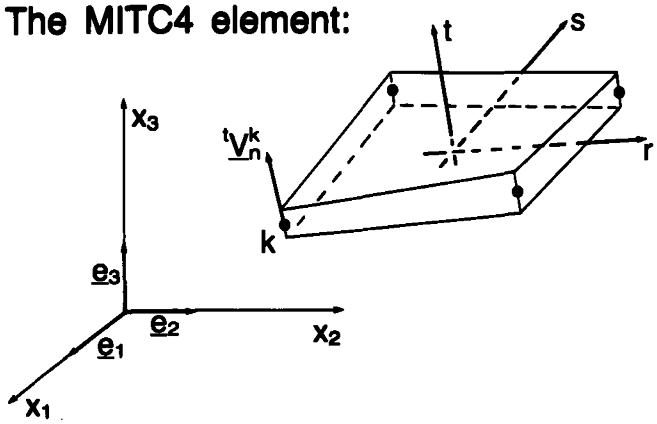

- For analysis of plates
- For analysis of moderately thick shells and thin shells

Transparency 20-44

- The key step in the formulation is to interpolate the geometry and displacements as earlier described, but
  - — To interpolate the transverse shear strain tensor components separately, with judiciously selected shape functions
  - — To tie the intensities of these components to the values evaluated using the displacement interpolations

rt transverse shear strain tensor
component interpolation

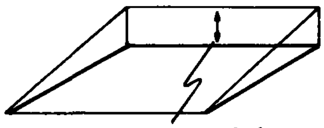

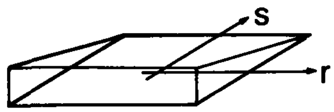

evaluated from
displacement interpolations

st transverse shear strain tensor
component interpolation

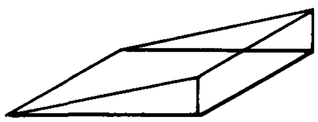

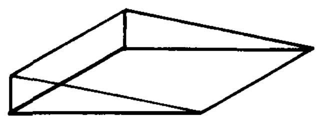

Transparency 20-45

The MITC4 element

- has only six zero eigenvalues (no spurious zero energy modes)
- passes the patch test

What do we mean by the patch test?

The key idea is that any arbitrary patch of elements should be able to represent constant stress conditions.

Transparency 20-46

Transparency 20-47

THE PATCH TEST

- We take an arbitrary patch of elements (some of which are geometrically distorted) and subject this patch to
  - — the minimum displacement/rotn. boundary conditions to eliminate the physical rigid body modes, and
  - — constant boundary tractions, corresponding to the constant stress condition that is tested.

Transparency 20-48

- We calculate all nodal point displacements and element stresses.

The patch test is passed if the calculated element internal stresses and nodal point displacements are correct.

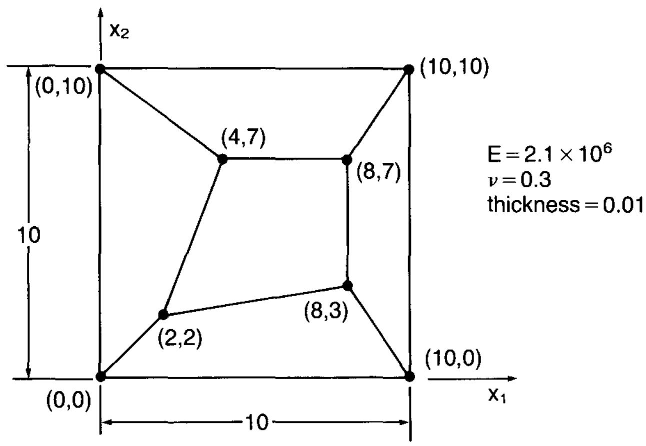

PATCH OF ELEMENTS CONSIDERED

Transparency 20-49

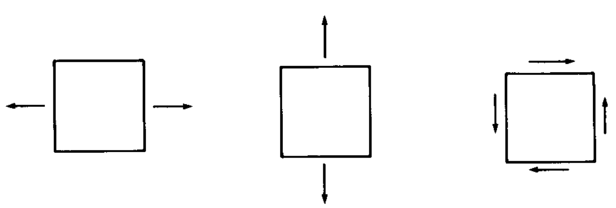

MEMBRANE TESTS

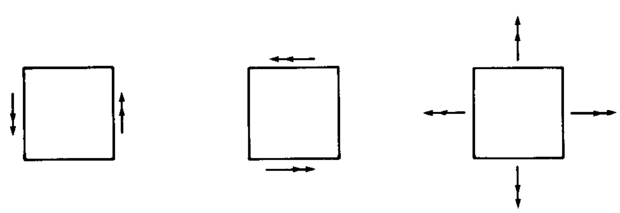

BENDING/TWISTING TESTS

Transparency 20-50

Transparency 20-51

Example: Spherical shell

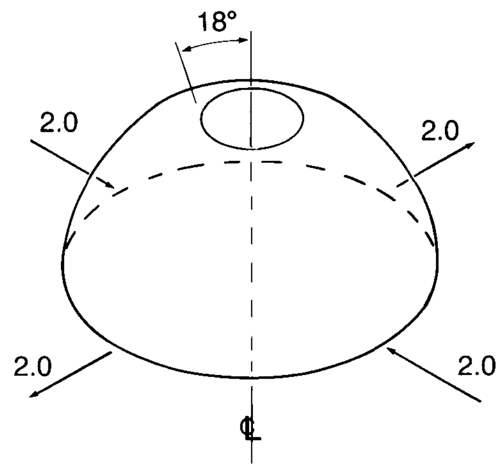

radius = 10.0
thickness = 0.04
$E = 6.825 \times 10^7$
$\nu = 0.3$

Transparency 20-52

Selection of director vectors:

- One director vector is generated for each node.
- The director vector for each node is chosen to be parallel to the radial vector for the node.
- In two dimensions:

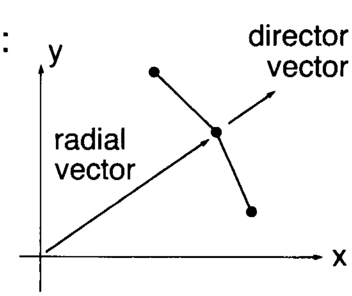

Selection of displacement boundary conditions:

- Consider a material fiber that is parallel to a director vector. Then, if this fiber is initially located in the x-z plane, by symmetry this fiber must remain in the x-z plane after the shell has deformed:

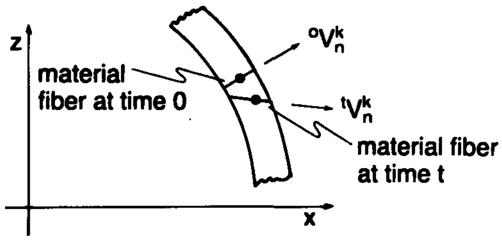

Transparency 20-53

Finite element mesh: Sixty-four MITC4 elements

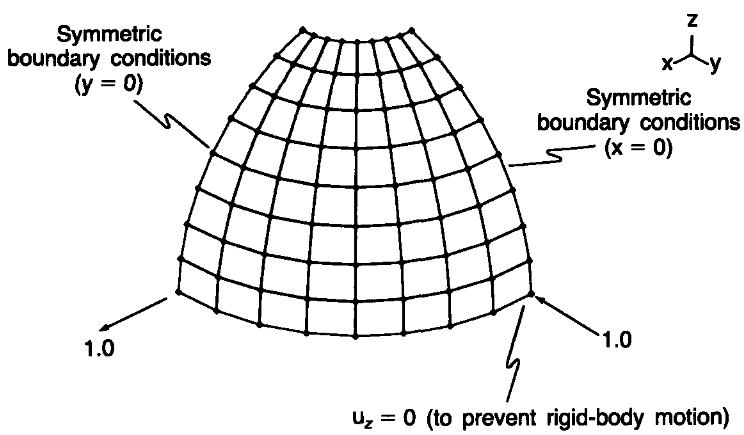

Transparency 20-54

Transparency 20-55

This condition is applied to each node on the x-z plane as follows:

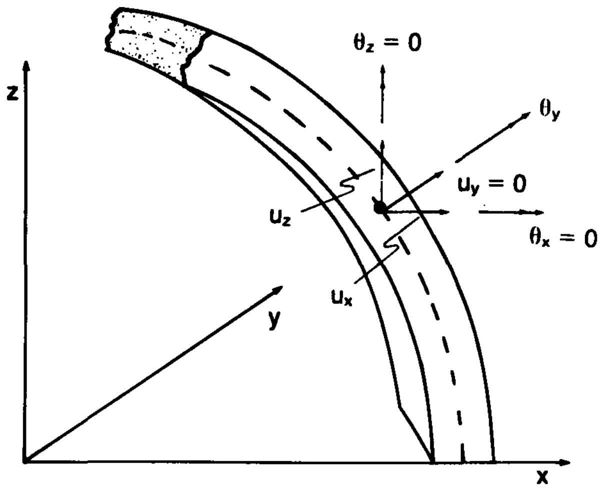

Transparency 20-56

- A similar condition is applied to nodes initially in the y-z plane.
- These boundary conditions are most easily applied by making each node in the x-z or y-z plane a 6 degree of freedom node. All other nodes are 5 degree of freedom nodes.
- To prevent rigid body translations in the z-direction, the z displacement of one node must be set to zero.

Linear elastic analysis results:

- Displacement at point of load application is 0.0936 (analytical solution is 0.094).
- Pictorially,

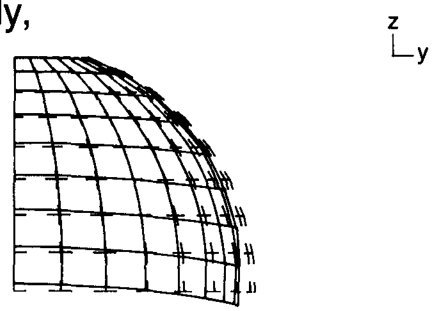

Transparency 20-57

<u>Example</u>: Analysis of an open (five-sided) box:

Box is placed open-side-down/Add on a frictionless surface.

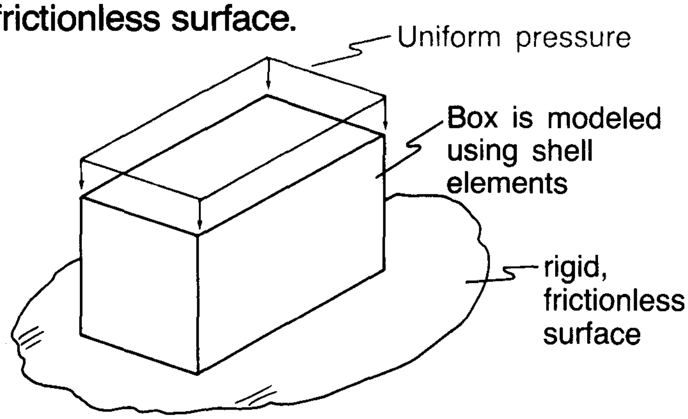

Transparency 20-58

Transparency 20-59

Modeling of the box with shell elements:

— Choose initial director vectors.

— Choose 5 or 6 degrees of freedom for each node.

— Choose boundary conditions.

Transparency 20-60

— Instead of input of director vectors, one for each node, it can be more effective to have ADINA generate mid-surface normal vectors.

— If no director vector is input for a node, ADINA generates for each element connected to the node a nodal point mid-surface normal vector at that node (from the element geometry).

— Hence, there will then be as many different nodal point mid-surface normal vectors at that node as there are elements connected to the node (unless the surface is flat).

Nodal point mid-surface normal vectors for the box:

— We use the option of automatic generation of element nodal point mid-surface normal vectors.

— At a node, not on an edge, the result is one mid-surface normal vector (because the surface is flat).

— At an edge where two shell elements meet, two mid-surface normal vectors are generated (one for each element).

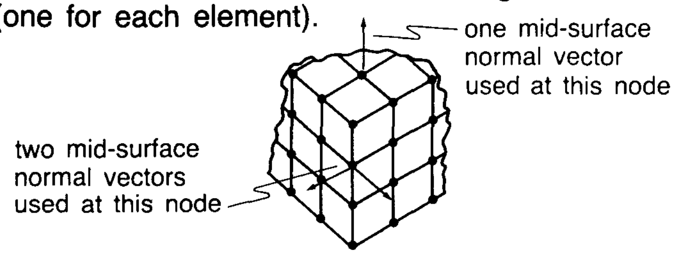

Transparency 20-61

Degrees of freedom:

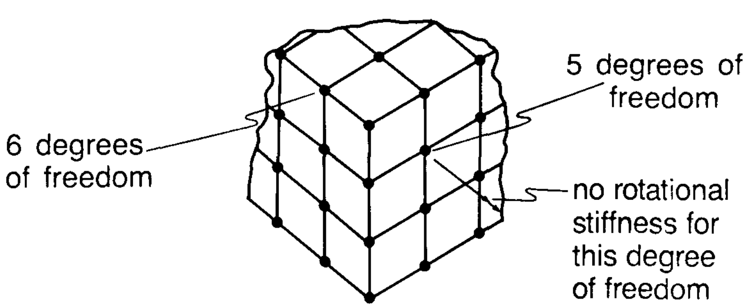

Transparency 20-62

Note added in preparation of study-guide

In the new version of ADINA (ADINA 84 with an update inserted, or ADINA 86) the use of the 5 or 6 shell degree of freedom option has been considerably automatized:

- The user specifies whether the program is to use 5 or 6 degrees of freedom at each shell mid-surface node N
  - IGL(N).EQ.0→6 d.o.f. with the translations and rotations corresponding to the global (or nodal skew) system
  - IGL(N).EQ.1→5 d.o.f. with the translations corresponding to the global (or nodal skew) system but the rotations corresponding to the vectors V_1 and V_2
- The user (usually) does not input any mid-surface normal or director vectors. The program calculates these automatically from the element mid-surface geometries.
- The user recognizes that a shell element has no nodal stiffness corresponding to the rotation about the mid-surface normal or director vector. Hence, a shell mid-surface node is assigned 5 d.o.f. unless
  - a shell intersection is considered
  - a beam with 6 d.o.f. is coupled to the shell node
  - a rotational boundary condition corresponding to a global (or skew) axis is to be imposed
  - a rigid link is coupled to the shell node

For further explanations, see the ADINA 86 users manual.

Transparency 20-63

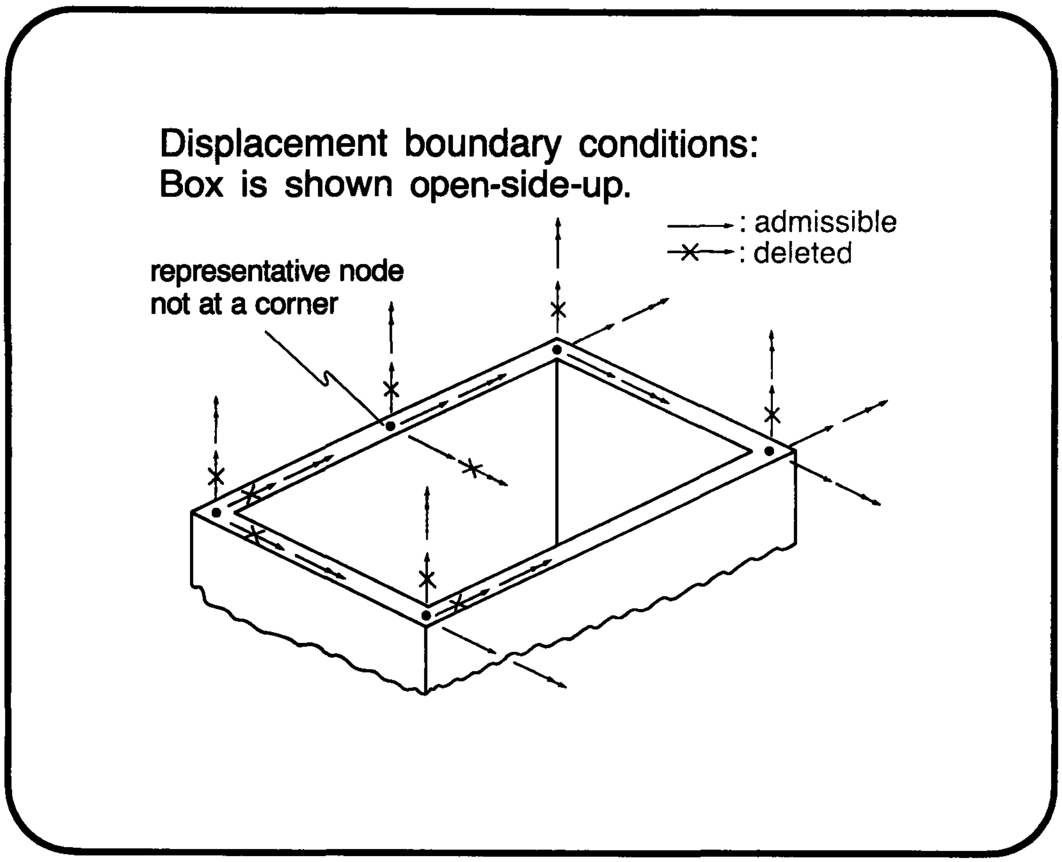

Consider a linear elastic static analysis of the box when a uniform pressure load is applied to the top.
We use the 128 element mesh shown (note that all hidden lines are removed in the figure):

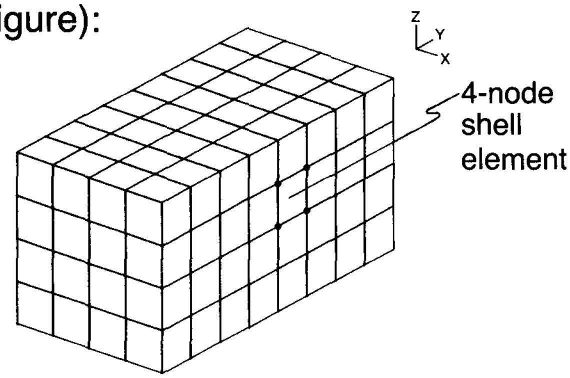

Transparency 20-64

We obtain the result shown below (again the hidden lines are removed):

- The displacements in this plot are highly magnified.

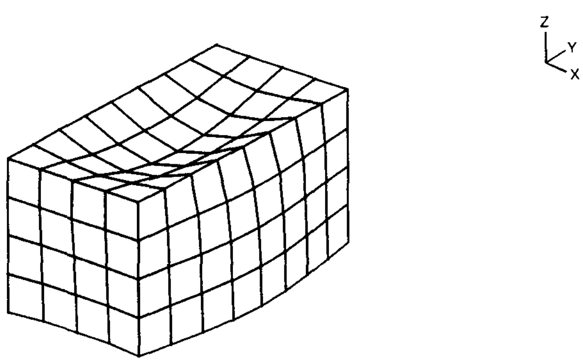

Transparency 20-65

Slide 20-3

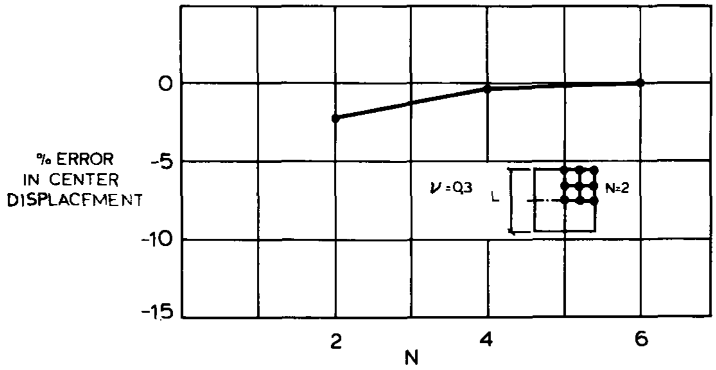

Simply-supported plate under uniform pressure, L/h = 1000

Slide 20-4

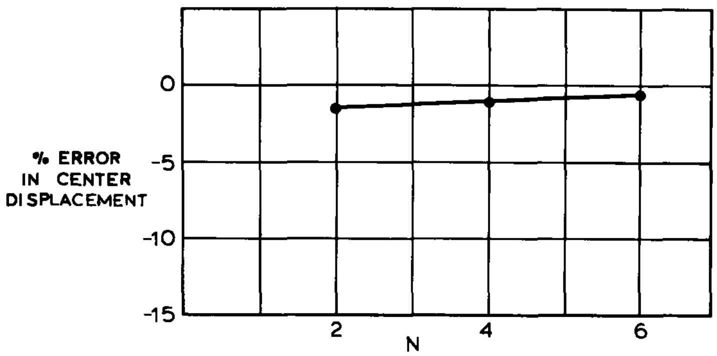

Simply-supported plate under concentrated load at center, L/h = 1000

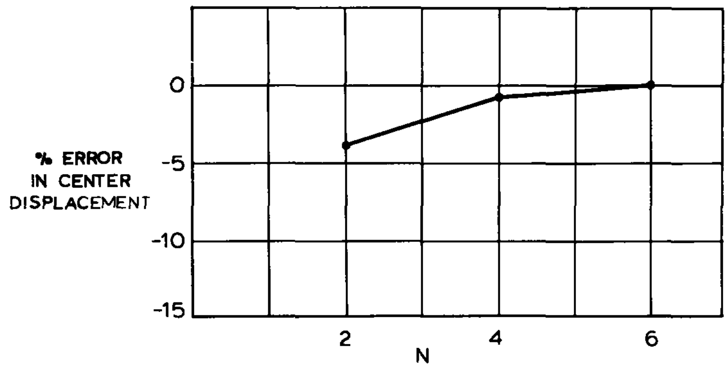

Clamped plate under uniform pressure, L/h = 1000

Slide
20-5

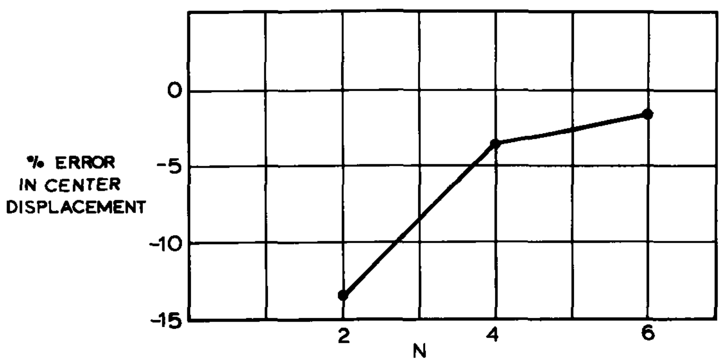

Clamped plate under concentrated load at center, L/h = 1000

Slide
20-6

Slide 20-7

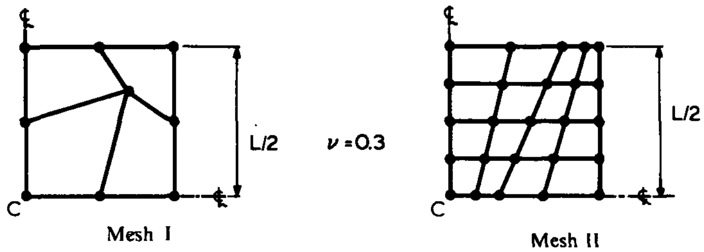

$\left.\dfrac{w^{FEM}}{w^{KIRCHHOFF}}\right\|_C$	Mesh I	0·93
	Mesh II	1·01
$\left.\dfrac{M^{FEM}}{M^{KIRCHHOFF}}\right\|_C$	Mesh I	0.85
	Mesh II	1.02

Effect of mesh distortion on results in analysis of a simply-supported plate under uniform pressure ($L/h = 1000$)

Slide 20-8

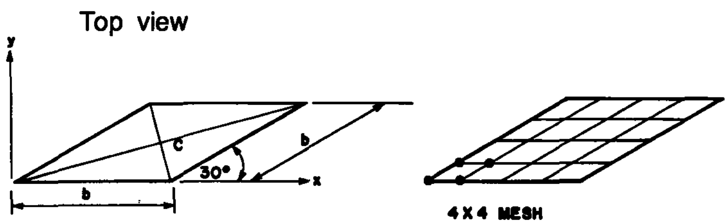

SIMPLY SUPPORTED EDGES

$E = 30 \cdot 10^6$

$\nu = 0.3$

$b = 1$

thickness = 0.01

uniform pressure p = 1

BOUNDARY CONDITION w = 0 ON FOUR EDGES

Analysis of skew plate

MESH	w_C^{FEM} / w_C^{MO}	$M_{max}^{FEM} / M_{max}^{MO}$	$M_{min}^{FEM} / M_{min}^{MO}$
4 X 4	0.879	0.873	0.852
8 X 8	0.871	0.928	0.922
16 X 16	0.933	0.961	0.919
32X32	0.985	0.989	0.990

Solution of skew plate at point C using uniform skew mesh

Slide 20-9

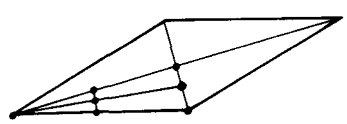

2 X 2 MESH

MESH	w_C^{FEM} / w_C^{MO}	$M_{max}^{FEM} / M_{max}^{MO}$	$M_{min}^{FEM} / M_{min}^{MO}$
2 X 2	0.984	0.717	0.602
4 X 4	0.994	0.935	0.878

Solution of skew plate using a more effective mesh

Slide 20-10

Slide 20-11

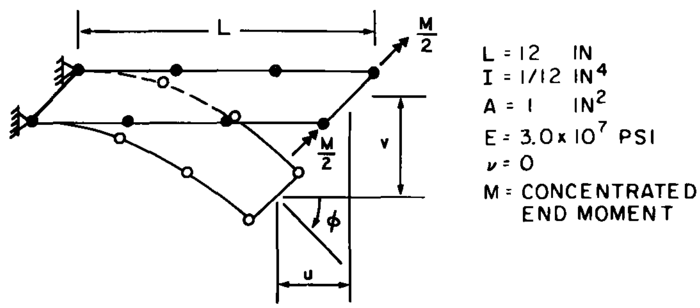

Large displacement analysis of a cantilever

Slide 20-12

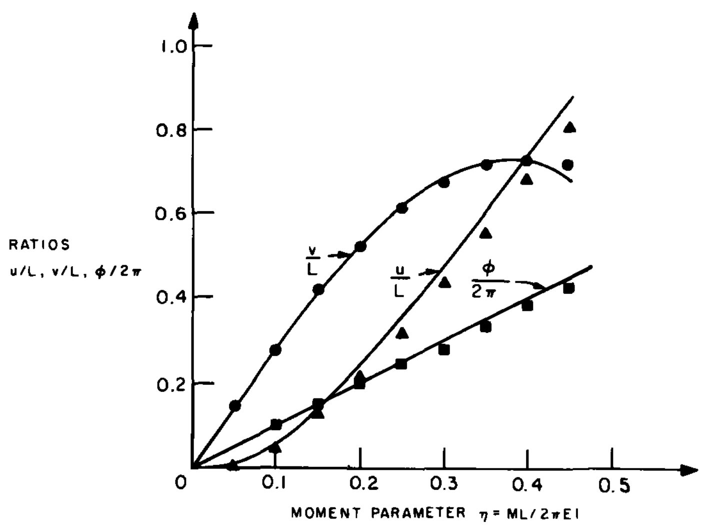

Response of cantilever

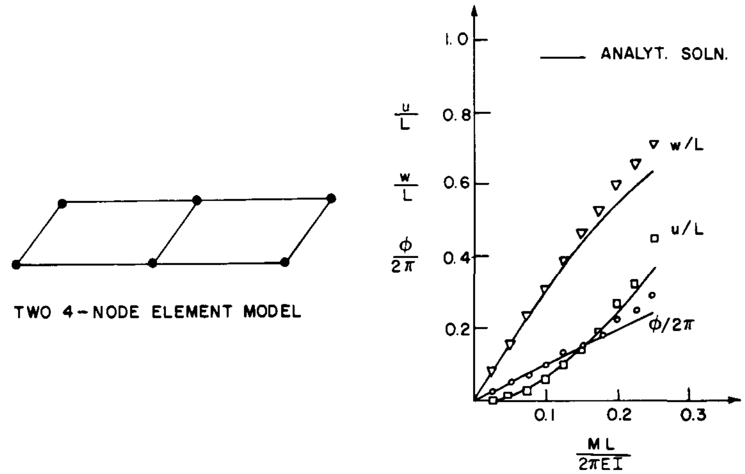

Large displacement/rotation analysis of a cantilever

Slide 20-13

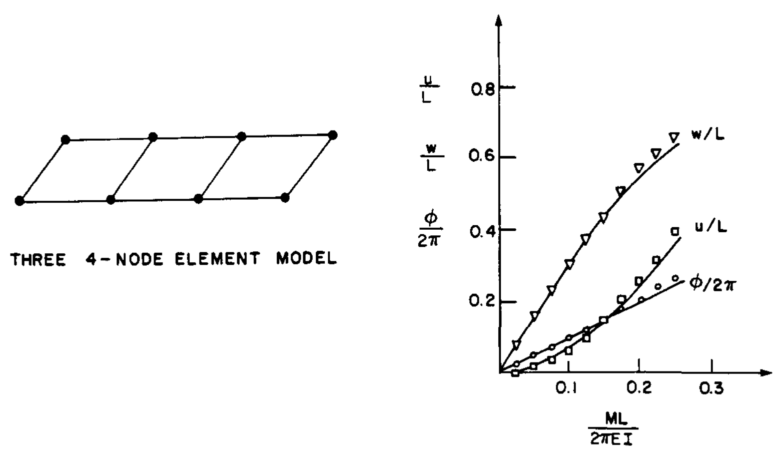

Slide 20-14

Slide 20-15

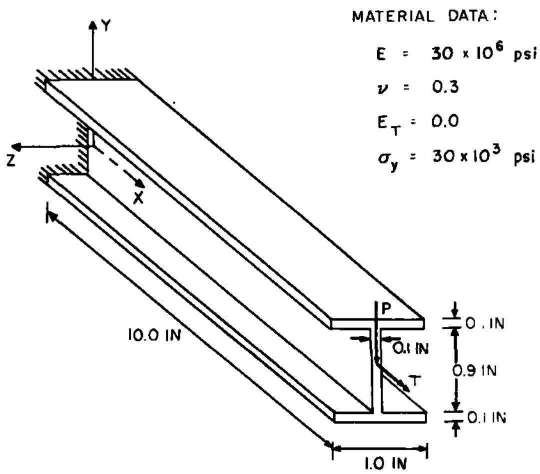

Analysis of I-beam

Slide 20-16

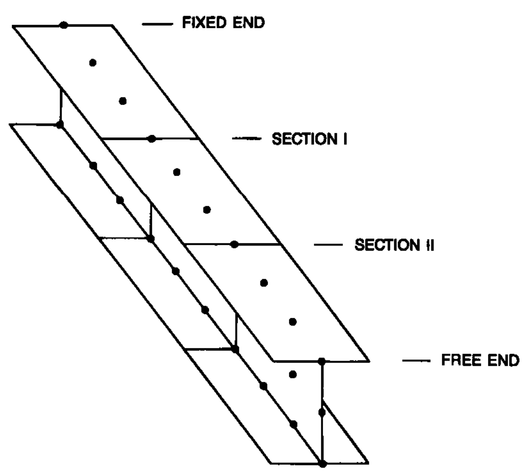

Iso-beam model

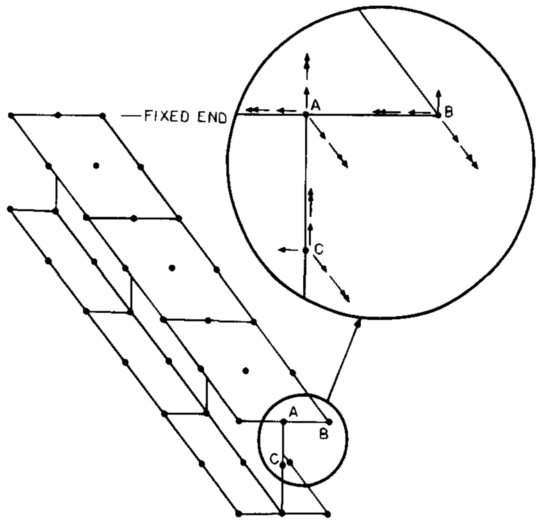

Shell model

Slide 20-17

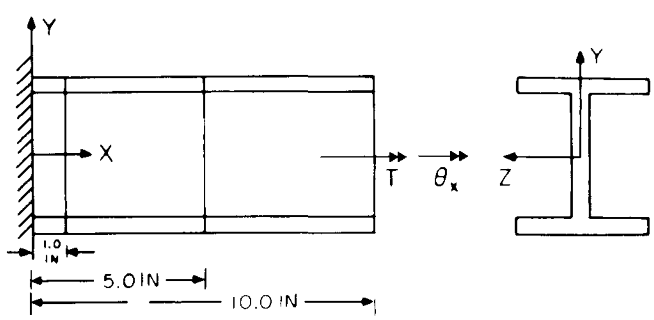

I-beam

Slide 20-18

Slide 20-19

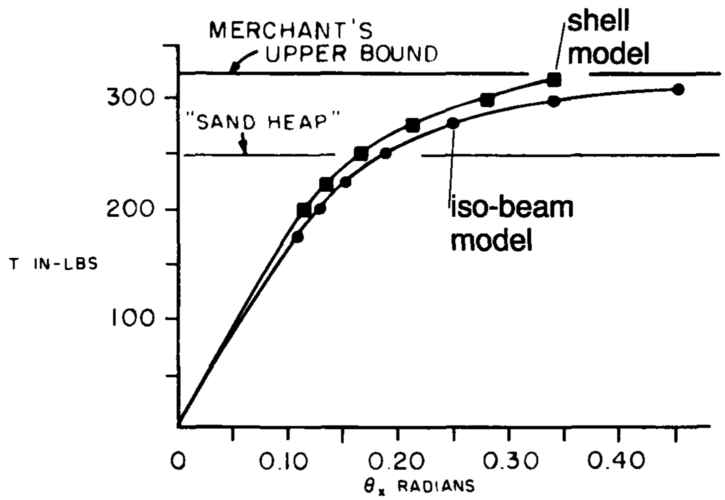

Rotation of I-beam about X-axis for increasing torsional moment.

Slide 20-20

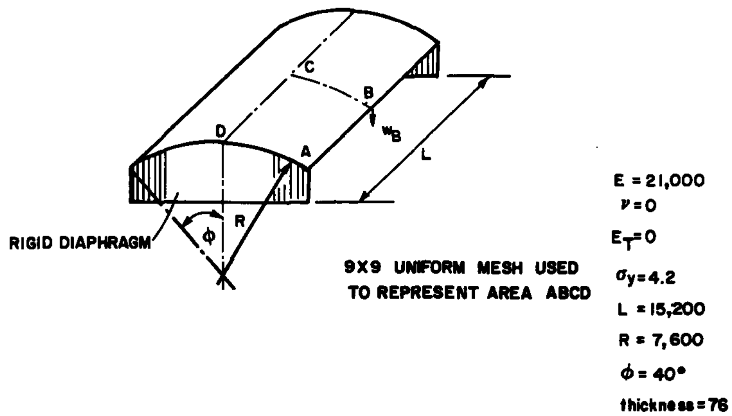

Large deflection elastic-plastic analysis of a cylindrical shell

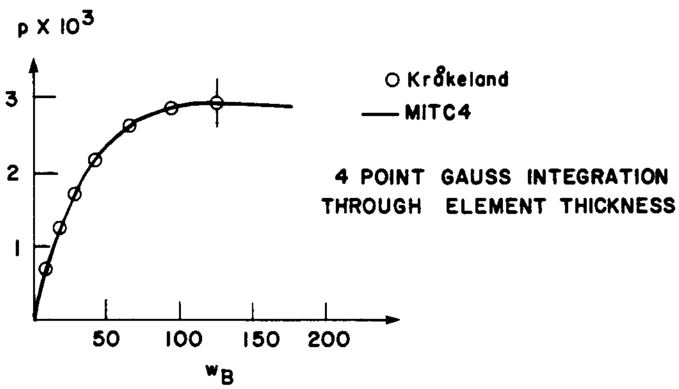

Response of shell

Slide 20-21

Topic 21

A Demonstrative Computer Session Using ADINA—Linear Analysis

Contents:

- **Use of the computer program ADINA for finite element analysis, discussion of data preparation, program solution, and display of results**
- **Capabilities of ADINA**
- **Computer laboratory demonstration—Part I**
- **Linear analysis of a plate with a hole for the stress concentration factor**
- **Data input preparation and mesh generation**
- **Solution of the model**
- **Study and evaluation of results using plots of stresses, stress jumps, and pressure bands**

Textbook: Appendix

References:

The use of the ADINA program is described and sample solutions are given in

Bathe, K. J., "Finite Elements in CAD — and ADINA," *Nuclear Engineering and Design*, to appear.

ADINA, ADINAT, ADINA-IN, and ADINA-PLOT Users Manuals, ADINA Verification Manual, and ADINA Theory and Modeling Guide, ADINA Engineering, Inc., Watertown, MA 02172, U.S.A.

Proceedings of the ADINA Conferences, (Bathe, K. J., ed.)
Computers & Structures
13, 5–6, 1981
17, 5–6, 1983
21, 1–2, 1985

References:
(continued)

The use of pressure band plots to evaluate meshes is discussed in

Sussman, T., and K. J. Bathe, "Studies of Finite Element Procedures—Stress Band Plots and the Evaluation of Finite Element Meshes," *Engineering Computations*, to appear.

A FINITE ELEMENT ANALYSIS — LINEAR SOLUTION

- We have presented a considerable amount of theory and example solution results in the lectures.
- The objective in the next two lectures is to show how an actual finite element analysis is performed on the computer.

Transparency 21-1

- We cannot discuss in detail all the aspects of the analysis, but shall summarize and demonstrate on the computer the major steps of the analysis, and concentrate on
  - — possible difficulties
  - — possible pitfalls
  - — general recommendations

Transparency 21-2

Transparency 21-3

We will use as the example problem the plate with a hole already considered earlier, and perform linear and nonlinear analyses

— elastic analysis to obtain the stress concentration factor
— elasto-plastic analysis to estimate the limit load
— an analysis to investigate the effect of a shaft in the plate hole

Transparency 21-4

Plate with hole: Schematic drawing

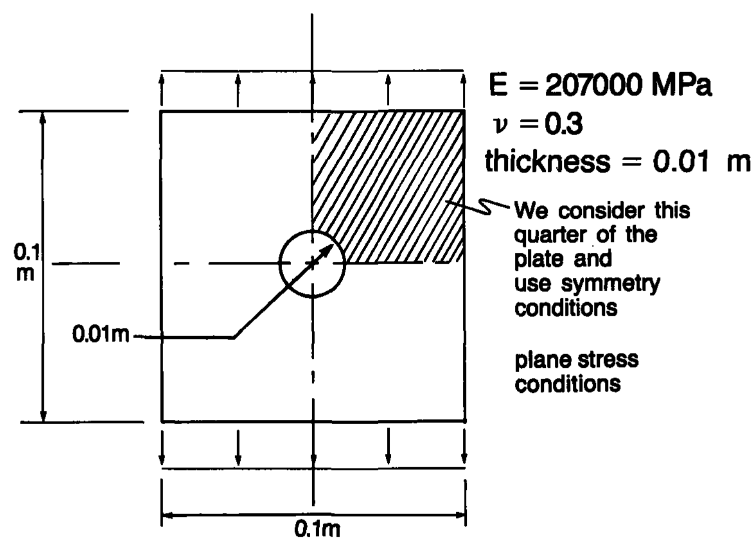

- The first step for a finite element analysis is to select a computer program. We use the ADINA system.

ADINA-IN	to prepare, generate the finite element data
ADINA	to solve the finite element model
ADINA-PLOT	to display numerically or graphically the solution results

Transparency 21-5

Schematically:

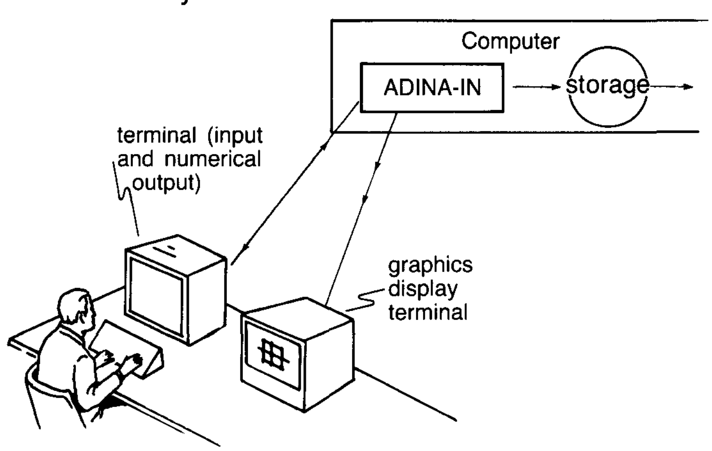

User work-station

Transparency 21-6

Transparency 21-7

- User types into terminal ADINA-IN commands interactively or for batch mode processing. User checks input and generated data on graphics display terminal.

Transparency 21-8

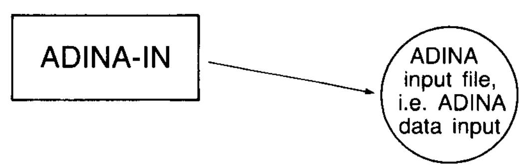

- ADINA-IN generates the input data for ADINA.
- The input data is checked internally in ADINA-IN for errors and consistency and is displayed as per request by the user.
- The degree of freedom numbers are generated (for a minimum bandwidth).

Transparency 21-9

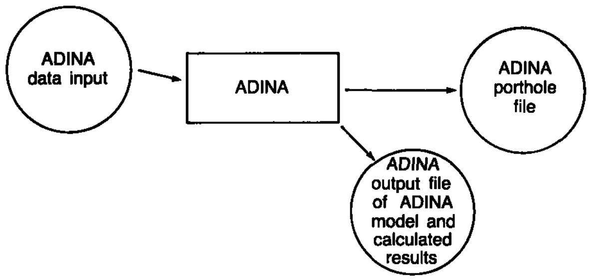

- User runs ADINA to calculate the response of the finite element model. ADINA writes the model data and calculated results on an output file and stores the model data and calculated results on the porthole file.

Transparency 21-10

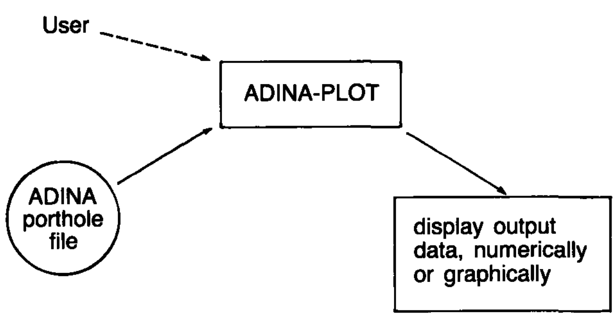

- User runs ADINA-PLOT to access the output data and display selected results; displacements, stresses, mode shapes, maxima, . . .

Transparency 21-11

A brief overview of ADINA

- Static and dynamic solutions
- Linear and nonlinear analysis
- Small and very large finite element models can be solved.

The formulations, finite elements and numerical procedures used in the program have largely been discussed in this course.

Transparency 21-12

DISPLACEMENT ASSUMPTIONS

- Infinitesimally small displacements
- Large displacements/large rotations but small strains
- Large deformations/large strains

MATERIAL MODELS

Isotropic Linear Elastic

Orthotropic Linear Elastic

Isotropic Thermo-Elastic

Curve Description Model for Analysis of Geological Materials

Concrete Model

Transparency 21-13

MATERIAL MODELS

Isothermal Plasticity Models

Thermo-Elastic-Plastic and Creep Models

Nonlinear Elastic, Incompressible Models

User-Supplied Models

Transparency 21-14

Transparency 21-15

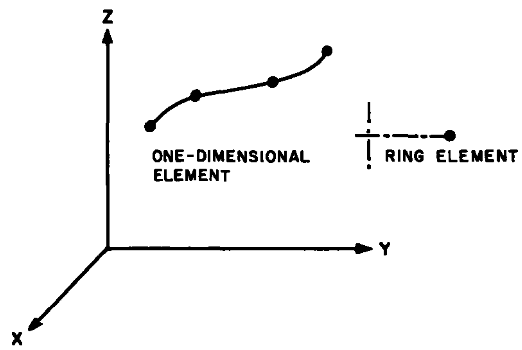

Truss and Cable Element
(2, 3, or 4 nodes)

Transparency 21-16

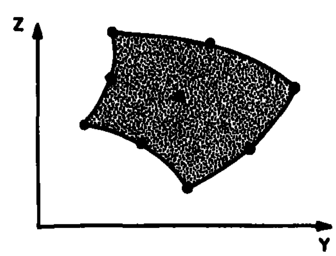

Two-Dimensional Solid Element
(variable number of nodes)

Transparency 21-17

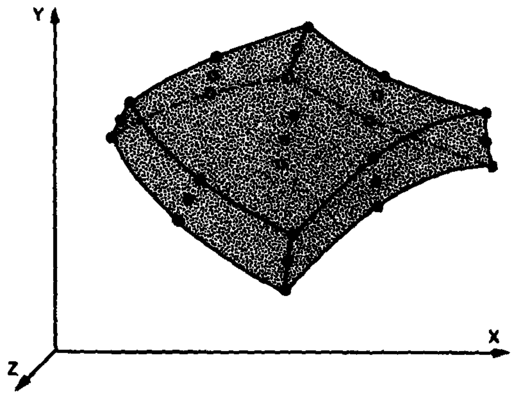

Three-Dimensional Solid Element
(variable number of nodes)

Transparency 21-18

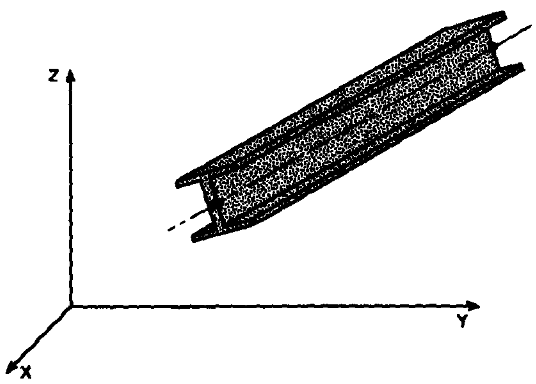

Two-Node Beam Element

Transparency 21-19

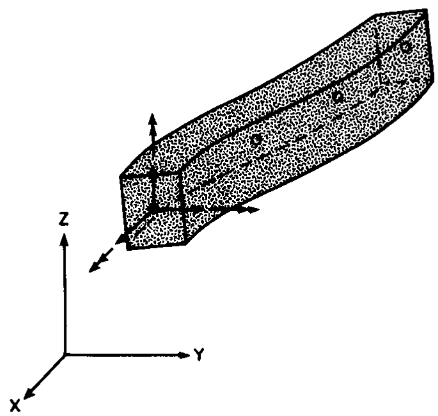

Isoparametric Beam Element
(2, 3, 4 nodes)

Transparency 21-20

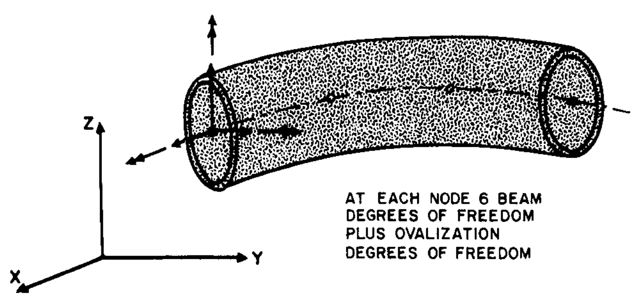

Pipe Element with Ovalization

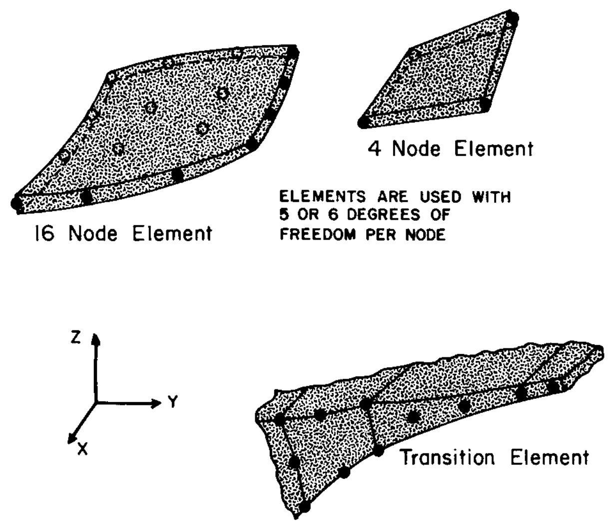

Plate and Shell Elements

Transparency 21-21

A SUMMARY OF IMPORTANT OBSERVATIONS

- We need to check the finite element data input carefully
  - — prior to the actual response solution run, and
  - — after the response solution has been obtained by studying whether the desired boundary conditions are satisfied, whether the displacement and stress solution is reasonable (for the desired analysis).

Transparency 21-22

Transparency 21-23

- We need to carefully evaluate and interpret the calculated response
  - — study in detail the calculated displacements and stresses along certain lines, study stress jumps
  - — stress averaging, stress smoothing should only be done after the above careful evaluation

Transparency 21-24

Data for Construction of 64 Element Mesh:

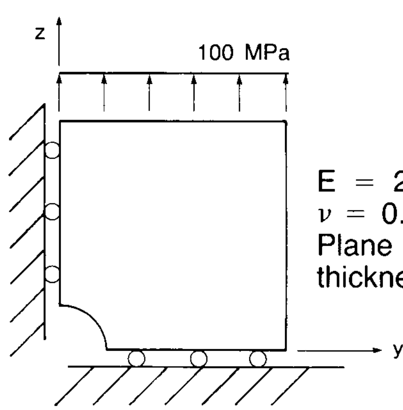

E = 207,000 MPa
ν = 0.3
Plane stress
thickness = 0.01 m

Transparency 21-25

Finite element mesh to be generated using ADINA-IN:

- Mesh contains 64 elements, 288 nodes.

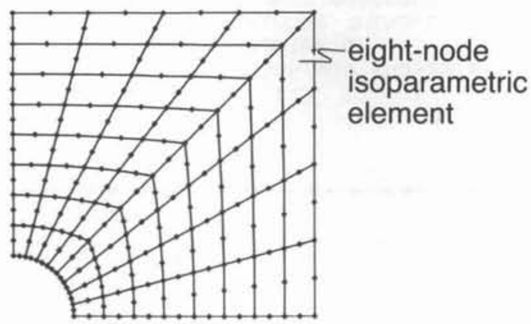

Demonstration Photograph 21-1

Finite Element Research Group Laboratory computer configuration

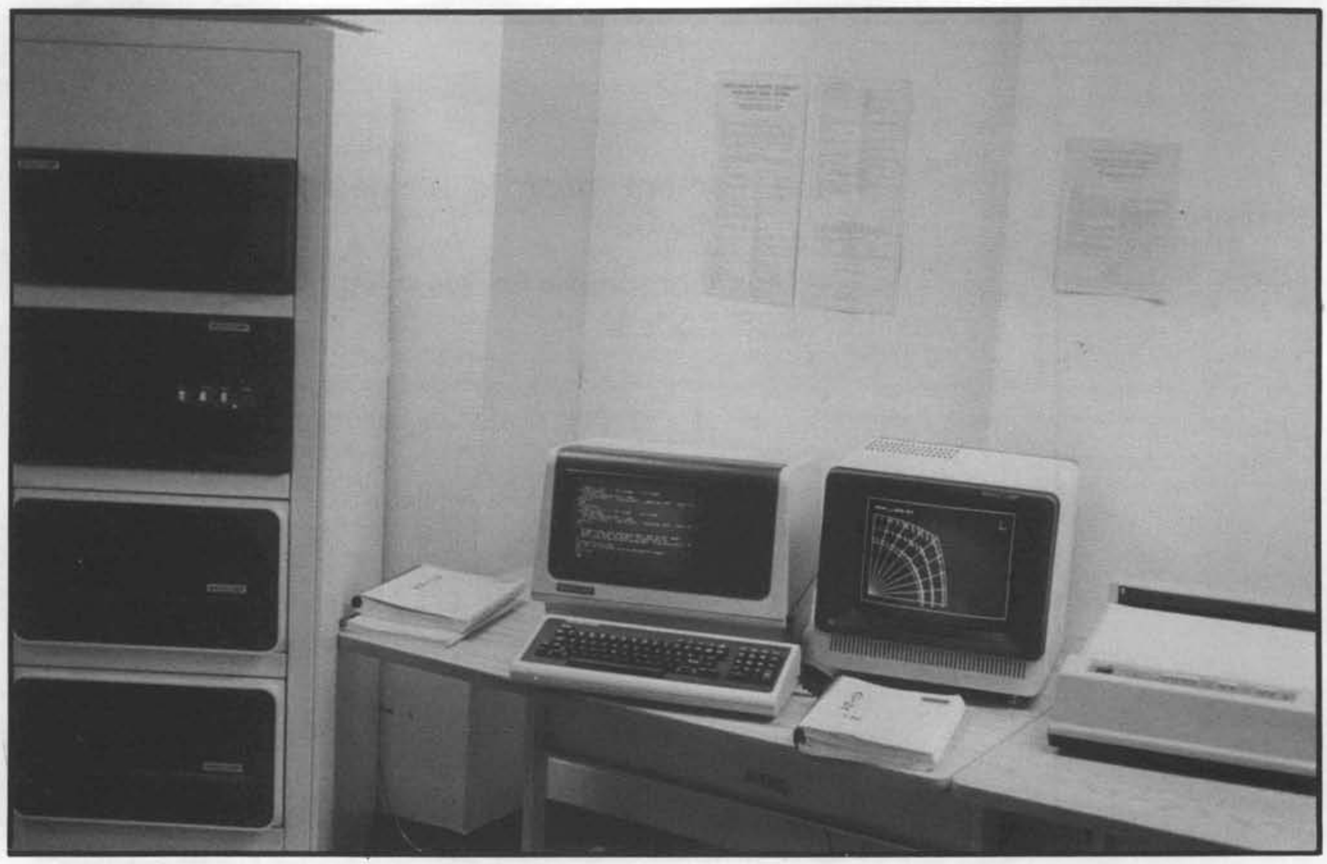

ADINA Demonstration 21-1
Input data

```
QUARTER PLATE WITH HOLE - 64 ELEMENTS
 2261001110  1    0     1     1 1.0000000
C***  MASTER CONTROL
99999    0    0    1    0    0    1   50 30.
C***  3  LOAD CONTROL
    0    4    0    0    0    0    0    0
C***  4  MASS AND DAMPING CONTROL
    0    0    0    0         .0         .0
C***  5  EIGENVALUE SOLUTION CONTROL
    0    0    0    0    0    0
C***  6  TIME INTEGRATION METHOD CONTROL
    0    20.500000000.25000000    0    0
C***  7  INCREMENTAL SOLUTION CONTROL
    1    1     210 15.001000000.010000000.05
C***  8  PRINT-OUT CONTROL
    1    1    1    1    1    1    0
```

Transparency 21-26
(Repeat 21-25)

Finite element mesh to be generated using ADINA-IN:

- Mesh contains 64 elements, 288 nodes.

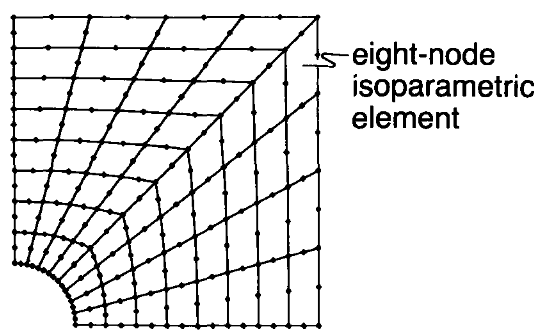

Stress vector output: Example

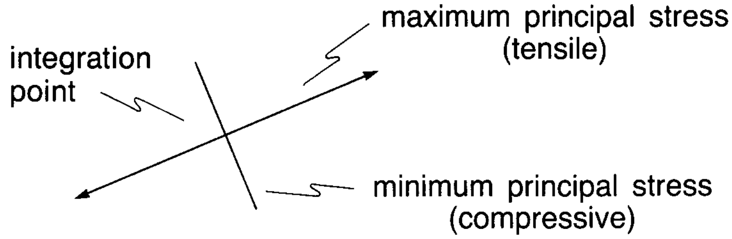

The length of the line is proportional to the magnitude of the stress.

Transparency 21-27

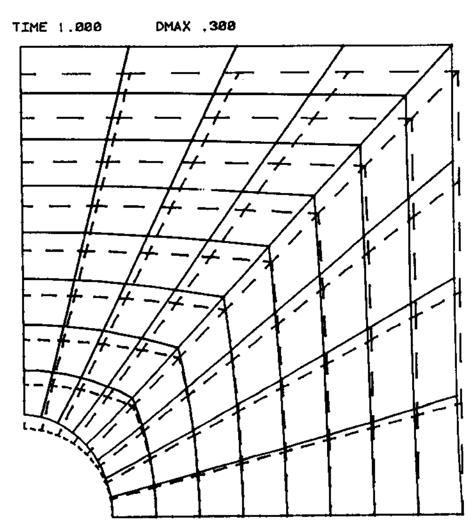

ADINA Demonstration 21-2

Deformed mesh plot

Transparency 21-28

Plate with hole: Schematic drawing

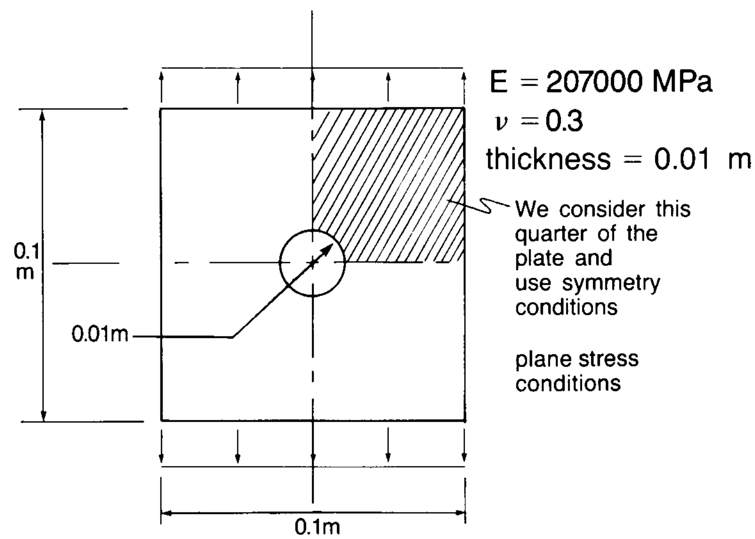

Transparency 21-29
(Repeat 21-25)

Finite element mesh to be generated using ADINA-IN:

- Mesh contains 64 elements, 288 nodes.

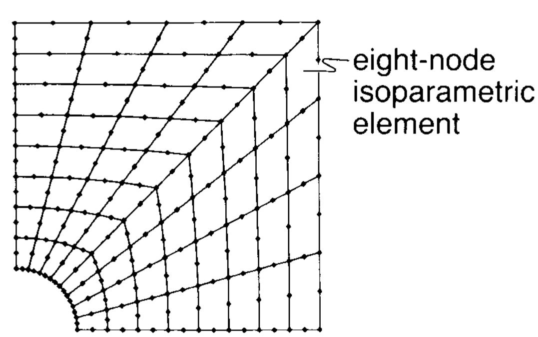

Stress point numbers and integration point numbers for element 57

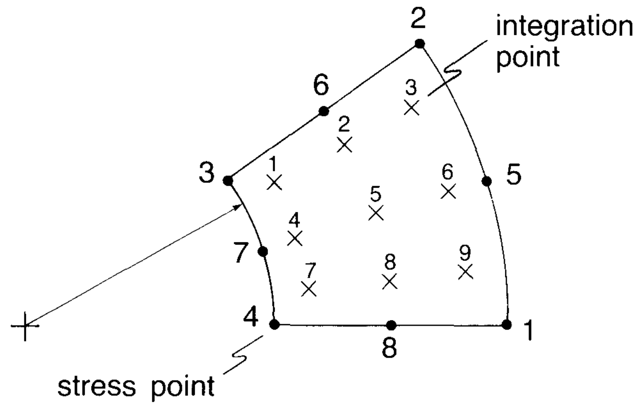

Transparency 21-30

Behavior of stresses near the stress concentration:

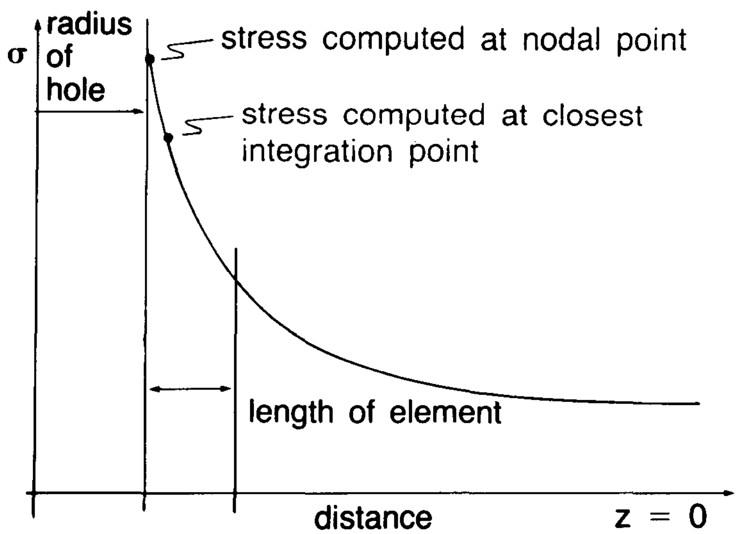

Transparency 21-31

Transparency 21-32

Maximum principal stress calculation:

$$\sigma_1 = \frac{\sigma_{yy} + \sigma_{zz}}{2} + \sqrt{\frac{(\sigma_{yy} - \sigma_{zz})^2}{4} + \sigma_{yz}^2}$$

Transparency 21-33
(Repeat 21-30)

Stress point numbers and integration point numbers for element 57

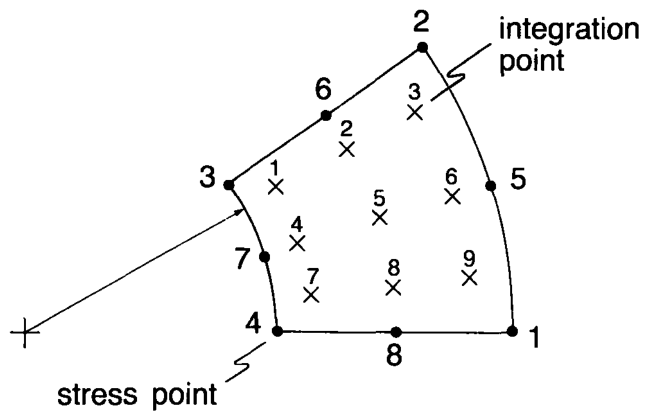

```
RESULTANT = SMAX        ARITHMETIC EXPRESSION:

(TYY+TZZ)/TWO+SQRT((TYY-TZZ)*(TYY-TZZ)/FOUR+TYZ*TYZ)

TYY       = YY-STRESS
TZZ       = ZZ-STRESS
TYZ       = YZ-STRESS
TWO       =  2.00000
FOUR      =  4.00000

EXTREME ELEMENT RESULTS PER ELEMENT GROUP FOR WHOLE MODEL

INTERVAL  TSTART= 1.0000      TEND= 1.0000      SCANNED FOR ABSOLUTE MAXIMUM

ELEMENT GROUP NO =   1  (2-D SOLID)          LISTED RESULTS ARE MEASURED IN
                                             GLOBAL COORDINATE SYSTEM
    RESULTANT SMAX        ELEMENT  POINT        TIME       STEP

  0.345151E+03               57       4    0.10000E+01       1
```

ADINA Demonstration 21-3

Close-up of calculations

Finite element mesh to be generated using ADINA-IN:

- Mesh contains 64 elements, 288 nodes.

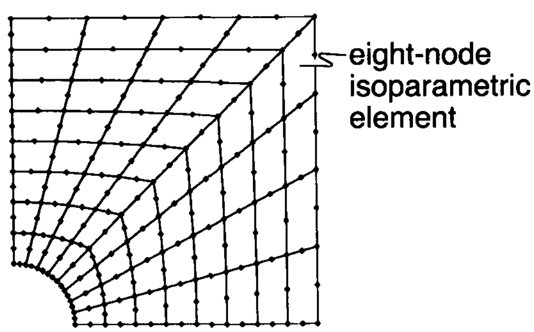

Transparency 21-34

(Repeat 21-25)

Transparency 21-35
(Repeat 2-33)

- To be confident that the stress discontinuities are small everywhere, we should plot stress jumps along each line in the mesh.
- An alternative way of presenting stress discontinuities is by means of a pressure band plot:
  - — Plot bands of constant pressure where

$$\text{pressure} = \frac{-(\tau_{xx} + \tau_{yy} + \tau_{zz})}{3}$$

Transparency 21-36
(Repeat 2-35)

Sixty-four element mesh: Pressure band plot

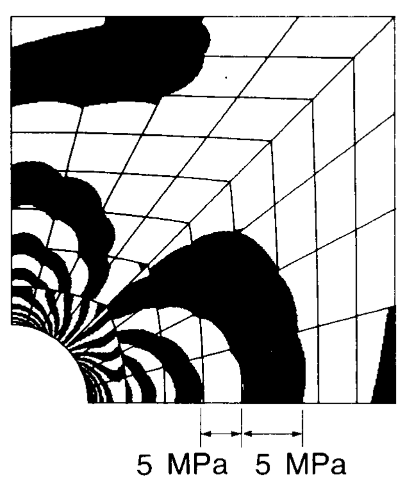

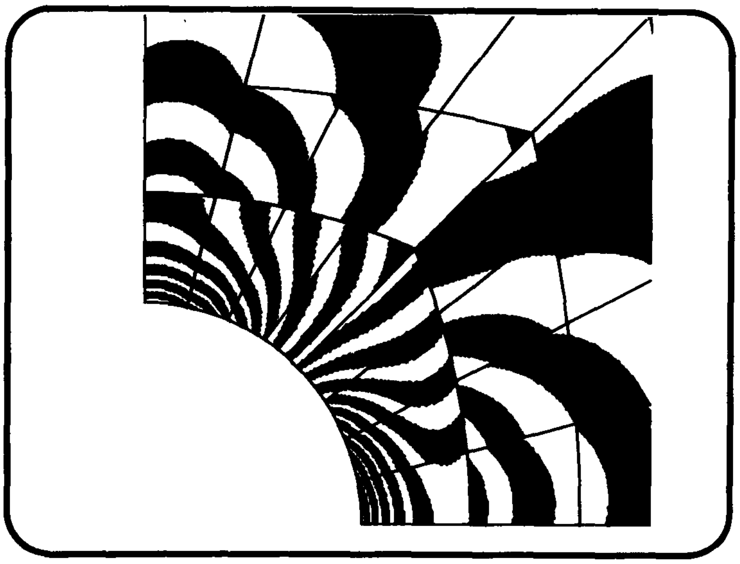

ADINA Demonstration 21-4
Close-up of pressure bands

A SUMMARY OF IMPORTANT OBSERVATIONS

- We need to check the finite element data input carefully
  - — prior to the actual response solution run, and
  - — after the response solution has been obtained by studying whether the desired boundary conditions are satisfied, whether the displacement and stress solution is reasonable (for the desired analysis).

Transparency 21-37
(Repeat 21-22)

Transparency 21-38
(Repeat 21-23)

- We need to carefully evaluate and interpret the calculated response
  - — study in detail the calculated displacements and stresses along certain lines, study stress jumps
  - — stress averaging, stress smoothing should only be done after the above careful evaluation

Topic 22

A Demonstrative Computer Session Using ADINA—Nonlinear Analysis

Contents:

- **Use of ADINA for elastic-plastic analysis of a plate with a hole**
- **Computer laboratory demonstration—Part II**
- **Selection of solution parameters and input data preparation**
- **Study of the effect of using different kinematic assumptions (small or large strains) in the finite element solution**
- **Effect of a shaft in the plate hole, assuming frictionless contact**
- **Effect of expanding shaft**
- **Study and evaluation of solution results**

Textbook: Appendix

References: The use of the ADINA program is described and sample solutions are given in

Bathe, K. J., "Finite Elements in CAD — and ADINA," *Nuclear Engineering and Design,* to appear.

ADINA, ADINAT, ADINA-IN, and ADINA-PLOT Users Manuals, ADINA Verification Manual, and ADINA Theory and Modeling Guide, ADINA Engineering, Inc., Watertown, MA 02172, U.S.A.

References:
(continued)

Proceedings of the ADINA Conferences, (K. J. Bathe, ed.)
Computers & Structures
13, No. 5–6, 1981
17, No. 5–6, 1983
21, No. 1–2, 1985

The contact solution procedure used in the analysis of the plate with the shaft is described in

Bathe, K. J., and A. Chaudhary, "A Solution Method for Planar and Axisymmetric Contact Problems," *International Journal for Numerical Methods in Engineering, 21*, 65–88, 1985.

A FINITE ELEMENT ANALYSIS — NONLINEAR SOLUTION

- We continue to consider the plate with a hole.
- A nonlinear analysis should only be performed once a linear solution has been obtained.
  The linear solution checks the finite element model and yields valuable insight into what nonlinearities might be important.

Transparency 22-1

Plate with hole: Schematic drawing

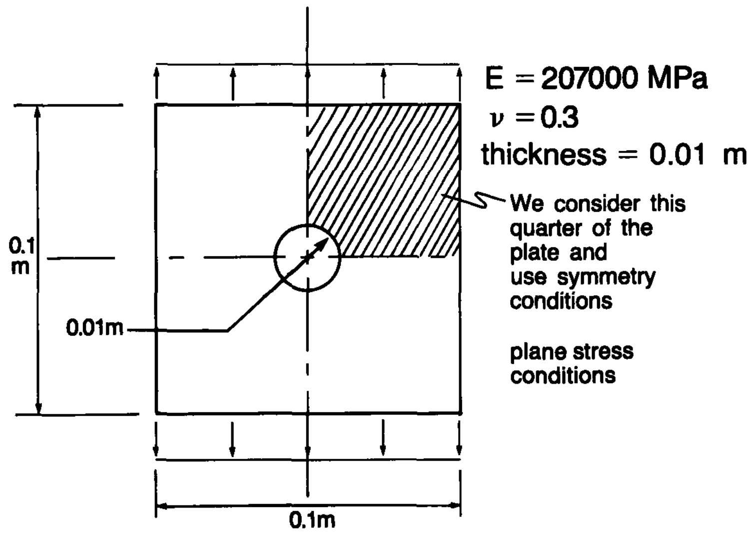

Transparency 22-2
(Repeat 21-4)

Transparency 22-3
(Repeat 21-25)

Finite element mesh to be generated using ADINA-IN:

- Mesh contains 64 elements, 288 nodes.

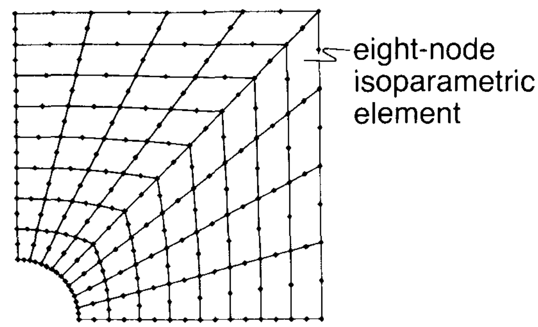

Transparency 22-4

- Some important considerations are now
  - What material model to select
  - What displacement/strain assumption to make
  - What sequence of load application to choose
  - What nonlinear equation solution strategy and convergence criteria to select

Transparency 22-5

- We use the ADINA system to analyse the plate for its elasto-plastic static response.
- We also investigate the effect on the response when a shaft is placed in the plate hole.

Transparency 22-6

Some important observations:

- The recommendations given in the linear analysis are here also applicable (see previous lecture).
- For nonlinear analysis we need to, in addition, be careful with the
  - — sequence and incremental magnitudes of load application
  - — choice of convergence tolerances

Transparency 22-7

Limit load calculations:

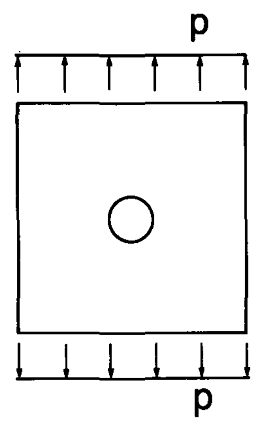

- Plate is elasto-plastic.

Transparency 22-8

Elasto-plastic analysis:

Material properties (steel)

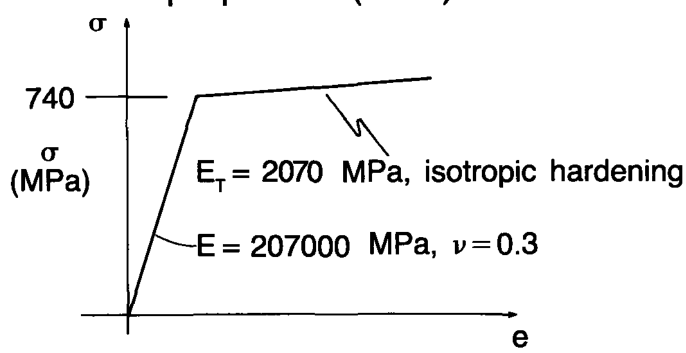

- This is an idealization, probably inaccurate for large strain conditions ($e > 2\%$).

Load history:

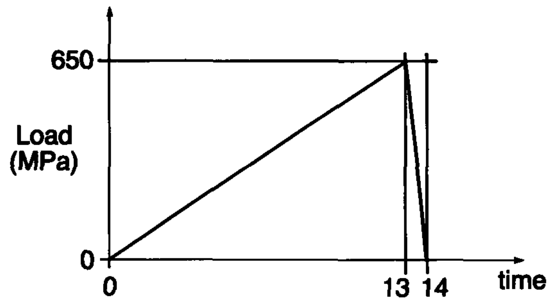

- Load is increased 50 MPa per load step.
- Load is released in one load step.

Transparency 22-9

```
USER-SUPPLIED

MATERIAL 1 PLASTIC E=207000 NU=0.3 ET=2070 YIELD=740
MATERIAL 1 PLASTIC E=207000 NU=0.3 ET=2070 YIELD=740
DELETE EQUILIBRIUM-ITERATIONS
DELETE EQUILIBRIUM-ITERATIONS
ADINA
ADINA
```

ADINA Demonstration 22-1
Input data

Transparency 22-10
(Repeat 21-25)

Finite element mesh to be generated using ADINA-IN:

- Mesh contains 64 elements, 288 nodes.

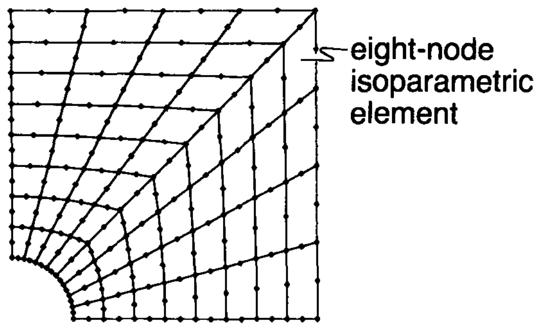

Transparency 22-11

Load history:

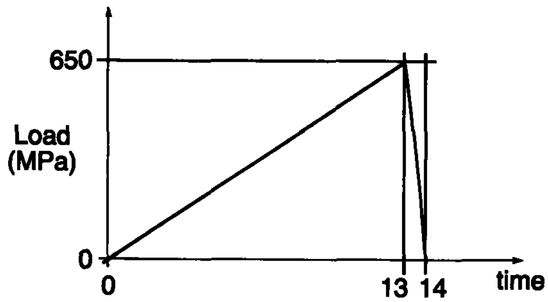

- Load is increased 50 MPa per load step.
- Load is released in one load step.
- The BFGS method is employed for each load step.

Convergence criteria:

Energy:

$$\frac{\Delta \underline{U}^{(i)T}\left[{}^{t+\Delta t}\underline{R} - {}^{t+\Delta t}\underline{F}^{(i-1)}\right]}{\Delta \underline{U}^{(1)T}\left[{}^{t+\Delta t}\underline{R} - {}^{t}\underline{F}\right]} \leq \text{ETOL} = 0.001$$

Force:

$$\frac{\left\|{}^{t+\Delta t}\underline{R} - {}^{t+\Delta t}\underline{F}^{(i-1)}\right\|_2}{\text{RNORM}} \leq \text{RTOL} = 0.01$$

$$(\text{RNORM} = \underbrace{100\ \text{MPa}}_{\substack{\text{nominal}\\ \text{applied}\\ \text{load}}} \times \underbrace{0.05\ \text{m}}_{\text{width}} \times \underbrace{0.01\ \text{m}}_{\text{thickness}})$$

Transparency 22-12

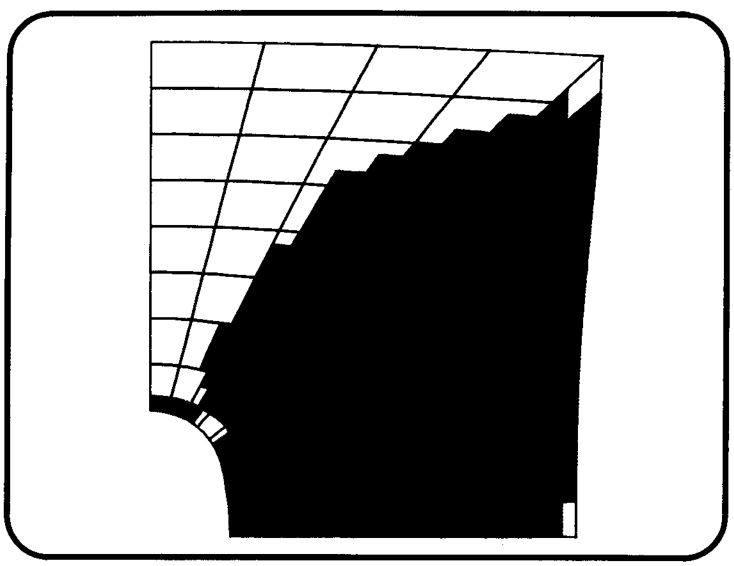

ADINA Demonstration 22-2
Plot of plasticity in plate with hole

Transparency 22-13

Stress vector output: Example

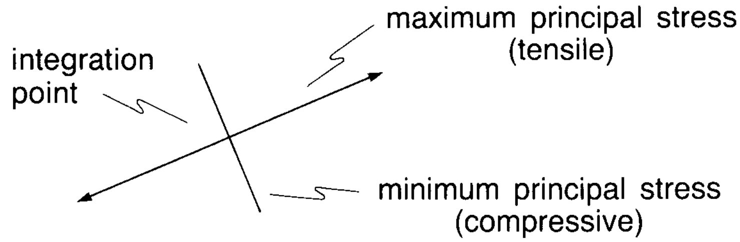

The length of the line is proportional to the magnitude of the stress.

ADINA Demonstration 22-3
Close-up of stress vectors around hole

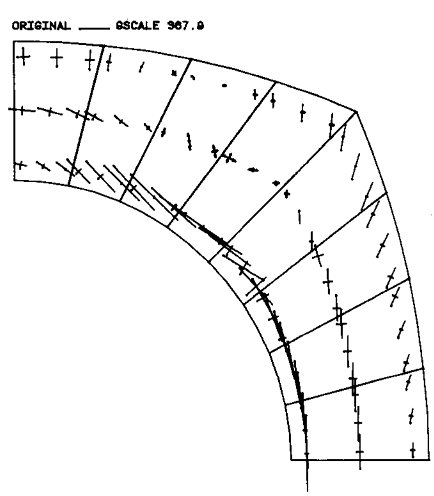

Finite element mesh to be generated using ADINA-IN:

- Mesh contains 64 elements, 288 nodes.

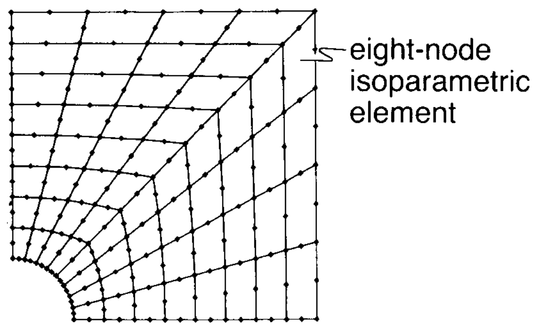

Transparency 22-14
(Repeat 21-25)

M.N.O.	Materially-Nonlinear-Only analysis
T.L.	Total Lagrangian formulation
U.L.	Updated Lagrangian formulation

Transparency 22-15

Transparency 22-16
(Repeat 21-25)

Finite element mesh to be generated using ADINA-IN:

- Mesh contains 64 elements, 288 nodes.

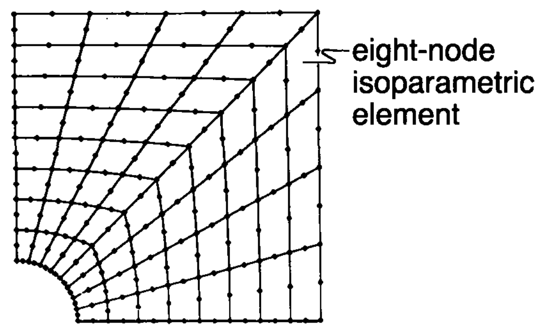

ADINA Demonstration 22-4
Elasto-plastic load displacement response

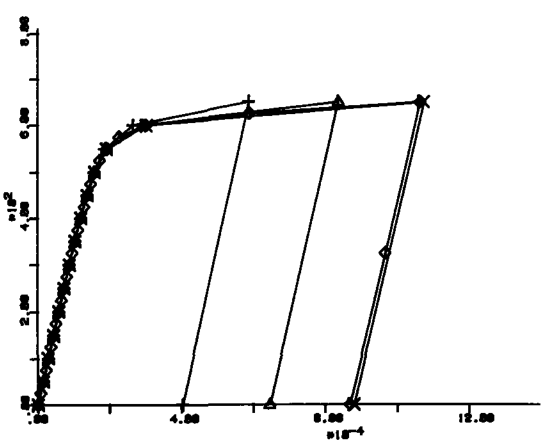

Plate with shaft:

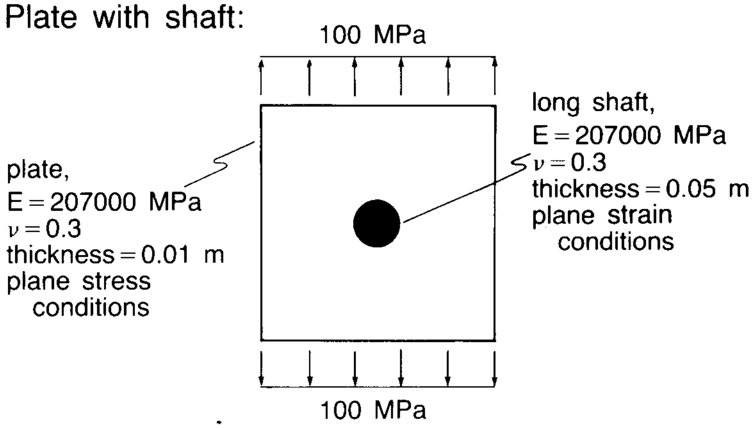

- The shaft is initially flush with the hole.
- We assume no friction between the shaft and the hole.

Transparency 22-17

Detail of shaft:

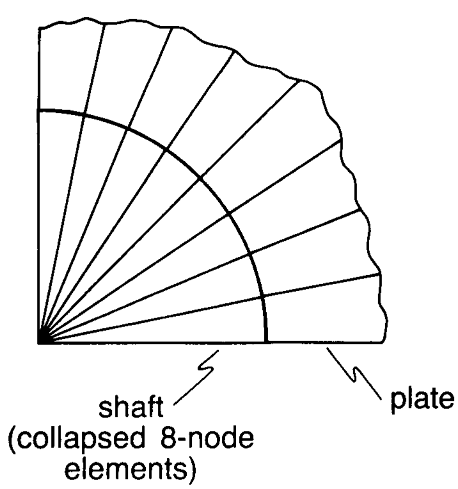

Transparency 22-18

Transparency 22-19

Solution procedure: Full Newton iterations without line searches

Convergence criteria:

Energy: ETOL = 0.001

Force: RTOL = 0.01 , RNORM = 0.05 N

Incremental contact force:

$$\frac{\|\Delta \underline{R}^{(i-1)} - \Delta \underline{R}^{(i-2)}\|_2}{\|\Delta \underline{R}^{(i-1)}\|_2} \leq \text{RCTOL} = 0.05$$

ADINA Demonstration 22-5

Deformed mesh

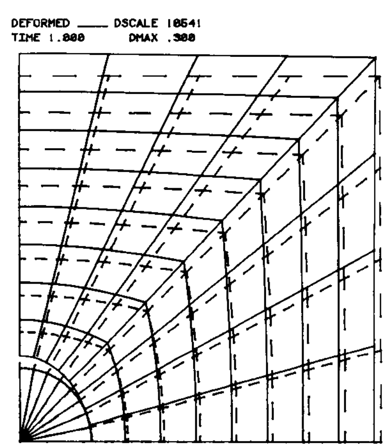

Plate with expanding shaft:

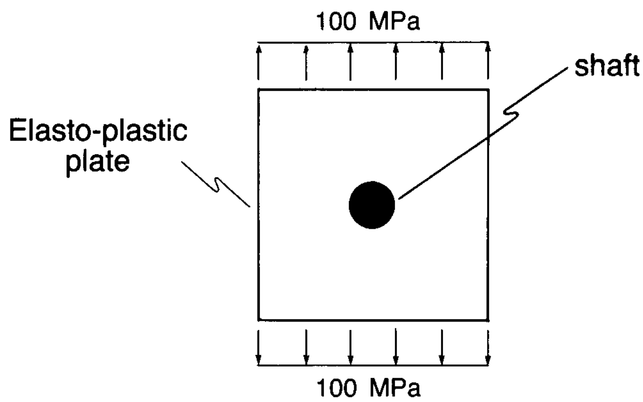

• The shaft now uniformly expands.

Transparency 22-20

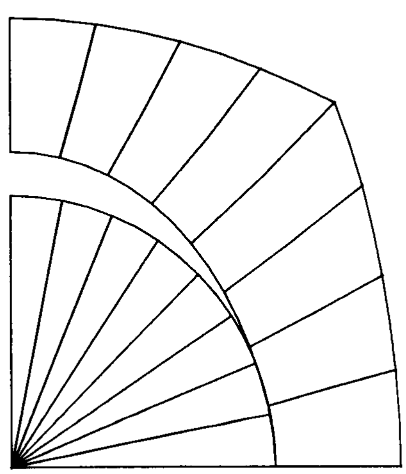

ADINA Demonstration 22-6
Close-up of deformations at contact

Glossary of Symbols

Contents:

Glossary of Roman Symbols

$\| \; \|_2$	The Euclidean norm or "two-norm." For a vector $\underline{a}$ $$\|\underline{a}\|_2 = \sqrt{\sum_k (a_k)^2}$$
$\tilde{}$	When used above a symbol, denotes "in the rotated coordinate system."
a_k, b_k	Cross-sectional dimensions of a beam at nodal point *k*.
${}^tA$	Cross-sectional area at time *t*.
$\underline{A}^{(i)}$	A square matrix used in the BFGS method.
$\underline{B}_L$	Linear strain-displacement matrix used in linear or M.N.O. analysis.
${}^t_0\underline{B}_L$	Linear strain-displacement matrix used in the T.L. formulation.
${}^t_t\underline{B}_L$	Linear strain-displacement matrix used in the U.L. formulation.
${}^t_0\underline{B}_{L0}, {}^t_0\underline{B}_{L1}$	Intermediate matrices used to compute ${}^t_0\underline{B}_L$; ${}^t_0\underline{B}_{L1}$ contains the "initial displacement effect."
${}^t_0\underline{B}_{NL}$	Nonlinear strain-displacement matrix used in the T.L. formulation.
${}^t_t\underline{B}_{NL}$	Nonlinear strain-displacement matrix used in the U.L. formulation.
c	The wave speed of a stress wave (dynamic analysis).
c_{ii}	Diagonal element corresponding to the *i*th degree of freedom in the damping matrix (dynamic analysis).
$\underline{C}$	The damping matrix (dynamic analysis).
C_1, C_2	The Mooney-Rivlin material constants (for rubberlike materials).
${}^t_0C_{ij}$	Components of the Cauchy-Green deformation tensor (basic concepts of Lagrangian continuum mechanics).
$\underline{C}_\ell$	Matrix containing components of the constitutive tensor referred to a local coordinate system.
$\underline{C}$	Matrix containing components of the constitutive tensor, used in linear and M.N.O. analysis.
${}_0\underline{C}$	Matrix containing components of the constitutive tensor ${}_0C_{ijrs}$, used in the T.L. formulation.
${}_t\underline{C}$	Matrix containing components of the constitutive tensor ${}_tC_{ijrs}$, used in the U.L. formulation.
C^E_{ijrs}	Components of elastic constitutive tensor relating $d\sigma_{ij}$ to de^E_{rs}
C^{EP}_{ijrs}	Components of elasto-plastic constitutive tensor relating $d\sigma_{ij}$ to de_{rs}
${}_0C_{ijrs}$	Components of tangent constitutive tensor relating d_0S_{ij} to $d_0\varepsilon_{rs}$
${}_tC_{ijrs}$	Components of tangent constitutive tensor relating d_tS_{ij} to $d_t\varepsilon_{rs}$
DNORM	Reference displacement used with displacement convergence tolerance DTOL (solution of nonlinear equations).
DMNORM	DMNORM is the reference rotation used when rotational degrees of freedom are present.
DTOL	Convergence tolerance used to measure convergence of the displacements and rotations (solution of nonlinear equations).

det	The determinant function, for example, $\det {}_0^t\underline{X}$.
${}^t dV$	A differential element of volume evaluated at time t.
${}^0 dV$	A differential element of volume evaluated at time 0.
$d\,{}^t\underline{x}$	Vector describing the orientation and length of a differential material fiber at time t (basic concepts of Lagrangian continuum mechanics).
$d\,{}^0\underline{x}$	Vector describing the orientation and length of a differential material fiber at time 0 (basic concepts of Lagrangian continuum mechanics).
${}^t\bar{e}^C$	Effective creep strain, evaluated at time t (creep analysis).
e_{ij}	Components of infinitesimal strain tensor (linear and M.N.O. analysis).
${}_0e_{ij}$	Linear (in the incremental displacements) part of ${}_0\varepsilon_{ij}$ (T.L. formulation)
${}_te_{ij}$	Linear (in the incremental displacements) part of ${}_t\varepsilon_{ij}$ (U.L. formulation).
${}^te_{ij}^{IN}$, ${}^te_{ij}^{C}$, ${}^te_{ij}^{P}$, ${}^te_{ij}^{TH}$, ${}^te_{ij}^{VP}$	Various types of inelastic strains evaluated at time t (inelastic analysis): IN inelastic C creep P plastic TH thermal VP viscoplastic
$\underline{e}_r$, $\underline{e}_s$, $\underline{e}_t$	Unit vectors in the r, s, and t directions (shell analysis).
$\bar{\underline{e}}_r$, $\bar{\underline{e}}_s$	Unit vectors constructed so that $\bar{\underline{e}}_r$, $\bar{\underline{e}}_s$, $\underline{e}_t$ are mutually orthogonal (shell analysis).
E	Young's modulus.
E_a, E_b	Young's moduli in the a and b directions (orthotropic analysis).
E_T	Strain hardening modulus (elasto-plastic analysis).
ETOL	Convergence tolerance used to measure convergence in energy (solution of nonlinear equations).
$f(x)$	A function that depends on x (solution of nonlinear equations).
$\underline{f}(\underline{U})$	A vector function that depends on the column vector $\underline{U}$ (solution of nonlinear equations).
${}^tf_i^B$, ${}^tf_i^S$	Components of externally applied forces per unit current volume and unit current surface area.
${}^tF$	Yield function (elasto-plastic analysis).
${}^t\underline{F}$	Vector of nodal point forces equivalent to the internal element stresses.
${}_0^t\underline{F}$	Vector of nodal point forces equivalent to the internal element stresses (T.L. formulation).
${}_t^t\underline{F}$	Vector of nodal point forces equivalent to the internal element stresses (U.L. formulation).
$\underline{F}_I(t)$	Column vector containing the inertia forces for all degrees of freedom (dynamic analysis).
$\underline{F}_D(t)$	Column vector containing the damping forces for all degrees of freedom (dynamic analysis).
$\underline{F}_E(t)$	Column vector containing the elastic forces (nodal point forces equivalent to element stresses) for all degrees of freedom (dynamic analysis).
g	Acceleration due to gravity.
G_{ab}	Shear modulus measured in the local coordinate system a-b (orthotropic analysis).
h	Cross-sectional height (beam element).
h_k	Interpolation function corresponding to nodal point k.

$\underline{H}$	Displacement interpolation matrix (derivation of element matrices).
$\underline{H}^S$	Displacement interpolation matrix for surfaces with externally applied tractions (derivation of element matrices).
I_1, I_2, I_3	The invariants of the Cauchy-Green deformation tensor (analysis of rubberlike materials).
$\underline{J}$	The Jacobian matrix relating the x_i coordinates to the isoparametric coordinates (two- and three-dimensional solid elements).
${}^t\underline{J}$	The Jacobian matrix relating the ${}^tx_i$ coordinates to the isoparametric coordinates (two- and three-dimensional solid elements in geometrically nonlinear analysis).
k	Shear factor (beam and shell analysis).
${}^t\underline{K}$	The tangent stiffness matrix, including all geometric and material nonlinearities.
${}^t_0\underline{K}$	The tangent stiffness matrix, including all geometric and material nonlinearities (T.L. formulation).
${}^t_t\underline{K}$	The tangent stiffness matrix, including all geometric and material nonlinearities (U.L. formulation).
${}^t_0\underline{K}_L$, ${}^t_t\underline{K}_L$	The contribution to the total tangent stiffness matrix arising from the linear part of the Green-Lagrange strain tensor. ${}^t_0\underline{K}_L$ - T.L. formulation ${}^t_t\underline{K}_L$ - U.L. formulation
${}^t_0\underline{K}_{NL}$, ${}^t_t\underline{K}_{NL}$	The contribution to the total tangent stiffness matrix arising from the nonlinear part of the Green-Lagrange strain tensor. ${}^t_0\underline{K}_{NL}$ - T.L. formulation ${}^t_t\underline{K}_{NL}$ - U.L. formulation
$\hat{\underline{K}}$	Effective stiffness matrix, including inertia effects but no nonlinear effects (dynamic substructure analysis).
${}^t\hat{\underline{K}}$	Effective stiffness matrix, including inertia effects and nonlinear effects (dynamic substructure analysis).
$\hat{\underline{K}}_c$	$\hat{\underline{K}}$ after static condensation (dynamic substructure analysis).
${}^t\hat{\underline{K}}_c$	${}^t\hat{\underline{K}}$ after static condensation (dynamic substructure analysis).
${}^t\underline{K}_{nonlinear}$	Nonlinear stiffness effects due to geometric and material nonlinearities (dynamic substructure analysis).
${}^tL$	Length, evaluated at time t.
L_e	Element length, chosen using the relation $L_e = c\,\Delta t$ (dynamic analysis).
L_w	Wave length of a stress wave (dynamic analysis).
m_{ii}	Lumped mass associated with degree of freedom i (dynamic analysis).
$\underline{M}$	The mass matrix (dynamic analysis).
${}^tp_{ij}$	Quantities used in elasto-plastic analysis, defined as ${}^tp_{ij} = -\left.\dfrac{\partial\, {}^tF}{\partial\, {}^te^P_{ij}}\right\rvert_{{}^t\sigma_{ij}\text{ fixed}}$
${}^tq_{ij}$	Quantities used in elasto-plastic analysis defined as ${}^tq_{ij} = \left.\dfrac{\partial\, {}^tF}{\partial\, {}^t\sigma_{ij}}\right\rvert_{{}^te^P_{ij}\text{ fixed}}$
r , s , t	Isoparametric coordinates (two- and three-dimensional solid elements, shell elements).
${}^t_0\underline{R}$	Rotation matrix (polar decomposition of ${}^t_0\underline{C}$).
$\underline{R}$	Reference load vector (automatic load step incrementation).
${}^t\underline{R}$	Applied loads vector, corresponding to time t.

${}^{t}\mathfrak{R}$	Virtual work associated with the applied loads, evaluated at time t.
RNORM,	Reference load used with force tolerance RTOL (solution of nonlinear equations).
RMNORM	Reference moment used when rotational degrees of freedom are present.
RTOL	Convergence tolerance used to measure convergence of the out-of-balance loads (solution of nonlinear equations).
${}^{t}s_{ij}$	Deviatoric stress evaluated at time t (elasto-plastic analysis).
${}^{t}S$	Surface area, evaluated at time t.
${}_{0}^{t}S_{ij}$	Components of 2nd Piola-Kirchhoff stress tensor, evaluated at time t and referred to the original configuration (basic Lagrangian continuum mechanics).
${}_{0}S_{ij}$, ${}_{t}S_{ij}$	Components of increments in the 2nd Piola-Kirchhoff stress tensors: $${}_{0}S_{ij} = {}^{t+\Delta t}_{0}S_{ij} - {}^{t}_{0}S_{ij}$$ $${}_{t}S_{ij} = {}^{t+\Delta t}_{t}S_{ij} - {}^{t}\tau_{ij}$$
${}_{0}^{t}\underline{S}$	Matrix containing the components of the 2nd Piola-Kirchhoff stress tensor (T.L. formulation).
${}_{0}^{t}\hat{\underline{S}}$	Vector containing the components of the 2nd Piola-Kirchhoff stress tensor (T.L. formulation).
t , t+Δt	Times for which a solution is to be obtained in incremental or dynamic analysis. The solution is presumed known at time t and is to be determined for time $t+\Delta t$.
$\bar{t}$	"Effective" time (creep analysis).
$\underline{T}$	Displacement transformation matrix (truss element).
T_{co}	Cut-off period (the smallest period to be accurately integrated in dynamic analysis).
T_n	Smallest period in finite element assemblage (dynamic analysis).
${}^{t}u_i$	Total displacement of a point in the ith direction.
${}^{t}\ddot{u}_i$	Total acceleration of a point in the ith direction (dynamic analysis).
u_i	Incremental displacement of a point in the ith direction.
u_i^s	Components of displacement of a point upon which a traction is applied.
${}_{0}^{t}u_{i,j}$	Derivatives of the total displacements with respect to the original coordinates (T.L. formulation).
${}_{0}u_{i,j}$	Derivatives of the incremental displacements with respect to the original coordinates (T.L. formulation).
${}_{t}u_{i,j}$	Derivatives of the incremental displacements with respect to the current coordinates (U.L. formulation).
u_i^k	Incremental displacement of nodal point k in the ith direction.
${}^{t}u_i^k$	Total displacement of nodal point k in the ith direction at time t.
$\hat{\underline{u}}$	A vector containing incremental nodal point displacements.
${}^{t}\hat{\underline{u}}$	A vector containing total nodal point displacements at time t.
${}^{t}\ddot{\underline{U}}$	Vector of nodal point accelerations, evaluated at time t.
${}^{t}\dot{\underline{U}}$	Vector of nodal point velocities, evaluated at time t.
${}^{t}\underline{U}$	Vector of nodal point displacements, evaluated at time t.
${}_{0}^{t}\underline{U}$	Stretch matrix (polar decomposition of ${}_{0}^{t}\underline{C}$).
$\underline{v}^{(i)}$	Column vector used in the BFGS method (solution of nonlinear equations).

${}^{t}V$	Volume evaluated at time t.
${}^{t}\underline{V}_n^k$, ${}^{t}V_{ni}^k$	Director vector at node k evaluated at time t (shell analysis).
$\underline{V}_n^k$	Increment in the director vector at node k (shell analysis).
${}^{t}\underline{V}_1^k$, ${}^{t}\underline{V}_2^k$	Vectors constructed so that ${}^{t}\underline{V}_1^k$, ${}^{t}\underline{V}_2^k$ and ${}^{t}\underline{V}_n^k$ are mutually perpendicular (shell analysis).
${}^{t}\underline{V}_s^k$, ${}^{t}\underline{V}_t^k$	Director vectors in the s and t directions at node k, evaluated at time t (beam analysis).
$\underline{V}_s^k$, $\underline{V}_t^k$	Increments in the director vectors in the s and t directions at node k (beam analysis).
$\underline{w}^{(i)}$	Vector used in the BFGS method (solution of nonlinear equations).
W	Preselected increment in external work (automatic load step incrementation).
${}_0^tW$	Strain energy density per unit original volume, evaluated at time t (analysis of rubberlike materials).
${}^{t}W_P$	Plastic work per unit volume (elastoplastic analysis).
${}^{t}x_i$	Coordinate of a material particle in the ith direction at time t.
${}^{t}x_i^k$	Coordinate of node k in the ith direction at time t.
${}_0^t x_{i,j}$, ${}_0^t X_{ij}$	Components of the deformation gradient tensor, evaluated at time t and referred to the configuration at time 0.
${}_t^0 x_{i,j}$, ${}_t^0 \underline{X}_{ij}$	Components of the inverse deformation gradient tensor.

Glossary of Greek Symbols

α	Parameter used in the α-method of time integration. $\alpha = 0$ - Euler forward method $\alpha = \frac{1}{2}$ - Trapezoidal rule $\alpha = 1$ - Euler backward method
α_k	Incremental nodal point rotation for node k about the ${}^t\underline{V}_1^k$ vector (shell analysis).
${}^t\alpha$	Coefficient of thermal expansion (thermo-elasto-plastic and creep analysis).
β	Line search parameter (used in the solution of nonlinear equations).
β	Section rotation of a beam element.
β_k	Incremental nodal point rotation for node k about the ${}^t\underline{V}_2^k$ vector (shell analysis).
γ	Transverse shear strain in a beam element.
γ	Fluidity parameter used in visco-plastic analysis.
γ	Related to the buckling load factor λ through the relationship $\gamma = \frac{\lambda - 1}{\lambda}$
${}^t\gamma$	Proportionality coefficient between the creep strain rates and the total deviatoric stresses (creep analysis).
$\underline{\gamma}^{(i)}$	Force vector in the BFGS method.
$\frac{\partial \underline{f}}{\partial \underline{U}}$	A square coefficient matrix with entries $\left[\frac{\partial \underline{f}}{\partial \underline{U}}\right]_{ij} = \frac{\partial f_i}{\partial U_j}$ (solution of nonlinear equations).
δ	When used before a symbol, this denotes "variation in."
δ_{ij}	Kronecker delta; $\delta_{ij} = \begin{cases} 0; & i \neq j \\ 1; & i = j \end{cases}$
$\underline{\delta}^{(i)}$	Displacement vector in the BFGS method.
$\Delta\ell$	"Length" used in the constant arc-length constraint equation (automatic load step incrementation).
Δt	Time step used in incremental or dynamic analysis.
Δt_{cr}	Critical time step (dynamic analysis).
$\Delta\underline{U}^{(i)}$	Increment in the nodal point displacements during equilibrium iterations $\Delta\underline{U}^{(i)} = {}^{t+\Delta t}\underline{U}^{(i)} - {}^{t+\Delta t}\underline{U}^{(i-1)}$
$\Delta\underline{\bar{U}}$	Vector giving the direction used for line searches (solution of nonlinear equations).
$\Delta\underline{\bar{U}}^{(i)}, \Delta\underline{\bar{\bar{U}}}$	Intermediate displacement vectors used during automatic load step incrementation.

$\Delta\underline{X}^{(k)}$	Increment in the modal displacements (mode superposition analysis).
$\Delta\tau$	A time step corresponding to a subdivision of the time step Δt (plastic analysis).
${}_0^t\varepsilon_{ij}$	Components of Green-Lagrange strain tensor, evaluated at time t and referred to time 0.
${}_0\varepsilon_{ij}$	Components of increment in the Green-Lagrange strain tensor: ${}_0\varepsilon_{ij} = {}^{t+\Delta t}_{0}\varepsilon_{ij} - {}_0^t\varepsilon_{ij}$
${}_t^t\varepsilon_{ij}^a$	Components of Almansi strain tensor.
η, ξ, ζ	Convected coordinate system (used in beam analysis).
${}_0\eta_{ij}$	The "nonlinear" part of the increment in the Green-Lagrange strain tensor.
θ_k	Nodal point rotation for node k (two-dimensional beam analysis).
θ_i^k	Nodal point rotation for node k about the x_i axis (beam analysis).
${}^t\theta$	Temperature at time t (thermo-elasto-plastic and creep analysis).
${}^t\kappa$	Variable in plastic analysis.
λ	Lamé constant (elastic analysis). $\lambda = \frac{E\nu}{(1+\nu)(1-2\nu)}$
λ	Scaling factor used to scale the stiffness matrix and load vector in linearized buckling analysis.
${}^t\lambda$	Load factor used to obtain the current loads from the reference load vector: ${}^t\underline{R} = {}^t\lambda\underline{R}$ (automatic load step incrementation).
${}^t\lambda$	Proportionality coefficient in calculation of the plastic strain increments (plastic analysis).
μ	Lamé constant (elastic analysis). $\mu = \frac{E}{2(1+\nu)}$
ν	Poisson's ratio.
ν_{ab}	Poisson's ratio referred to the local coordinate system a-b (orthotropic analysis).
Π	Total potential energy (fracture mechanics analysis).
${}^t\rho$	Mass density, evaluated at time t.
${}^t\sigma_{ij}$	Components of stress tensor evaluated at time t in M.N.O. analysis.
${}^t\bar{\sigma}$	Effective stress (used in creep analysis) ${}^t\bar{\sigma} = \sqrt{\frac{3}{2}\,{}^ts_{ij}\,{}^ts_{ij}}$
${}^t\sigma_y$	Yield stress at time t (plastic analysis).
σ_y	Initial yield stress (plastic analysis).
$\sum_m$	Denotes "sum over all elements."
${}^t\hat{\underline{\Sigma}}$	Vector containing the components of the stress tensor in M.N.O. analysis.
τ	(as a left superscript)—Denotes a time. Examples: ${}^\tau\underline{K}, {}^\tau\underline{R}$ - linearized buckling analysis; ${}^\tau\underline{K}$ - solution of nonlinear equations
${}^t\tau_{ij}$	Components of Cauchy stress tensor, evaluated at time t.
${}^t\underline{\tau}$	Matrix containing the components of the Cauchy stress tensor (U.L. formulation).

${}^{t}\hat{\underline{T}}$	Vector containing the components of the Cauchy stress tensor (U.L. formulation).
$\underline{\phi}$	A vector containing the nodal point displacements corresponding to a buckling mode shape.
$\underline{\phi}_i$	A vector containing the nodal point displacements corresponding to the *i*th mode shape.
ω_i	Natural frequency of the *i*th mode shape.
$\omega_n^{(m)}$	Largest natural frequency of element *m*.
$(\omega_n^{(m)})_{max}$	Largest natural frequency of all individual elements.

Resource: Finite Element Procedures for Solids and Structures
Klaus-Jürgen Bathe